Stony Brook University

The Role of Phospholipase D2 in golgi-architecture maintenance, vesicular trafficking and glucose- stimulated insulin release & Validation of a novel non-invasive approach to functional β-cell mass quantification

A Dissertation Presented

by

Oladapo Yeku

to

The Graduate School

In Partial fulfillment of the

Requirements

For the Degree of

Doctor of Philosophy

in

Molecular and Cellular Pharmacology

Stony Brook University

August 2010

Stony Brook University

The Graduate School

Oladapo Olumoroti Yeku

We, the dissertation committee for the above candidate for the Doctor of Philosophy degree, hereby recommend acceptance of this dissertation.

Michael A. Frohman, M.D., PhD.
Dissertation Director
Professor
Department of Pharmacological Sciences

David Talmage, Ph.D.
Chairperson of the Defense
Associate Professor
Department of Pharmacological Sciences

Ken-Ichi Takemaru, Ph.D.
Associate Professor
Department of Pharmacological Sciences

Richard Z. Lin, M.D.
Professor
Departments of Medicine and Physiology & Biophysics

This dissertation is accepted by the Graduate School.

Lawrence Martin
Dean of the Graduate School

Abstract of the Dissertation

The Role of Phospholipase D2 in golgi-architecture maintenance, vesicular trafficking and glucose- stimulated insulin release & Validation of a novel non-invasive approach to functional β-cell mass quantification

by

Oladapo Yeku

Doctor of Philosophy

In

Molecular and Cellular Pharmacology

Stony Brook University

2010

Phospholipase D (PLD) is essential for different aspects of vesicle trafficking and regulated exocytosis in a variety of biological models. PLD1 and PLD2 are the two major mammalian isoforms and both isoforms localize to different organelles where they generate phosphatidic acid (PA), the effector molecule of PLD activity. The role of PLD1 in glucose-stimulated insulin release (GSIR), a form of regulated exocytosis, has been well characterized. Additionally, the role of PLD1 in anterograde vesicle trafficking from the ER to the cis-golgi and from the trans-golgi to the plasma membrane has also been

described. The role of PLD2 in GSIR and vesicle trafficking has been less defined. Here we report an essential role for PLD2 in cis-golgi architecture maintenance and GSIR. Loss of PLD2 leads to increased GSIR and tubulated cis-golgi morphology. Dysregulation of Ca^{2+} homeostasis was found to be responsible for increased GSIR in PLD2 knockdown cells. We further identified a putative lipid sensor and phosphatidic acid phosphatase (PAP), PITPNM3, that plays a role downstream of PLD2 activity to support golgi architecture. For the first time, we suggest a role for PA to DAG conversion as an integral process for cis-golgi architecture maintenance. Finally, in insulin- secreting cells, we provide evidence that supports opposing roles for PLD1 and PLD2 in golgi architecture maintenance and GSIR. In renal epithelial cells, we found cis-golgi fragmentation and lysosomal trafficking defects when PLD2 was knocked down. Examination of $PLD2^{-/-}$ mouse kidneys showed vacuolization of the proximal tubules without any measurable decline in renal function.

Failure of insulin secretion by β-cells is the underlying cause of type-I diabetes. To date, there is no way to monitor functional β-cell mass non-invasively. Here we demonstrate a proof of principle approach to the detection and quantification of functional β-cell mass using an established metabolomic approach.

This is dedicated to my father, mother, sister and brother

Table of Contents

List of Abbreviations

PLD	Phsopholipase D
PLC	Phospholipase C
PA	Phosphatidic Acid
PX	Phox homology domain
PH	Pleckstrin homology domain
DAG	Diacylglycerol
PAP	Phosphatidic acid phosphatase
LPA	Lyso-phosphatidic acid
ER	Endoplasminc Reticulum
EGF	Epithelial Growth Factor
GLUT4	Glucose Transporter type 4
ARF1	ADP-ribosylation factor 1
ATP	Adenosine Triphosphate
GLP1	Glucagon-like peptide-1
GSIR	Glucose-Stimulated Insulin Release
CDK5	Cyclin Dependent Kinase 5
LPS	Lipopolysaccharide
PAS	Periodic Acid Schiff
VDCC	Voltage Dependent Calcium Channel
CAR8 (CARP)	Carbonic Anhydrase Related protein 8
NIR1 (PITPNM3)	Phosphatidyl Inositol Transfer Protein membrane associated
LDL	Low Density Lipoprotein
HDL	High Density Lipoprotein
AQP2	Aquaporin 2
RNAi	RNA interference

List of Figures

Chapter 1

Chapter 2

Chapter 3

Chapter 4

Chapter 5

Chapter 6

Acknowledgements

It takes a village……

I would like to thank my mentor, thesis advisor and friend; Dr. Michael Frohman. He offered me an opportunity when others would not have been so considerate. I have learned nearly everything I know about the scientific approach from him. I have him to thank for providing me with critical undergraduate research training that made me competitive for MSTP programs around the country. Subsequently, I have learned a great deal from him as a graduate student. As an apprentice, I could not have chosen a better mentor- thank you.

I would like to thank Dr. Guangwei Du and Dr. Ping Hung, the two post doctoral fellows who trained me at the bench. I have constantly strived to emulate their "experimentalist" attitude.

I would like to thank the many professors from Stony Brook and Medgar Evers College who have helped me along the way. Dr. Howard Crawford, Dr. Edward Catapane, Dr. Charles desBordes, Dr. Ann Brown, Dr. Anthony DePass, Dr. John Sumerlin, Dr. Carlyle Thompson, Dr. Henry Ricardo and too many others to list individually.

I would like to thank my many friends from SOM class of 2009, my MSTP class, the department of pharmacology and the graduate school. I would like to Iehab Talukder, my coffee buddy and general accomplice. I would also like to thank George Zanazzi for his many kind words and critical evaluation of my thesis.

I would like to thank the members of my lab, I have learned a lot from all of you.

I am greatly indebted to my committee members; Dr. David Talmage, Dr. Ken Takemaru and Dr. Richard Lin. I appreciate the commitment of your time and interest in my professional development.

I would like to thank the AGEP and Turner family, especially Nina Maung-Gaona, Kathryne Piazzola for taking me in and treating me like family.

Last but not least, I would like to thank Christine Li, your support has been instrumental throughout this process-thank you.

Chapter 1

Introduction

The phospholipase D (PLD) family of enzymes is found widely from plant, bacterial (Wang, 2000; Wang et al., 1993; Wang et al., 2002; Wang et al., 2000; Wang et al., 1994; Whitaker et al., 2001) and yeast (Ella et al., 1995; Rose et al., 1995) to mammals (Colley et al., 1997a; Colley et al., 1997b; Hammond et al., 1995; Hammond et al., 1997). The proteotypic catalytic activity of this family of enzymes involves the hydrolysis of phosphatidylcholine (PC) to phosphatidic acid (PA) (Fig 1-1) (Saito and Kanfer, 1975). PA can further be metabolized to diacylglycerol (DAG) by phosphatidic acid phosphatases (PAP) (Sciorra and Morris, 1999). The reverse reaction to phosphorylate DAG to generate PA is performed by DAG kinase. PA can also be reversibly converted to lysoPA (LPA) (Brindley and Waggoner, 1996). In the presence of primary alcohols, PLD generates phosphatidylalcohols (PEt) via a transphosphatidylation reaction, which is the more general form of the hydrolysis reaction described above (Edwards and Murray, 1995; Kobayashi and Kanfer, 1987; Yang et al., 1967) (fig 1-1). In mammalian cells, there are at least 5 isoforms of PLD, three of which are well studied (Choi et al., 2006; Colley et al., 1997a; Colley et al., 1997b; Hammond et al., 1997). Phospholipase D1 (PLD1), Phospholipase D2 (PLD2) and MitoPLD are all widely expressed in many tissues. PLD1 and PLD2 are structurally very similar with both enzymes containing a phox homology domain (PX), a pleckstrin homology domain (PH), and four conserved motifs. Motifs II and IV each encode an HKD half-catalytic domain that juxtapose in the folded structure to form the active catalytic site (Xie et al., 1998; Xie

et al., 2000) to hydrolyze PC (Stuckey and Dixon, 1999; Sung et al., 1997). PLD1 contains a unique 116-amino acid loop region between motifs II and III, deletion of which increases its activity 3-fold (Sung et al., 1999b), suggesting its role as a negative regulatory element. Addition of this loop region to PLD2 did not alter its activity (Hammond et al., 1997; Sung et al., 1999a).

PLD1 and PLD2 differ in their basal activity and regulation. PLD1 has very low basal activity and requires agonist stimulation, while PLD2 has been shown to exhibit high basal activity (Colley et al., 1997a; Colley et al., 1997b; Jenkins and Frohman, 2005; Sung et al., 1999a; Sung et al., 1999b). ADP ribosylation factors (ARF) are well-characterized stimulants of PLD activity. ARF1 (Brown et al., 1993; Cockcroft et al., 1994; Martin et al., 1996), ARF3 (Brown et al., 1995), ARF5 and ARF6 (Brown et al., 1995; Caumont et al., 1998) are potent activators of PLD1. Activation of PLD2 by ARF on the other hand is very modest by comparison (Lopez et al., 1998; Sung et al., 1999a). PLD catalytic activity is also strongly dependent on phosphoinositides. Phosphatidylinositol 4,5 bisphosphate ($PI4,5P_2$) is a potent stimulator of PLD and an essential cofactor for ARF stimulation of PLD (Brown et al., 1995; Brown et al., 1993). Phosphoinositides are generated by phosphoinositol kinases, which have been shown to also be positively regulated by PA (Jenkins et al., 1994; Moritz et al., 1992)

As mentioned earlier, PLD is expressed widely in various mammalian cells and tissues. However, its intracellular localization has been difficult to define. This is due in part to the relative unavailability of highly specific antibodies, and in part because the subcellular location may differ in different cell types, or even in cell lines in comparison to primary tissues. For instance, Hughes *et al.* (2004) (Hughes et al., 2004) originally

reported that PLD2 was not expressed in MIN6 insulinoma cell lines. This finding conflicted with Laine *et al.* who showed expression of both PLD isoforms in pancreatic tissue (Laine et al., 2000). Influenza epitope- tagged PLD1 microinjected into rat embryo fibroblasts showed a distribution that was consistent with golgi, endoplasmic reticulum (ER) and late endosomes (Colley et al., 1997b). Subcellular fractionation studies in insulinoma and rat kidney epithelial cells (NRK) also showed that PLD1 was associated with the golgi membrane (Freyberg et al., 2001). Studies in Cos 7 and CHO cell lines (Lucocq et al., 2001) suggested that PLD1 was present in multivesicular and tubulovesicular bodies, golgi structures and endosomal membranes. This study also reported PLD1 localization to punctate perinuclear structures, a finding not corroborated by Colley *et al* (Colley et al., 1997b). In contrast to these studies, other groups have reported PLD1 localization to the endosomal and lysosomal compartment (Hughes and Parker, 2001) without any localization to the ER or golgi (Toda et al., 1999). In insulinoma, neuroendocrine and mast cells, PLD1 has been reported to localize to secretory vesicles (Brown et al., 1998; Choi et al., 2002; Hughes et al., 2004; Vitale et al., 2001), presumably to facilitate secretion. Upon agonist stimulation, PLD1 has been shown to translocate to the plasma membrane (Brown et al., 1998; Choi et al., 2002; Du et al., 2003; Huang et al., 2005). On the other hand, PLD2 has mostly been reported to localize to the plasma membrane (Choi et al., 2002; Du et al., 2004; Honda et al., 1999). Upon stimulation by serum or EGF, PLD2 translocates to sub-membranous vesicles and membrane ruffles (Colley et al., 1997b; Honda et al., 1999). Cytoplasmic (Honda et al., 1999) and β-actin (Honda et al., 1999) localization have also been reported for PLD2. PLD activity has also been reported in the nucleus (Balboa et al., 1995) and mitochondria

(Madesh and Balasubramanian, 1997). Much of the discrepancy in the literature regarding PLD localization and function can be attributed to the methods used for the study. 1-butanol, a frequently used inhibitor, has potentially off-target effects (Su et al., 2009), some of the tags used for the study might natively prefer certain cellular compartments, and PLD could be playing different roles in different cell types. Additionally, both isoforms of PLD are dynamic, translocating to various organelle membranes to generate PA in response to the changing needs of the cell.

PLD activity, mainly via the generation of PA, has been described in many cell biological systems. PLD activity has been linked to actin cytoskeletal reorganization, membrane ruffling and stress fiber formation (Brown et al., 1998; Cross et al., 1996; Honda et al., 1999). GLUT4 receptor trafficking from the intracellular compartment to the plasma membrane in 3T3-L adipocytes is dependent on PLD activity (Emoto et al., 2000; Huang et al., 2005). In the liver, the conversion of apolipoprotein B-containing precursors to VLDL depends on ARF1 activation of PLD (Asp et al., 2000; Olofsson et al., 1999). In immune cells, PLD has been shown to play an important role in exocytosis. In neutrophils, inhibition of PLD activity led to a decrease in azurophilic granule release (Fensome et al., 1996). Inhibition of lysosomal granules from HL60 cells in mutant PLD-expressing cells has also been reported (Jones et al., 1999). In mast cells, inhibition of PLD prevented IgE agonist-stimulated insulin release (Way et al., 2000). In general, PLD, most often PLD1, is believed to play a role in vesicle trafficking and exocytosis. Experiments showing PLD co-localization with the golgi and cytoplasmic vesicles, butanol-inhibition studies showing golgi fragmentation and failure of exocytosis, and elegant experiments linking PLD localization/function to stimulus-driven exocytosis all

support a critical role for PLD in organelle maintenance, vesicle trafficking and exocytosis.

With rare exceptions, most of the investigations into the role of PLD listed above have involved the use of 1-butanol as a pan-PLD inhibitor. Because of the subversion of PA production, generation of phosphatidylbutanol has been used extensively to probe the role of PLD in many biological processes. There are however two drawbacks to this approach; 1-butanol possesses off-target effects (Su et al., 2009), and both isoforms are simultaneously inhibited, making it impossible to determine which PLD isoform is primarily responsible for the phenotype under investigation. In summary, the localization and function of the PLD isoforms has remained incompletely defined.

Vesicle trafficking in eukaryotic cells is a delicate balance of anterograde trafficking from the ER to the golgi, from the golgi to the plasma membrane, lysosome, or other vesicular body, and retrograde transport back from the plasma membrane to endosomes or the golgi and from there back to the ER. Vesicles leaving the ER to the Golgi primarily do so via recruitment of COPII proteins. COPII dependent trafficking is initiated by the ADP-ribosylation family (ARF) member Sar1p. Sar1p is activated from its GDP-bound state to a GTP-bound state by Sec12p, a transmembrane ER protein. Upon activation, Sar1-GTP associates with the ER and recruits COPII proteins. One of the recruited coatomer proteins, Sec23p, contains GAP activity that stimulates Sar1-GTP hydrolysis. Sar1p-GTP hydrolysis provided a convenient explanation for vesicle fission, but this notion has since been disputed (Barlowe et al., 1994; Oka and Nakano, 1994), suggesting that vesicle uncoating (Sar1-GTP hydrolysis) is separable from actual vesicle fission. Since ARF-family members are known to activate PLD, investigators proposed a

role for PLD in vesicle trafficking. Kistakis *et al* (Ktistakis et al., 1996) found that 1-butanol treatment inhibited vesicle budding without affecting coatomer binding. Secondary alcohols used as controls did not affect either coatomer binding or vesicle scission. This experiment suggested a role for PLD generated PA downstream of coatomer binding in vesicular trafficking. Further adding to this appeal was the knowledge that PA might promote vesicle scission because of its biophysical properties. On the other hand, COPI-coated vesicles mediate retrograde trafficking from the *cis*-golgi to the ER. ARF1 has been shown to regulate COPI recruitment, following which the activity of BARS protein has been reported to be critical for membrane fission (Yang et al., 2005; Yang et al., 2006). Recently, PA and possibly DAG have been implicated as required components for COPI – coated vesicle fission (Yang et al., 2008). Despite binding of COPI proteins and BARS, PA generation was found to be required for the final pinching-off of the vesicles *in vitro*. In many instances, conversion of PA to DAG by PAPs serves as a way to terminate PLD activity, but conversion to DAG might actually be a necessary continuum of PLD activity with respect to vesicle fission (Roth et al., 1999; Yang et al., 2008).

β-cells are specialized cells that secrete insulin upon glucose stimulation. This process, a form of regulated exocytosis, culminates in the release of insulin into the blood. Like many other proteins destined for secretion, insulin is synthesized in the ER and is trafficked through the golgi and insulin-containing vesicles that bud off the *trans*-golgi and aggregate adjacent to the plasma membrane ready for release. Electrophysiology studies and electron micrograph images show insulin granules at different regions of the β-cell. Some vesicles are extremely close to the plasma

membrane and these vesicles constitute the readily releasable pool (RRP) that is available for immediate release on cue. A second wave of vesicles are located deeper within the cell and are mobilized to replenish the RRP. Agents that interrupt or dismantle the golgi lead to diminished insulin release. Inhibition of PLD1 abolishes insulin secretion (Hughes et al., 2004) likely because of the role of PLD1 in promoting anterograde traffic from the ER to the golgi and from the *trans*-golgi to the plasma membrane. Also, 1-butanol treatment of cells leads to golgi fragmentation and abolishment of insulin release.

In the following study, I characterize the role of PLD2 and to a lesser extent, its relationship to PLD1 in β-cells. Because of the significance of β-cells to diabetes, characterization of the role of PLD2 in organelle function and glucose-stimulated insulin release could potentially have an impact on our therapeutic approach to the disease.

Figure 1-1. Overview of PA generation from PC by PLD. PLD hydrolyzes PC to PA (black branch point). PA can further be dephosphorylated to DAG or converted to lysoPA (LPA). In the presence of primary alcohols (e.g. 1-butanol), PC is instead transphosphatidylated to phosphatidylethanol (pink branch point). Image from Liscovitch *et al.* (2000)

Figure 1-1

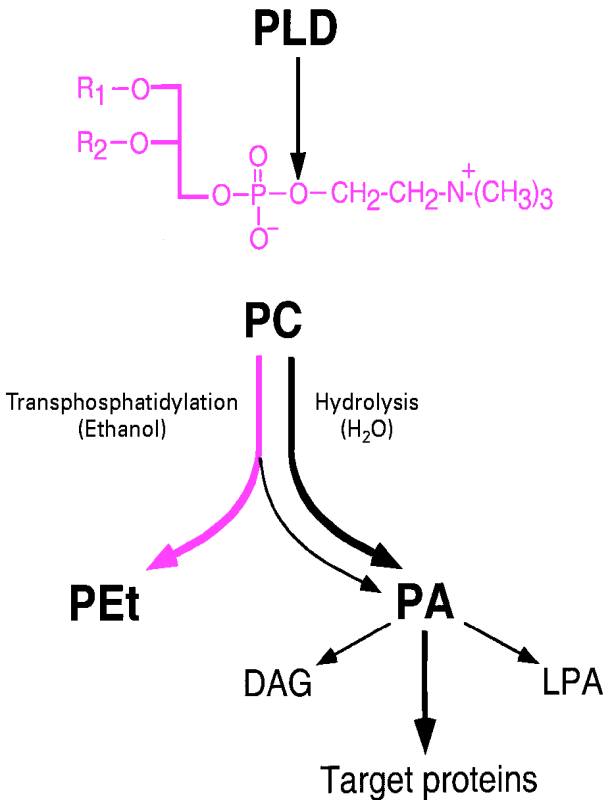

Liscovitch *et al.* (2000)

Chapter 2

The Role of PLD2 in GSIR

β-cells are insulin-secreting cells present in the pancreas of all mammals. These cells are responsible for the maintenance of euglycemia. Shortly after the consumption of a meal, rising serum glucose levels are sensed and internalized by GLUT2 receptors present on the surface of β-cells. This internalized glucose is metabolized to pyruvate to generate ATP. A shift in the ATP: ADP ratio inside the β-cell leads to closure of the ATP-sensitive K^+ channel which in turn leads to membrane depolarization. Membrane depolarization then opens L-type voltage-gated Ca^{2+} channels (VDCC) which permit Ca^{2+} influx, leading to insulin-loaded secretory vesicle fusion with the plasma membrane (exocytosis) and release of insulin into the bloodstream (Aguilar-Bryan et al., 2001; Ohara-Imaizumi et al., 2007; Srinivasan et al., 2000). β-cells are also responsive to secretagogues such as GLP1, small peptides, EGF and the parasympathetic nervous system (Asp et al., 2000; Hughes et al., 2004; Lee et al., 2008a; Lee et al., 2008b; Liu et al., 2008; MacDonald, 2007; Wei et al., 2005). These secretagogues potentiate insulin release by stimulating phospholipase C (PLC). PLC generates IP_3 and DAG from $PI(4,5)P_2$. Intracellular Ca^{2+} stores in the ER and golgi are gated by IP_3 receptors (IP_3R) (Pinton et al., 1998; Worley et al., 1994) and upon IP_3 binding release Ca^{2+}. There is evidence that suggests that there is a small burst of Ca^{2+} that occurs shortly after glucose triggered depolarization of the cell membrane but before the opening of the VDCC (Worley et al., 1994). Prevention of K^+ channel closure with diazoxide abolishes this small spike, but depletion of extracellular Ca^{2+} with EGTA has no effect, suggesting that

glucose triggers a small burst of Ca^{2+} release from intracellular stores prior to the opening of the VDCC.

The role of PLD in GSIR is unclear. While some reports suggested that only PLD1 was expressed in β-cells (Hughes et al., 2004), other reports have reported that PLD2 is also expressed (Laine et al., 2000). Exogenously-provided PA has been shown to stimulate insulin release (Metz and Dunlop, 1990), but not in the context of PLD activity. The use of 1-butanol has also impeded the delineation of the role of PLD2 in GSIR. Lee *et al* (Lee et al., 2008a; Lee et al., 2008b) reported EGF-stimulated PLD2 activity leads to insulin release. But this activity was largely due to CDK5 activation and EGF was used as the secretagogue activator; glucose-stimulated insulin release was actually not examined. With the new availability of mice lacking PLD2, I conducted preliminary studies to identify potential phenotypes, which, as described subsequently, led me to examine the role of PLD2 in GSIR.

Materials and Methods.

PLD2$^{-/-}$ mice and genotyping

WT and PLD2$^{-/-}$ mice were generated by Dr. Gilbert DiPaolo (Columbia University). Briefly, a loxP sequence was cloned upstream of PLD2 exon 13 and a FRT-Neo-FRT-LoxP cassette was inserted downstream of exon 15. The construct was microinjected into 129svj embryonic stem cells. PLD2-NEO/+ clones were selected and subsequently implanted into C57BL/6 blastocysts. Adult male mice were crossed with Cre-expressing mice leading to deletion of exons 13-15. PLD2$^{+/-}$ mice were crossed to generate PLD2$^{-/-}$ mice. Deletion of exons 13-15 was confirmed by genotyping using primers spanning the deleted region. Forward primers are 5'-GGGAATCTGAGGCTTCAAGACTGGG-3' and 5'-GCACGGGGCCCTCCCACATC-3' and 5'-GCTGGTGTTTTGAGGATGCTTG-3' for the reverse primer. Tails were snipped from the animals and incubated in 50 mM NaOH at 98°C for 50 min. The dissolved tails were briefly vortexed, neutralized with 1 M Tris (pH 8) and centrifuged for 6 min at 14000 RPM. The supernatant was collected and used for PCR. Primers generate a 150 bp band for WT and 521 bp for PLD2$^{-/-}$ mice. Heterozygous mice contained one of each band. All animals were maintained on a 12- hr light/dark cycle and fed standard mouse chow. All animal experiments were performed in accordance with the rules and regulations of the Animal Care and Use Committee, State University of New York at Stony Brook, Stony Brook, USA. For experiments, WT and PLD2 $^{-/-}$ pup littermates from heterozygous mice were initially used. Results from these studies were comparable to data from pure strain crosses and C57 backcrossed stain (F8 backcross).

Isolation of primary pancreatic islets and β-cells

Animals were sacrificed by CO_2 asphyxiation. A midline incision was made and the pancreas identified and removed. The pancreatic tissue was dissolved in Hanks balanced salt solution (HBSS) containing 2 mg/ml collagenase (Sigma) for 50 min at 37°C. The digestion was stopped by adding ice-cold HBSS containing 10% FBS (Hyclone). The mixture was centrifuged for 3 min and the pellet was washed 3 times with ice-cold HBSS and finally resuspended in 10 ml ice-cold HBSS. Aliquots were plated on a dish and islets were visually identified and hand picked under a dissecting microscope. Picked islets were cultured in Gibco RPMI 1640 (Invitrogen) supplemented with 10% FBS, 100 μg/ml streptomycin and 100 IU/ml penicillin. To prepare β-cells, primary islets were picked and incubated in trypsin for 5 min. Complete media (DMEM supplemented with 10% FBS, 100 μg/ml streptomycin and 100 IU/ml penicillin and L-glutamate) was added to terminate the trypsinization. The islets were then mechanically dispersed with a 25 G needle attached to a 10 mL capacity syringe. Dispersed β-cells were seeded unto poly-L-lysine coated plates/ coverslips and cultured in DMEM containing 5 mM glucose and 10% calf serum (Hyclone) and supplemented with 100 μg/ml streptomycin and 100 IU/ml penicillin (Sigma).

Intraperitoneal glucose and insulin tolerance tests

8-12 week old male WT and $PLD2^{-/-}$ mice were weighed and fasted overnight. The following morning, fasting plasma glucose was measured from tail bleeds using a glucometer (One Touch). They were then injected i.p with 1 g/kg of 25% D-glucose. Tail blood was then collected at various time points for glucose measurement. 2 mice were

used from each genotype and the experiment was repeated 3 times. For insulin tolerance test, mice were fasted for 6 hrs followed by i.p injection of 0.85 u/kg insulin (Novolin R; Novo Nordisk). Glucose measurements were taken from tail blood at different time points before and after the insulin injection. 2 animals per genotype were used and the experiment was repeated twice.

NIT-1 cell line and PLD2 RNAi transfection

The NIT-1 insulinoma cell line was purchased from ATCC and maintained in Hams F12 media supplemented with 10% FBS, 100 μg/ml streptomycin and 100 IU/ml penicillin and L-glutamate. PLD2 was transiently down-regulated using a PLD2 RNAi plasmid (PLD2-723). RNAi targeted against luciferase was used as a control vector. Vectors were transfected using Fugene HD (Roche) for 48 hrs. Knockdown efficiency was determined by RT-PCR.

RNA isolation and RT-PCR

Total RNA was isolated from cells transfected with either luciferase or PLD2 RNAi for 48 hrs using an RNA isolation kit (Qiagen). Isolated RNA was briefly treated with DNAase I (Qiagen) and subjected to one-step RT-PCR (Qiagen). PLD2 was amplified with 5'-CGAGAAGCTCCTGGTGGTAG-3' and 5'-CCAGTCCTTGGTGATGAGGT-3' to generate an amplicon size of 232 bp. 1 cycle of cDNA synthesis was performed at 50° C for 30 min, followed by 94° C for 2 min. PCR amplification was performed for 35 cycles as follows; 94 ° C for 15 sec (denaturation), 55° C for 30 s (annealing) and 72° C for 1 min (extension). A final extension step was performed at 72° C for 10 min.

Insulin secretion via static incubation

10 pancreatic islets from each genotype were picked under a dissecting microscope and incubated in 250 μL of KRBH buffer (KCl: 4.74 mmol/L, NaCl: 125 mmol/L, NaHCO3: 5 mmol/L, MgSO4: 1.2 mmol/L, CaCl2: 1 mmol/L, HEPES: 25 mmol/L, KH2PO4: 1.2 mmol/L, BSA: 0.10%) containing 2.5 mM D-glucose for 60 min at 37°. Subsequently, the buffer was removed and fresh KRBH media containing 2.5 mM D-glucose was added and placed at 37°C for 60 min. The buffer was collected, briefly centrifuged and the supernatant was collected as basal insulin secretion. For "stimulated" insulin secretion, the buffer was replaced with KRBH containing 20 mM glucose and incubated for 60 min at 37°C. The collected buffer was centrifuged and the supernatant preserved. All insulin-containing samples were placed on ice immediately after collection or stored at 20°C. To determine total insulin content, the islets were dissolved in 70% ethanol and 0.18 M HCl overnight, sonicated and centrifuged before samples were taken for ELISA measurements. ELISA measurements to determine basal, stimulated and total insulin concentrations were done with ultrasensitive mouse insulin ELISA (Mercodia: 10115010) and BioRad plate reader.

Microarray

Pancreatic islets were isolated from 8 WT (4 male and 4 female) and 8 $PLD2^{-/-}$ mice (4 male and 4 female). The islets were then matched and grouped according to sex (male 2 WT and 2 $PLD2^{-/-}$ mice; male 2 WT and 2 $PLD2^{-/-}$; female 2 WT and 2 $PLD2^{-/-}$; female 2 WT and 2 $PLD2^{-/-}$) and subjected to microarray analysis by Agilent whole genome

microarray (Miltenyi Biotech). Gene expression was compared between WT and PLD2$^{-/-}$ mice and repeated in quadruplicate.

Ca^{2+} measurements

NIT-1 cells were cultured in a 100 mm dish until they reached 85% - 90% confluency. The cells were subsequently trypsinized and diluted 1:5 into black-walled 96-well plates (Falcon). 24 hours after after seeding, the cells were transfected with luciferase or PLD2 RNAi for 48 hrs. The cells were washed once with KRBH containing 2.5 mM D-glucose and loaded with Fluo-4 cell- permeable Ca^{2+} dye for 45 min at 37° and 15 min at room temperature. Base-line intracellular measurements were taken using a Fluostar microplate reader exciting the dye at 488nm (argon laser) and emitted light was acquired at 505-530 nm. 20 mM glucose was then added to the cells and the scan was repeated 10 min later. Fold intracellular Ca^{2+} was calculated by dividing stimulated fluorescence values by baseline values. Data for each drug treatment was collected over 3 independent experiments.

Inhibitors and general reagents

PLC inhibitor U-73122 and IP_3 receptor (IP_3R) inhibitor Xestospongin were purchased from Calbochem. VDCC inhibitors Nifedipine and Diltiazem were purchased from Sigma.

Statistical analysis

Student's *t*-test was performed and significance was set at $p < 0.05$ unless otherwise stated in individual figure legends.

Results

PLD2 $^{-/-}$ mice exhibit exaggerated insulin release upon glucose stimulation

Insulin release from pancreatic beta cells and immortalized insulinoma cell lines is triggered by an increase in extracellular glucose concentrations. Post-parandially, rising serum glucose is internalized by GLUT2 receptors on pancreatic beta cells and this signal is transduced into eventual membrane depolarization and an increase in cytoplasmic Ca^{2+}, a universal signal for vesicle fusion and exocytosis. To directly examine the role of PLD2 in regulated exocytosis, I measured both random and fasting plasma glucose in PLD2$^{-/-}$ and matched wildtype (WT) mice (Fig. 2-1a,b). PLD2$^{-/-}$ mice exhibited lower random and fasting serum glucose, suggesting a sustained increase in circulating serum insulin. *In vivo* insulin secretion was directly stimulated by injecting PLD2$^{-/-}$ mice with an intraperitoneal bolus of glucose (Fig. 2-1c). Serum glucose measurements showed a blunted rise in PLD2$^{-/-}$ animals when compared to WT. Since serum glucose levels can also be affected by peripheral tissue sensitivity to glucose, I performed an insulin tolerance test (ITT) (Fig. 2-1d). WT and PLD2$^{-/-}$ animals showed comparable decreases in serum glucose over time, suggesting that peripheral glucose uptake in these animals were similar. However, in order to directly test the hypothesis that attenuation of PLD2 promotes exocytosis, I performed an *ex vivo* glucose stimulation test. Pancreatic islets were dissected from matched WT and PLD2$^{-/-}$ animals and directly stimulated with glucose (Fig. 2-1e). Both low (2.5 mM) and high (20 mM) glucose stimulation led to a greater increase in insulin secretion by islets from PLD2$^{-/-}$ mice compared to WT islets. Possible explanations for increased insulin release by PLD2$^{-/-}$ islets could be attributable to differences in islet size, or total insulin content. I found no differences in gross islet

size by histology and electron microscopy (Fig. 2-2a-b). Total insulin content was also similar between both groups (Fig. 2-2c-d). In summary, genetic deficiency of PLD2 leads to increased exocytosis of insulin in response to glucose stimulation. Exaggerated insulin release in $PLD2^{-/-}$ mice leads to decreased resting serum glucose and a heightened response to rising serum glucose levels.

Transient inhibition of PLD2 leads to increased GSIR

Increased GSIR in $PLD2^{-/-}$ islets could be the result of long term compensation not directly related to PLD2 knockdown. To address this possibility, I transfected the NIT-1 insulinoma cell line with PLD2 RNAi to acutely deplete PLD2 (48 hr transfection). NIT-1 cells showed greater than 90% transfection efficiency. PLD2 knockdown in NIT-1 cells led to increased GSIR in NIT-1 cells compared to luciferase RNAi controls (Fig. 2-3).

Microarray analysis shows alterations in Ca^{2+} homeostasis

To elucidate the underlying mechanism of increased GSIR, I subjected islets dissected from WT and $PLD2^{-/-}$ mice to microarray analysis. I expected compensation from other genes involved in PA metabolism. Unexpectedly, I did not find any changes in genes known to be directly involved in PA generation and metabolism. No differences were seen in PLD1, DAG kinase, phosphatidic acid phosphatase (PAP), and LPA phosphatase transcript levels (data not shown). Interestingly, transcripts of genes involved in PC transport were downregulated (Fig. 2-4). Specifically, levels of membrane-associated phosphatidylinositol transfer protein 3 (PITPNM3, also known as

Nir1 – (Lev et al., 1999)), a member of the PI/PC transport protein family (Bankaitis, 2009) was downregulated 5-fold (Fig. 2-4). ATP binding cassette, sub-family b, member 1b (Abcb1b), a p-glycoprotein reported to be involved in positively regulating second phase insulin release (Tang et al., 2009) showed a 3-fold upregulation. Finally, transcript levels of carbonic anhydrase related protein (CAR8/CARP), an IP_3 receptor (IP_3R) inhibitor (Hirota et al., 2003) were reduced 5-fold. I became interested in CAR8 because of its function as an IP_3R inhibitor.

PLD2-silenced cells show increased intracellular calcium levels upon stimulation

Intracellular calcium influx is the step immediately prerequisite to exocytosis and insulin release. To further characterize the mechanism of increased GSIR in PLD2 knockdown cells, I performed measurements of intracellular calcium ($^{i}Ca^{2+}$) upon glucose stimulation in PLD2 silenced and control cells. Luciferase and PLD2 knockdown cells were loaded with Fluo-4, a cell-permeable Ca^{2+} dye. Baseline scans were taken, following which the cells were stimulated with 20mM glucose and a repeat scan performed 10min later. The fold-change in intracellular Ca^{2+} levels is shown (Fig. 2-5a). Upon stimulation, control cells showed a 1.19 ± 0.05-fold increase in intracellular Ca^{2+}. PLD2-silenced cells showed a 2.07 ±0.04-fold increase over basal. Compared to control cells, PLD2-silenced cells showed a 73.9% fold greater increase in intracellular Ca^{2+}. Involvement of CAR8 downregulation in increased intracellular Ca^{2+} in PLD2 silenced cells was explored by co-expressing PLD2 RNAi and a CAR8 expression construct and assessing GSIR and intracellular Ca^{2+} (Fig. 2-5b,c). Expression of CAR8 caused a 42% decrease in basal GSIR and 31% in stimulated GSIR in control cells (Fig. 2-5b) but most

importantly, it abolished the increased insulin release seen in PLD2-silenced cells (decreased by 56% in basal and 58% in stimulated conditions). Measurement of intracellular Ca^{2+} revealed a 39% decrease in control cells and a 59% decrease in PLD2 RNAi and CAR8 co-expressing cells compared to controls (Fig. 2-5c). There was no difference between cells co-expressing CAR8/Luciferase RNAi and CAR8/PLD2 RNAi (0.99 ± 0.01 versus 0.92 ± 0.03 respectively). These results support a role for down-regulation of CAR8, an IP_3R inhibitor, in the increased GSIR observed in PLD2-silenced cells. Reduced expression of CAR8 in cells with depleted PLD2 leads to increased intracellular Ca^{2+} and GSIR. To test the hypothesis that increased IP_3R-gated calcium was responsible for increased GSIR in PLD2-silenced cells directly, luciferase control and PLD2 knockdown cells were treated with xestospongin c, an IP_3R inhibitor, and subjected to GSIR (Fig. 2-5d). Inhibition of the IP_3R decreased basal and stimulated GSIR in control cells (32% and 54% respectively) and abolished the increased GSIR in PLD2-depleted cells at both low and high glucose concentrations (62% and 77% respectively) compared to controls. Phospholipase C (PLC) generates IP_3, the ligand for the IP_3R, by hydrolyzing PIP_2 to yield IP_3 and DAG. Since PLC levels were unaltered in our microarray, I treated PLD2 knockdown and control cells with U-73122, a PLC inhibitor, and stimulated the cells with glucose (Fig. 2-5d). PLC inhibition led to a reduction in basal and stimulated GSIR in control cells (27% and 69% respectively) but had no effect on low glucose insulin secretion in PLD2 knockdown cells (7%). However, high glucose insulin secretion was diminished by 80% in PLD2 knockdown compared to control. Intracellular Ca^{2+} was also reduced in both PLC (5% in control, 4% in PLD2 RNAi) and IP_3R (31% in control, 50% in PLD2 RNAi) inhibitor treatments (Fig. 2-5e)

and the increased glucose-stimulated intracellular Ca^{2+} in PLD2-silenced cells was reduced to "no treatment" levels. Treatment with thapsigargin also abolished the differences in intracellular Ca^{2+} between control and PLD2-silenced cells (1.37-fold in control versus 1.4-fold in PLD2-silenced cells) (Fig. 2-5f). Glucose-stimulated PLC activity has been reported to be downstream of membrane depolarization (Gromada et al., 1996; Vadakekalam et al., 1996), but VDCC activation is still the major contributor to intracellular Ca^{2+} upon glucose stimulation. To validate that in our system, I treated control and PLD2-silenced NIT-1 cells with different L-type Ca^{2+} inhibitors (Nifedipine, Diltiazem) and measured intracellular Ca^{2+} and GSIR. Both intracellular Ca^{2+} (Fig. 2-5g) and GSIR (Fig. 2-5h) were quenched in the presence of VDCC inhibitors. VDCC inhibition leading to reduced cytoplasmic Ca^{2+} influx and GSIR is in agreement with established literature (Gromada et al., 1996; Vadakekalam et al., 1996). Overall, our data suggests an accentuating role for PLC-derived IP_3 in glucose stimulated GSIR. PLD2, by downregulating CAR8, increases VDCC-dependent intracellular Ca^{2+} and insulin release upon glucose stimulation.

Discussion

PLD1 and PLD2 have been described as facilitators of secretagogue- stimulated insulin release (Hughes et al., 2004; Lee et al., 2008a; Lee et al., 2008b). Thus far, the role of PLD in glucose-stimulated insulin release (GSIR) has not been described. Pancreatic β-cells and insulinoma cell lines are exocytosis models that can yield insight into the pathophysiology of diabetes. In pancreatic β-cells, PLD1 and PLD2 are expressed (Laine et al., 2000) and generate PA from PC (Hughes et al., 2004; Lee et al., 2008b). I found that PLD2$^{-/-}$ mice had lower random and fasting serum glucose. When challenged with i.p glucose, there was a blunted rise in serum glucose in PLD2$^{-/-}$ mice compared to WT animals. This suggested a hyper-insulinemic phenotype that was subsequently confirmed by direct stimulation of pancreatic islets with glucose. This was surprising because attenuation of PLD2 activity has been shown to inhibit secretagogue-stimulated insulin release (Lee et al., 2008b) and hexoseaminidase secretion in mast cells (Choi et al., 2002). RNAi inhibition of PLD2 in NIT-1 cell-lines also led to an increase in GSIR suggesting that increased insulin secretion was an acute (48 hour RNAi silencing) and reproducible phenotype. Importantly, these earlier studies focused on secretagogues, which utilize a distinct mechanism from glucose stimulation (Cheng et al., 2007; Liu et al., 2008; MacDonald, 2007). Additionally, use of 1-butanol and over-expression of a catalytically-inactive mutant PLD allele as a dominant negative isoform in these studies may have masked the true role of PLD2 by inhibiting both PLD isoforms and /or inducing off-target effects through sequestering PLD2-interacting proteins and lipids. My data suggest that the increased GSIR may be a direct result of dysregulated Ca^{2+} homeostasis. This is not surprising because tight regulation of intracellular (ER)-stored

Ca^{2+} is important for maintaining membrane potential in beta cells (Worley et al., 1994). Failure to maintain a hyperpolarized membrane in our PLD2 KO islets might lead to inappropriate or premature membrane depolarization, increased Ca^{2+} influx and insulin release. Microarray data from isolated $PLD2^{-/-}$ islets has led to an interesting novel target that may yield further insight into the mechanism of increased GSIR in $PLD2^{-/-}$ islets. Car8 (CARP) is an IP_3R inhibitor (Hirota et al., 2003) that was down-regulated in our microarray screen. Expression of CAR8 in PLD2-silenced cells reduced insulin secretion and intracellular Ca^{2+} to WT levels. This is consistent with the reduction of $^{i}Ca^{2+}$ and insulin secretion in PLD2 knockdown cells when treated with PLC and IP_3 inhibitors. PLC is known to be activated upon high glucose treatment via Ca^{2+}-induced Ca^{2+} release (CICR) (Gromada et al., 1996; Vadakekalam et al., 1996; Vadakekalam et al., 1997). This would partly explain the effect of PLC inhibition on high-glucose stimulated insulin release but not on low-glucose stimulation. Inhibition of L-type VDCC abolished most of the intracellular Ca^{2+} and insulin release in both PLD2 silenced and control cells, suggesting that PLD2 exacerbation of Ca^{2+} influx and insulin release is upstream of the VDCC opening. This data agrees with published literature by Gromada *et al* (1996) and Vadakekalam *et al* (1996) (Gromada et al., 1996; Vadakekalam et al., 1996) describing PLC activation and IP_3 generation downstream of K^+ channel closure and membrane depolarization. Ablation of PLD2 might be increasing sensitivity to glucose-stimulated IP_3 generation (via CAR8 downregulation) leading to a greater increase in Ca^{2+} influx and insulin secretion. The key question that remains unanswered is the mechanism by which PLD2 regulates CAR8.

Figure 2-1. PLD2$^{-/-}$ mice exhibit lower random and fasting glucose, enhanced GTT and increased GSIR. (a). Serum glucose were taken at 3 time points during the day for 3 consecutive days from matched WT and PLD2$^{-/-}$ mice (n=4 mice from each group. *, $p < 0.03$). (b). Serum glucose measurements were taken from matched WT and PLD2$^{-/-}$ animals fasted overnight (n=4 mice from each group. * $p < 0.01$. Experiment repeated 3 times). (c). WT and PLD2$^{-/-}$ mice were injected i.p with 1g/kg of 25% glucose. Serum glucose was subsequently measured over plotted time course. (n=2 mice from each group. Experiment repeated 3times.*, $p < 0.03$, student's *t*-test). (d). Insulin tolerance test performed on matched WT and PLD2$^{-/-}$ mice. (n = 2 mice per group, experiment repeated 2 times) (e) 10 islets isolated each from WT and PLD2$^{-/-}$ mice were stimulated with 2.5 mM (basal) and 20 mM (stimulated) glucose and secreted glucose measured. (*, $p < 0.03$. Representative of 10 sets of experiments performed over 3 days, n= 100 islets).

Figure 2-1

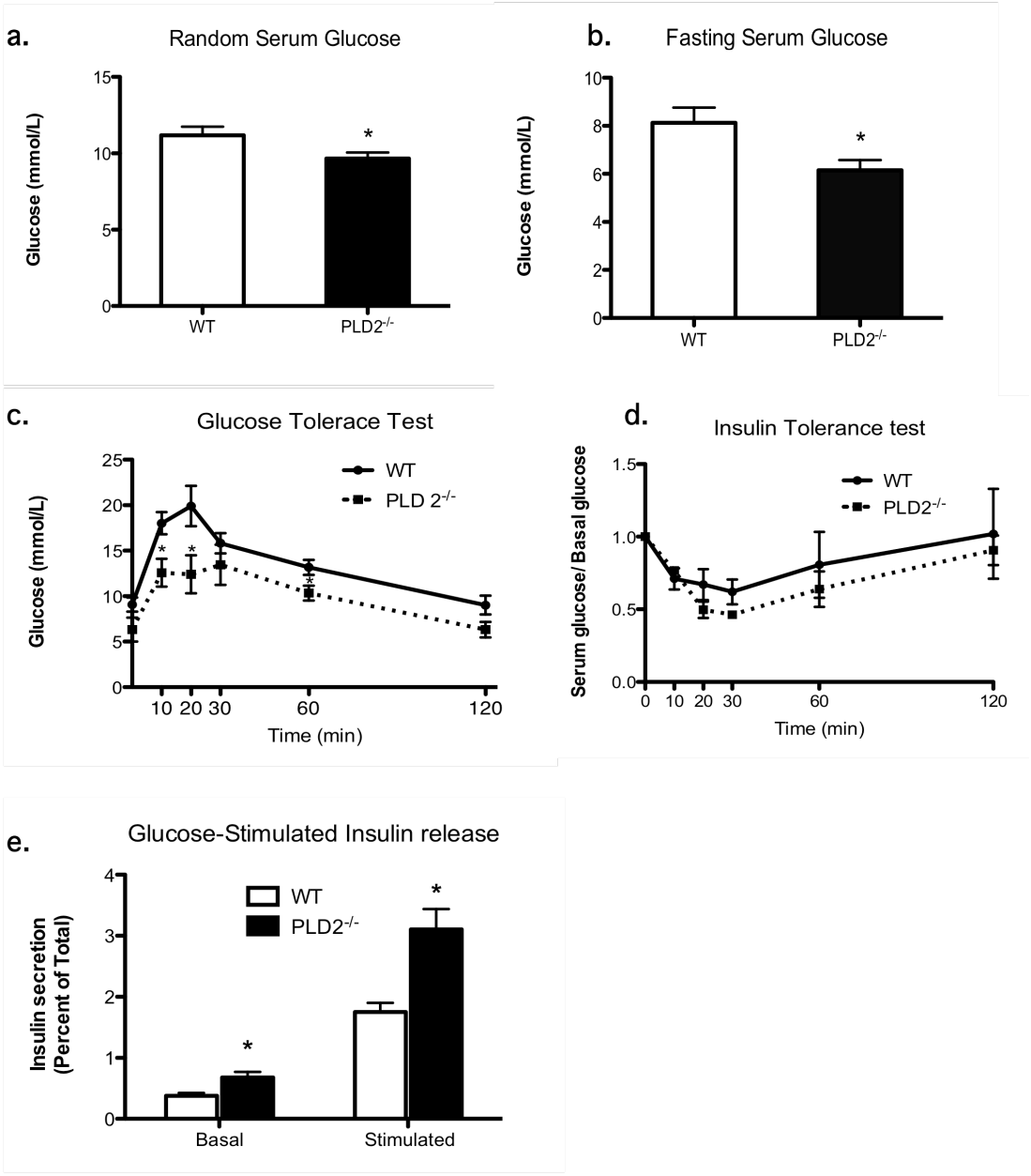
a.
Random Serum Glucose
Glucose (mmol/L)
15
10
5
0
*
WT
PLD2-/-
b.
Fasting Serum Glucose
Glucose (mmol/L)
10
8
6
4
2
0
*
WT
PLD2-/-
c.
Glucose Tolerace Test
Glucose (mmol/L)
25
20
15
10
5
0
WT
PLD 2-/-
* *
10 20 30
60
120
Time (min)
d.
Insulin Tolerance test
Serum glucose/ Basal glucose
1.5
1.0
0.5
0.0
WT
PLD2-/-
0 10 20 30
60
120
Time (min)
e.
Glucose-Stimulated Insulin release
Insulin secretion (Percent of Total)
4
3
2
1
0
WT
PLD2-/-
*
*
Basal
Stimulated

Figure 2-2. PLD2$^{-/-}$ islets are morphologically similar to WT and do not contain more insulin. (a). Pancreatic tissue from WT and PLD2$^{-/-}$ mice were fixed, embedded and stained with H&E. Islets of beta cells are indicated in text and exocrine acinar cells are also labeled (b). EM images of WT and PLD2$^{-/-}$ islets. Dense black dots in the cytoplasm represent insulin granules (white arrow). Nucleus is marked as "N" (c). WT and PLD2$^{-/-}$ pancreatic tissue were fixed and stained with anti-insulin antibodies. Islets shown. Endocrine Islets and exocrine acinar cells are marked (d). Total insulin was extracted (see methods) from WT and PLD2$^{-/-}$ islets and measured by ELISA (Experiment repeated 3 times, 10 islets per group per experiment total islets: WT; n = 200 islets. PLD2$^{-/-}$; n = 170 islets.).

Figure 2-2

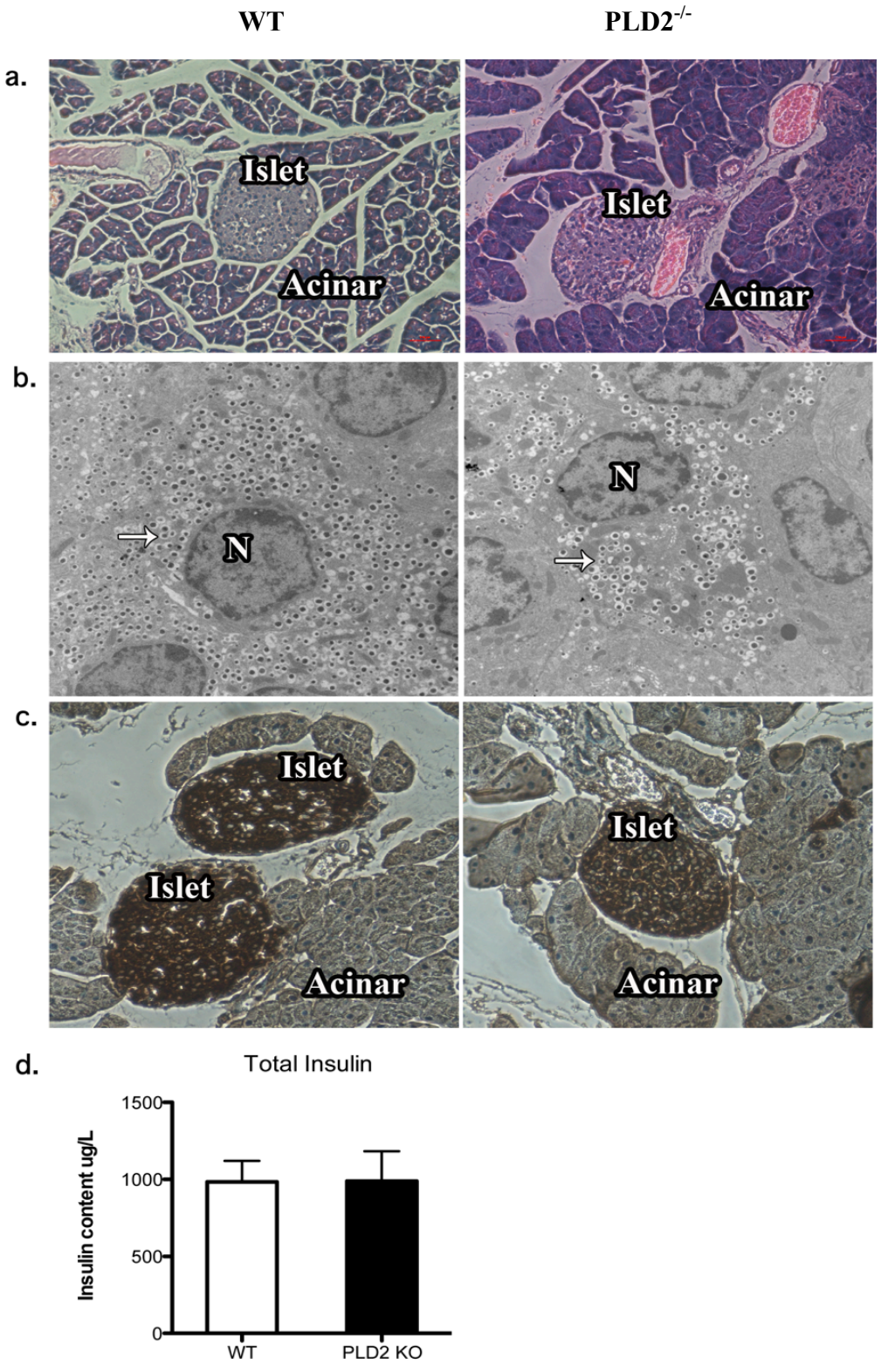
WT
PLD2-/-
a.
Islet
Acinar
Islet
Acinar
b.
N
N
c.
Islet
Islet
Acinar
Islet
Acinar
d.
Total Insulin
Insulin content ug/L
1500
1000
500
0
WT
PLD2 KO

Figure 2-3. RNAi–silencing of PLD2 in NIT-1 cells leads to increased GSIR Cultured NIT-1 cells were transfected with PLD2 RNAi and stimulated with 2.5 mM and 20 mM glucose 48 hours later ($n = 4$ *, $p < 0.03$. Experiment repeated twice). Secreted insulin was collected and quantified by ELISA. NIT-1 cells were transfected for 48 hours with either luciferase RNAi or PLD2 RNAi. 100 ng of total RNA isolated from the transfected cells was subjected to RT-PCR (see materials and methods).

Figure 2-3

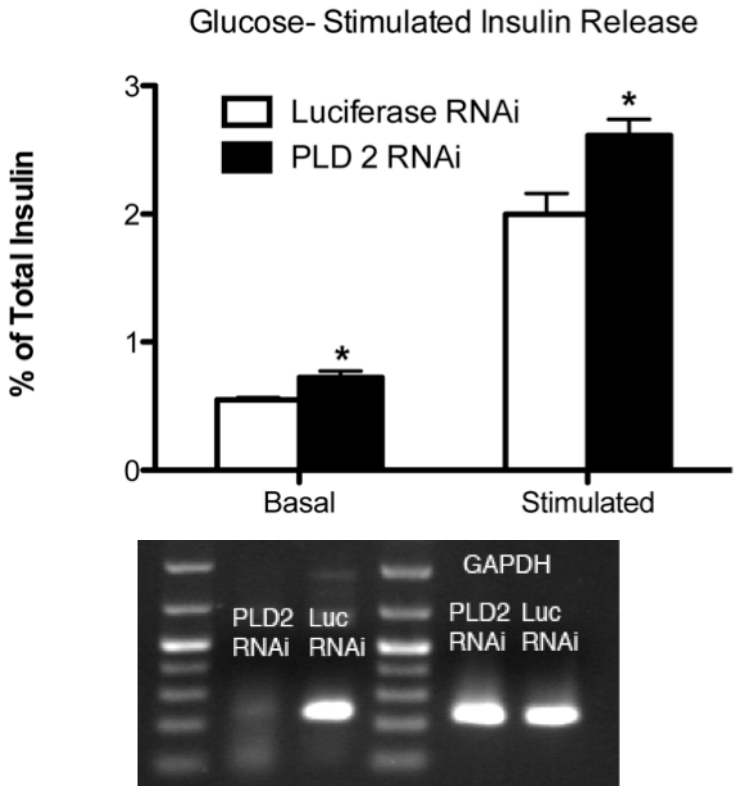
Glucose- Stimulated Insulin Release
% of Total Insulin
3
2
1
0
Luciferase RNAi
PLD 2 RNAi
*
*
Basal
Stimulated
GAPDH
PLD2 RNAi
Luc RNAi
PLD2 RNAi
Luc RNAi

Figure 2-4. Microarray analysis of WT and PLD 2$^{-/-}$ primary islets. WT and PLD2$^{-/-}$ islets were dissected and subjected to microarray analysis. Islets were pooled from two mice for each group and paired. A total of 4 groups (n=4, 8 animals for each genotype), were used (*, $p < 0.05$). Hits column represents number of times a candidate appears in our screen.

Figure 2-4

Hits	Sequence name	Sequence description	Fold change
4	Pitpnm3	PITPNM family member 3	**-5.2**
4	Mid1	Midline 1; E3 ubiquitin ligase; TRIM family member	-4.9
4	Car8	Carbonic anhydrase related protein 8	-4.6
4	Xaf1	XIAP associated factor 1	-3.6
4	Cap1	CAP, adenylate cyclase-associated protein 1	2.4
4	Cftr	Cystic fibrosis transmembrane conductance regulator homolog	2.4
4	Abcb1b	ATP-binding cassette, sub-family B (MDR/TAP), member 1B	3.1
4	Cap1	CAP, adenylate cyclase-associated protein 1 (yeast)	2.4
4	Ptprz1	Protein tyrosine phosphatase, receptor type Z, polypeptide 1	4.3
4	Inpp4b	Inositol polyphosphate-4-phosphatase, type II	3.9
3	Kcna1	Potassium voltage-gated channel, shaker-related subfamily, member 1	-3.1
3	Inpp4b	Inositol polyphosphate-4-phosphatase, type II	3.8
3	Ppp1r3a	Protein phosphatase 1, regulatory (inhibitor) subunit 3A	27.1
3	Pou5f1	POU domain, class 5, transcription factor 1	33.1
2	Pde3a	Phosphodiesterase 3A, cGMP inhibited	-2.9
2	Golim4	Golgi integral membrane protein 4	-2.5
2	Rab5b	RAB5B, member RAS oncogene family	-2.4
2	Kcna6	Potassium voltage-gated channel, shaker-related,	-2.4

		subfamily, member 6	
2	Scfd1	Sec1 family domain containing 1	-2.3
2	Sh3gl3	SH3-domain GRB2-like 3	-2.3
2	Hps1	Hermansky-Pudlak syndrome 1 homolog (human)	-2.1
2	Rnd1	Rho family GTPase 1	2.3
2	Mdr	Mus musculus multidrug resistant protein (Mdr) mRNA, partial cds.	2.3
2	Plcxd1	Phosphatidylinositol-specific phospholipase C, X domain containing 1	2.5
2	Rab38	Rab38, member of RAS oncogene family	2.9
2	Pik3cg	Phosphoinositide-3-kinase, catalytic, gamma polypeptide	4.8
2	Rabl3	RAB, member of RAS oncogene family-like 3	5.2
2	Ap1m2	Adaptor protein complex AP-1, mu 2 subunit	10.4
2	Grm1	Glutamate receptor, metabotropic 1	16.9

Figure 2.5. PLD2 knockdown cells show increased intracellular Ca^{2+} upon stimulation. (a) Luc and PLD2-silenced cells were loaded with Fluo-4 Ca^{2+} dye in 2.5 mM glucose for 45 min. Baseline fluorescence was recorded and then the cells were stimulated with 20mM glucose for 10 min. Fold-increase in Ca^{2+} is shown ($n = 5$ *, $p < 0.003$. (b). PLD2 RNAi and CAR8 cotransfected cells were stimulated with low and high glucose and secreted insulin levels were measured ($n = 4$ *, $p < 0.05$). (c). NIT-1 cells were cotransfected 1:1 with PLD2 RNAi and CAR8. 48 hours later, cells were loaded with Fluo-4 and intracellular Ca^{2+} measured ($n = 7$ *, $p < 0.05$). (d). Cultured NIT-1 cells were transfected with Luciferase RNAi or PLD2 RNAi and treated with 1 μM Xestospongin or 10 μM U-73122 for 60 min before being stimulated with 2.5 mM or 20 mM glucose for another 60 min in the presence of the drug (see materials and methods for details). Secreted insulin was measured and shown ($n = 4$ *, $p < 0.05$). (e). Luciferase RNAi or PLD2 RNAi transfected cells were treated with 1 μM Xestospongin or 10 μM U-73122 and loaded with fluo-4 and intracellular Ca^{2+} was measured ($n = 4$ *, $p < 0.05$). (f). Luciferase RNAi transfected or PLD2 RNAi transfected cells were loaded with Fluo-4 in the presence of thapsigargin for 60 min and then stimulated with 20 mM glucose for 10 min. (g). Control and PLD2 silenced cells were treated with 2 different L-type VDCC inhibitors (Nifedipine: 10 μM, Diltiazem: 50 μM) for 60 min and intracellular Ca^{2+} was measured ($n = 6$ *, $p < 0.05$). (h). Same drug treatments as (g) but secreted insulin in response to glucose stimulation was measured. ($n = 4$ *, $p < 0.05$).

Figure 2-5

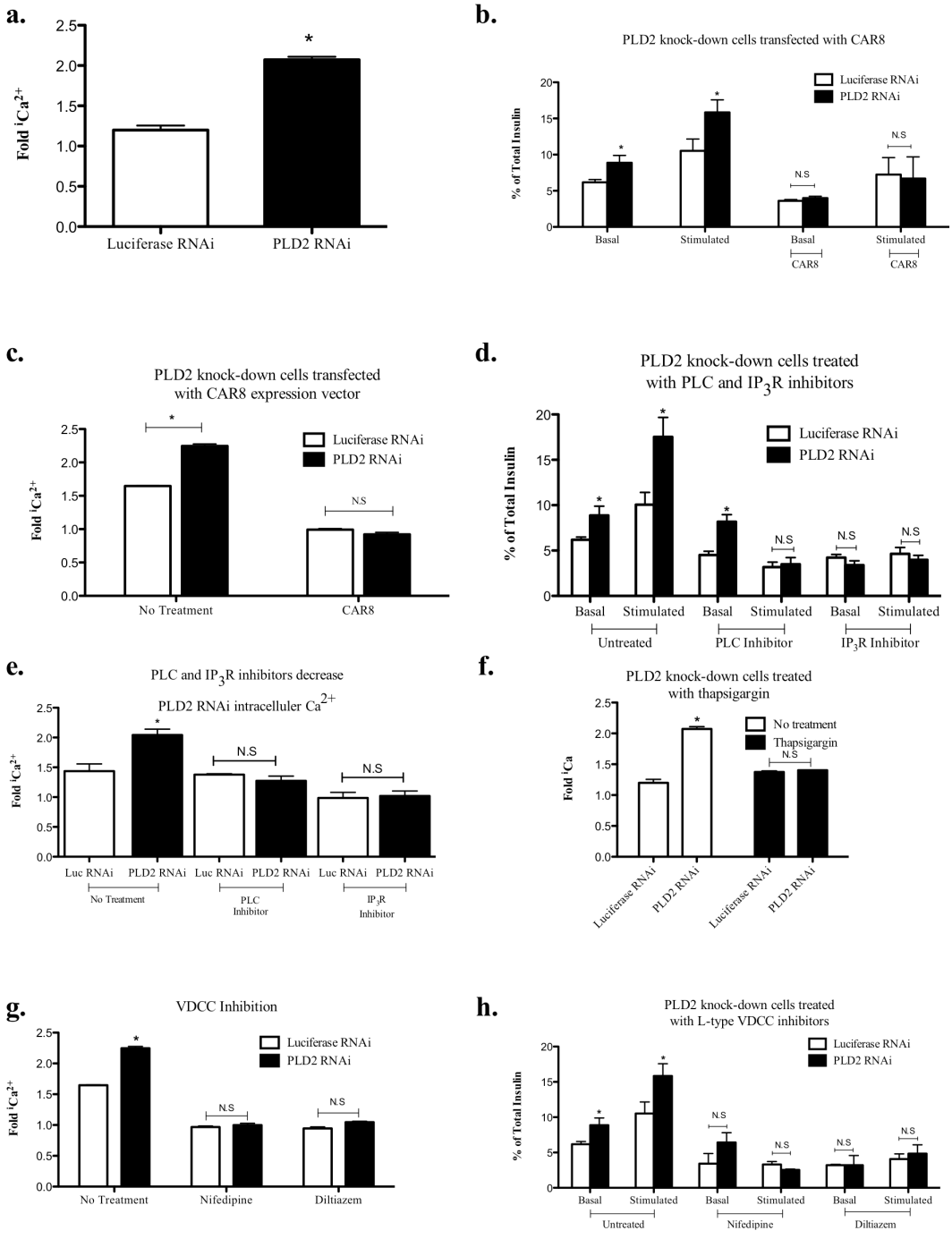
a.
Fold $^{i}Ca^{2+}$
Luciferase RNAi
PLD2 RNAi
b.
PLD2 knock-down cells transfected with CAR8
% of Total Insulin
Luciferase RNAi
PLD2 RNAi
Basal
Stimulated
Basal
CAR8
Stimulated
CAR8
N.S
c.
PLD2 knock-down cells transfected
with CAR8 expression vector
Fold $^{i}Ca^{2+}$
Luciferase RNAi
PLD2 RNAi
No Treatment
CAR8
d.
PLD2 knock-down cells treated
with PLC and IP_3R inhibitors
% of Total Insulin
Luciferase RNAi
PLD2 RNAi
Untreated
PLC Inhibitor
IP_3R Inhibitor
e.
PLC and IP_3R inhibitors decrease
PLD2 RNAi intracelluler Ca^{2+}
Fold $^{i}Ca^{2+}$
Luc RNAi
PLD2 RNAi
No Treatment
PLC Inhibitor
IP_3R Inhibitor
f.
PLD2 knock-down cells treated
with thapsigargin
Fold ^{i}Ca
No treatment
Thapsigargin
Luciferase RNAi
PLD2 RNAi
g.
VDCC Inhibition
Fold $^{i}Ca^{2+}$
Luciferase RNAi
PLD2 RNAi
No Treatment
Nifedipine
Diltiazem
h.
PLD2 knock-down cells treated
with L-type VDCC inhibitors
% of Total Insulin
Luciferase RNAi
PLD2 RNAi
Untreated
Nifedipine
Diltiazem

Chapter 3

The role of PLD2 in golgi architecture maintenance

Insulin synthesized in the ER is trafficked to the *cis*-golgi and subsequently to the *trans*-golgi and the plasma membrane. PLD1 associates with the ER, recruits Sar1p and facilitates COPII-mediated anterograde trafficking to the *cis*-golgi (Pathre et al., 2003). PLD1 activity stimulates vesicle budding from the *trans*-golgi (Chen et al., 1997) and co-localizes with insulin vesicles destined for secretion (Hughes et al., 2004). However, as described below, a broad-based morphological characterization of islet cells in $PLD2^{-/-}$ mice revealed alterations in Golgi structure. Although PLD2 is best known for being at the plasma membrane and affecting cell shape and endocytosis, there have been a few reports that proposed roles for PLD2 at the golgi. For example, golgi membrane tubulation experiments have suggested a role for PLD2 in vesicle scission and COPI-mediated retrograde transport (Yang et al., 2008), albeit these experiments utilized an *in vitro* reconstitution system that only model in part the complexity of an intact cell. Other experiments have shown that 1-butanol treatment of neuroendocrine cells leads to golgi membrane fragmentation and cessation of exocytosis (Siddhanta et al., 2000) but these experiments, like all 1-butanol experiments, cannot delineate between the role of PLD1 and PLD2. Additionally, caution is advised in the interpretation of experiments using 1-butanol because of its potential off-target effects (Su et al., 2009). The role of PLD2-generated PA in golgi architecture maintenance has yet to be determined *in vivo*. To this end, I set out to delineate the role of PLD2 in golgi-architecture maintenance.

Materials and Methods.

Antibodies, inhibitors and general reagents

cis-golgi antibody GM-130, *cis*/mid golgi antibody Giantin and *Trans*-golgi antibody TGN38 were purchased from ABCAM. IP_3 receptor antibody was purchased from Thermo scientific. PMA was purchased from Sigma. Mouse and Rabbit Alexia fluorescently conjugated secondary antibodies and rhodamine-conjugated phalloiden were purchased from Invitrogen. FIPI, a pan-PLD1/PLD2 inhibitor was prepared as described previously (Su et al., 2009) and isoform-specific PLD inhibitors purchased from Cayman Chemicals.

Immunocytochemistry and Immunohistochemistry

Dispersed β-cells were seeded on poly-L-lysine coated coverslips for 48 hrs. Cells were fixed in 4% paraformaldehyde for 10 min and rinsed with room temperature PBS. Cells were then permeabilized with 0.1% triton X-100 for 10 min. After rinsing with PBS, cells were then probed with primary antibody for 60 min, followed by 60 min incubation with fluorescently-labeled secondary antibodies. The same protocol was used for staining NIT-1 cells that had been transected with either Luc or PLD2 RNAi. For immunohistochemistry, 4 μm sections of WT and $PLD2^{-/-}$ paraffin-embedded pancreas were immunostained with the various primary antibodies as indicated followed by biotinylated secondary antibodies.

Electron Microscopy

WT and PLD2$^{-/-}$ islets were fixed in 2% paraformaldehyde/2% EM grade glutaraldehyde in 0.1 M phosphate buffer, pH 7.4 for 15 min, postfixed in 2% OsO4 in PBS for 1h, dehydrated, infiltrated and embedded in plastic resin. Ultrathin sections were cut on an Ultracut E ultramicrotome (Reichert-Jung), stained with uranyl acetate and lead citrate before examination with a FEI BioTwinG2 Transmission Electron Microscope (TEM)**.**

Inhibition of PITPNM3

PITPNM3 siRNA and control (Negative) oligos were purchased from Invitrogen. Oligo 1: 5'-UUUACUUAGCCUCCGUUCUGUGCGC-3', Oligo 3: 5'-AGAUCAUGCCCUGUGGGAAGUUGUG-3'. Knockdown was verified using RT-PCR with primers 5'-GTTCAGAGTCCTCGGACAGC-3' (forward) and 5'-CCAGACCAGTGCTCTCCTTC-3' (reverse). Knockdown efficiency was examined by RT-PCR. 1 cycle of cDNA synthesis was performed at 50° C for 30 min, followed by 94° C for 2 min. PCR amplification was performed for 35 cycles as follows; 94 ° C for 15 sec (denaturation), 55° C for 30 s(annealing) and 72° C for 1 min (extension). A final extension step was performed at 72° C for 10 min.

Overexpression of PLD1 and PLD2

NIT-1 cells seeded on coverslips were transfected with pCGN vectors expressing human PLD1 or mouse PLD2 for 48 hrs or the empty vector as control. The PLD1-expressing cells were stimulated with PMA for 60 min. Cells were fixed and stained with the indicated antibodies.

Golgi quantification

Golgi images were analyzed using image J software. For each cell, the Golgi highlighted and the fluorescence intensity threshold was set and "Area fraction" function was used. Cells were counted over the course of 3 independent experiments.

Statistical analysis

Student's *t*-test was performed and significance was set at $p < 0.05$ unless otherwise stated in individual figure legends.

Results

PLD2$^{-/-}$ islets show expanded *cis*-golgi morphology

In an effort to initially characterize the mechanism underlying GSIR in PLD2$^{-/-}$ islets (chapter 2), I performed immunohistochemical analysis of WT and PLD2$^{-/-}$ pancreatic tissue. Surprisingly, I found an intense and expanded staining of the *cis*-golgi architecture (Fig. 3-1a) using anti-GM130 antibodies. In both the endocrine (islet) and exocrine pancreas, the *cis*-golgi appeared longer and more tortuous. WT and PLD2$^{-/-}$ pancreatic islets were dissociated into β-cells and probed with a *cis*-golgi antibody (Fig. 3-1b). In WT β-cells, the *cis*-golgi structure was compact and peri-nuclear while in PLD2$^{-/-}$ β-cells, the *cis*-golgi appeared distended and, as quantitated, revealed a 2-fold expansion compared to WT β-cells (Fig. 3-1c). PLD2$^{-/-}$ islets examined by electron microscopy showed dilated structures that extended to the plasma membrane (Fig. 3-1d. plasma membrane in red, dilated structures are marked by blue asterisk) consistent with our immunohistochemical data. In order to examine the extent of the perturbation, the *trans*-golgi was examined using TGN 48 antibodies (not shown). The early endosomal marker EEA1 was also used to examine perturbations in endocytosis (not shown) and the lysosomal antibody LAMP1 was used the visualize lysosomes (not shown). Finally, membrane transferrin localization was examined using the anti-transferrin antibody (not shown). No differences were found in any of these trafficking events.

Transient inhibition of PLD2 leads to tubulated *cis*-golgi

Tubulated *cis*-golgi in PLD2$^{-/-}$ islets could be the result of long-term compensation in my primary β cells. To address this possibility, I transfected NIT-1 insulinoma cell lines

with PLD2 RNAi. Additionally, the NIT-1 cell line would permit experiments that would be difficult in primary cells (for example, transfection of plasmids). Knockdown of PLD2 led to a 2-fold expansion of the *cis*-golgi over Luciferase RNAi-transfected control cells (Fig. 3-2a,b). Probing the *cis*-golgi with another antibody that localizes to the *cis* and medial golgi also showed 2-fold tubulated golgi architecture (Fig. 3-2c,d). This independently confirms our finding of an expanded *cis*-golgi and it also suggests an expansion of the *cis*-golgi into the medial-golgi space. Examination of the *trans*-golgi did not show differences between control and PLD2 knockdown cells (Fig. 3-2e,f). I also did not find differences in the ER (Fig. 3-3a) or microtubule (Fig. 3-3b) morphology.

Micro-array analysis shows alterations in PC transport gene

Among the targets described in chapter 2, we focused on PITPNM3/ NIR1. Specifically, levels of membrane-associated Phosphatidyl Inositol Transfer protein (PITPNM3/ NIR1), a member of a large family of PI transfer proteins, were downregulated 5-fold (Fig. 2-4). Surprisingly, analysis of PITPNM3 showed that it had a c-terminus haloacid dehalogenase (HAD)- like domain similar to the Lipin HAD domain. The Lipin HAD domain converts PA to DAG, raising the possibility of this or a related enzymatic activity for PITPNM3.

Inhibition of PITPNM3 leads to tubulated *cis*-golgi

PITPNM3 is a transmembrane protein containing a Lipin-like HAD domain (unpublished) without the N-terminal PC sensing domain of other PITP family members (Lev et al., 1999). First, I wanted to test if PITPNM3 was downstream of PLD2

knockdown as suggested by my microarray analysis. Silencing of PITPNM3 using 2 different oligos in NIT-1 cells showed a 2.3-fold (Oligo 1) and 2.2-fold (Oligo 3) expansion of the *cis*-golgi (Fig. 3-4a,b). This suggested that knockout of PLD2 leads to downregulation of PITPNM3, which subsequently leads to tubulation of the *cis*-golgi. PLD2 KO islets and PLD2-silenced NIT-1 cells also showed increased GSIR in addition to tubulated *cis*-golgi. In the previous chapter, I found increased GSIR as a consequence of PLD2 knockdown and decided to investigate if PITPNM3 had any role in this. To test the hypothesis that PITPNM3 also played a role in GSIR, I silenced PITPNM3 in NIT-1 cells and stimulated the cells *in vitro* with low and high glucose levels. No differences were observed in GSIR between the control and PITPNM3 silenced cells (Fig. 3-4c), suggesting that *cis*-golgi tubulation and GSIR are separable consequences of PLD2 ablation.

PLD overexpression leads to tubulated *cis*-golgi

PLD2 generates PA and proteins with PAP domains metabolize PA to DAG (Reue and Brindley, 2008). I became interested in the idea that conversion of PA to DAG not only served to terminate PA action, but the product, DAG, was necessary for continuation of the vesicle budding process. DAG has already been shown to play an important role in vesicle fission from the *trans*-golgi (Baron and Malhotra, 2002; Diaz Anel, 2007; Guo et al., 2007), and Yang *et al* reported increased DAG levels on the *cis*-golgi (Yang et al., 2008). To test the hypothesis that PA alone is not enough to promote fission, I transfected NIT-1 cells with constructs overexpressing PLD1 and PLD2. To my surprise, overexpression of PLD2 led to a 3.4-fold tubulation of the *cis*-golgi (Fig. 3-5a,b) without

any changes to the *trans*-golgi (not shown). PLD1 has very low basal activity (1.3-fold tubulation) and was stimulated with PMA and that lead to a 3.7-fold *cis*-golgi tubulation. I did not see significant tubulation in control cells transfected with the empty vector or cells transfected with PLD1 without PMA stimulation.

Overexpression of PITPNM3 rescues PLD2 knockdown tubulation phenotype.

Next, I examined if expression of PITPNM3 would decrease tubulation in PLD2-silenced cells. To do this, I constructed C-terminal fused PITPNM3-GFP plasmid and a HAD-domain mutant PITPNM3-mut-GFP. The mutation was performed in the HAD consensus sequence among all 3 PITPNM3 family members. This mutant contains an alanine in place of an aspartic acid (SI**D**GS was mutated to SI**A**GS). In the yeast homolog of lipin, PAH1p, mutations in the aspartic acid residue in the HAD domain abolished phosphatase activity by 99% (Han et al., 2007). Hence, we rationalized that mutation of the aspartic acid residue in the HAD domain of PITPNM3 would also abolish any catalytic activity it might have. Both constructs were expressed in NIT-1 cells, and they both displayed cytoplasmic localization (Fig. 3-6a). Neither construct had any appreciable effect on golgi morphology (Fig. 3-6a,b). I then co-expressed PLD2 RNAi and PITPNM3/mut for 48 hours in NIT-1 cells and reexamined the *cis*-golgi. I found *cis*-golgi tubulation in PLD2 silenced cells expressing PITPNM3 mutant but normal *cis*-golgi in PLD2-silenced cells expressing WT PITPNM3. This result suggests that PITPNM3 has enzymatic activity because expression of the protein rescues the PLD2 knockdown phenotype while the mutant PITPNM3 does not. The nature of this enzymatic activity is currently unknown. The implication that both generation of PA and the subsequent conversion of

PA to DAG (by PITPNM3) are required for proper golgi architecture maintenance is attractive but this speculation remains to be proven.

Discussion

Cis-golgi tubulation in PLD2$^{-/-}$ cells was an unexpected finding. Germline deletion and RNAi-mediated silencing of PLD2 led to a 2-fold expansion of the golgi membrane. Earlier studies had indicated PLD2 localization to the golgi apparatus (Freyberg et al., 2002) and PLD2-generated PA has been shown to be required for COPI-mediated budding and vesicle scission (Yang et al., 2008). Complete abolishment of PLD activity leads to golgi-membrane fragmentation and cessation of exocytosis (Chen et al., 1997; Freyberg et al., 2003; Siddhanta et al., 2000). Microarray analysis of PLD2$^{-/-}$ islets led to the identification of PITPNM3, a member of a family of PI transfer proteins (Bankaitis et al., 2005). PITP proteins are known as Sec14p in yeast and have been found to be essential for golgi secretory activity and cell viability (Bankaitis et al., 1989; Novick et al., 1980). Sec14p bypass mutants were found to be proteins that caused decreased PC biosynthesis or increased PC metabolism to other lipids. Specifically, PLD activity was also critical for Sec14p bypass (Li et al., 2000; Sreenivas et al., 1998; Xie et al., 1998). Presumably, PLD activity is required to consume some of the PC by converting it to PA. When I downregulated PITPNM3 in NIT-1 cells, I saw a 2-fold expansion of the *cis*-golgi, consistent with what I saw in PLD2 knockout and knockdown cells. This would suggest that the activity of PLD2 on the *cis*-golgi involves more than just the generation of PA. The role of other lipid metabolizing enzymes in golgi architecture maintenance has been described (Bankaitis, 2009; Schmidt and Brown, 2009). Yang *et al* (2009) described increased production of DAG on the golgi membrane but this was described as a metabolic consequence of PA generation, i.e. PA generated on the golgi membrane is metabolized to DAG. When I increased the production of PA in

the cell by overexpressing PLD2 or stimulating PLD1 activity with PMA, I saw golgi tubulation. This phenotype is the same I observed with PLD2 knockdown, suggesting that PLD activity is only one aspect of *cis*-golgi membrane trafficking. Overexpression of PLD2 provides the prerequisite PA needed for the recruitment of membrane fission machinery. Based on this data, I speculate that failure to generate DAG at an equivalent level inhibits adequate fission (despite the production of PA).

Figure 3-1. PLD2$^{-/-}$ islets and β-cells show tubulated *cis*-golgi architecture. (a). Fixed WT and PLD2$^{-/-}$ pancreatic tissue was probed with anti-GM130 *cis*-golgi antibody. Endocrine islet and exocrine acinar cells are indicated. Inset shown represents enlarged cell (N: nucleus). Arrow points to *cis*-golgi (b) Primary β-cells from WT and PLD2$^{-/-}$ islets were stained with anti-GM130 and anti-insulin antibodies and imaged with a confocal microscope. (c). Golgi area from (b) quantified using area fraction analysis in Image J (see materials and methods). (n = 6 for 3 independent experiments. *, $p < 0.05$.) (d). Electron micrographs of WT and PLD2$^{-/-}$ islets. Each horizontal image is a magnification of the preceding panel. The red line corresponds to plasma membrane while the blue asterisks indicate golgi. (N: nucleus. I: insulin granule).

Figure 3-1

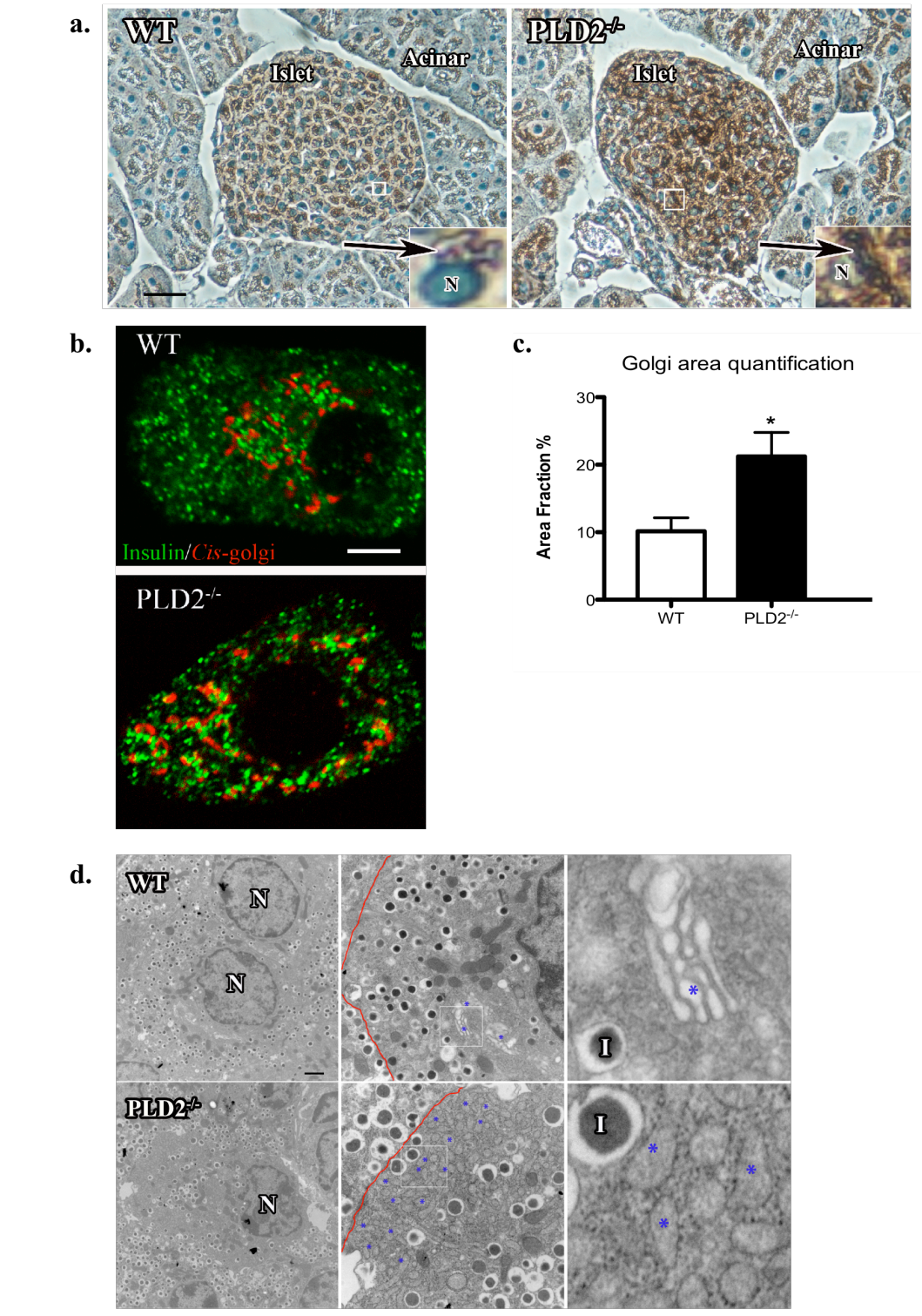
a.
WT
Islet
Acinar
N
PLD2-/-
Islet
Acinar
N
b.
WT
Insulin/Cis-golgi
PLD2-/-
c.
Golgi area quantification
Area Fraction %
30
20
10
0
*
WT
PLD2-/-
d.
WT
N
N
I
*
PLD2-/-
N
I
*
*
*

Figure 3-2. RNAi–silencing of PLD2 in NIT-1 cells leads to golgi tubulation. (a). Cultured NIT-1 cells were transfected with PLD2 RNAi and stained with anti-GM130 and anti-insulin antibodies 48 hours later. White arrow points to tubulated golgi. (b). Quantification of *cis*-golgi area from Fig. 3b (see materials and methods for quantification method) (*, $p < 0.0001$). (c). NIT-1 cells transfected with PLD2 RNAi for 48 hours was stained with anti-GM130 (*cis*-golgi) and anti- Giantin (*cis*/mid-golgi) antibodies. (d). Quantification of golgi area from Fig 3-2b ($n = 27$. *, $p < 0.003$). (e). Anti- TGN38 (*trans*-golgi) and phalloiden stains of NIT-1 cells transfected with PLD2 RNAi for 48 hours. (f). Quantification of *trans*-golgi. $n = 10$.

Figure 3-2

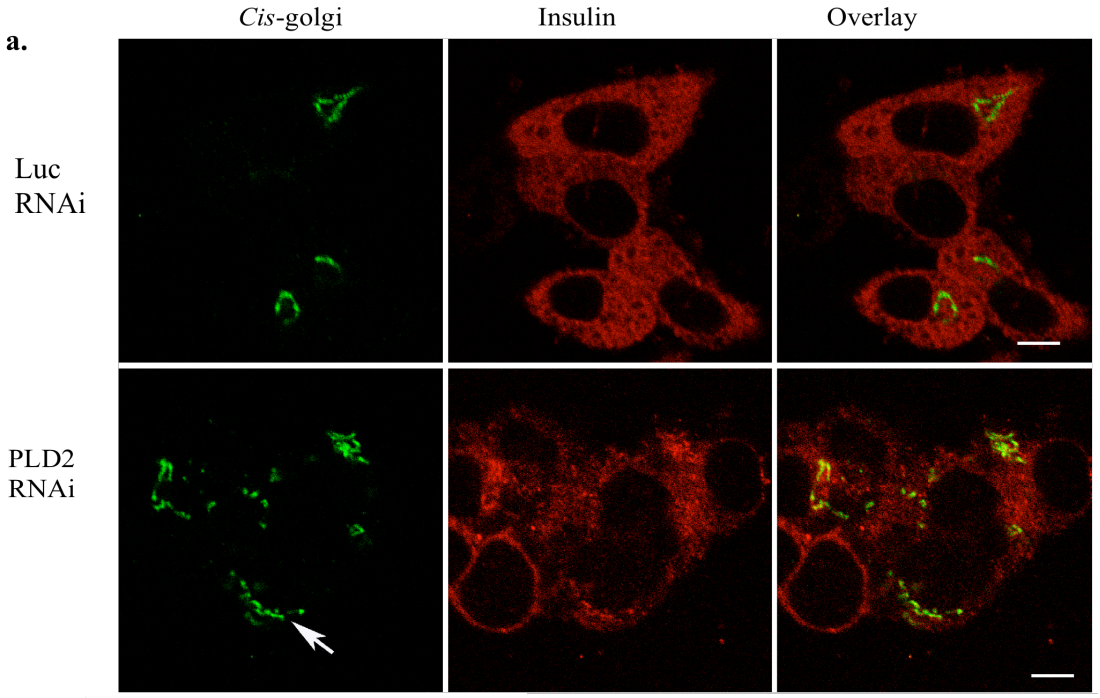
a.
Cis-golgi
Insulin
Overlay
Luc RNAi
PLD2 RNAi

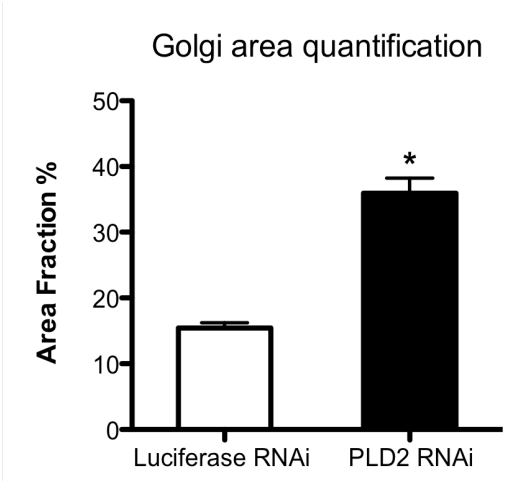
b.
Golgi area quantification
Area Fraction %
50
40
30
20
10
0
*
Luciferase RNAi
PLD2 RNAi

Figure 3-2

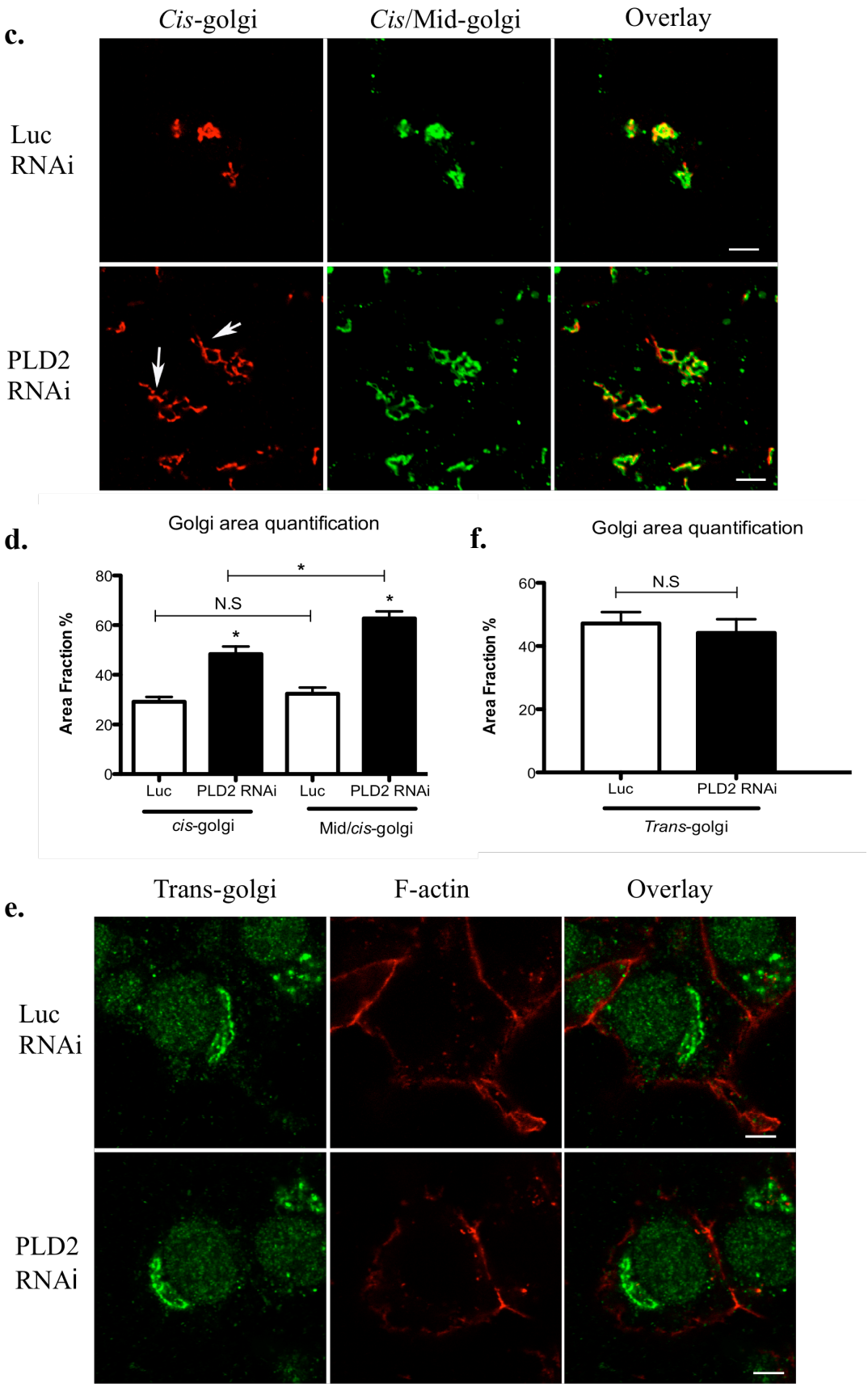
c.
Cis-golgi
Cis/Mid-golgi
Overlay
Luc RNAi
PLD2 RNAi
d.
Golgi area quantification
Area Fraction %
80
60
40
20
0
N.S
*
*
*
Luc
PLD2 RNAi
Luc
PLD2 RNAi
cis-golgi
Mid/*cis*-golgi
f.
Golgi area quantification
Area Fraction %
60
40
20
0
N.S
Luc
PLD2 RNAi
Trans-golgi
e.
Trans-golgi
F-actin
Overlay
Luc RNAi
PLD2 RNAi

Figure 3-3. PLD2 knockdown does not perturb ER or microtubular morphology. (a). PLD2-silenced NIT-1 cells were fixed (48-hours post transfection) and stained with the anti-KDEL ER marker and with phalloidin. (b). NIT-1 cells transfected with PLD2 or control luc RNAi for 48 hours were fixed and probed with an anti-tubulin antibodies and phalloidin.

Figure 3-3

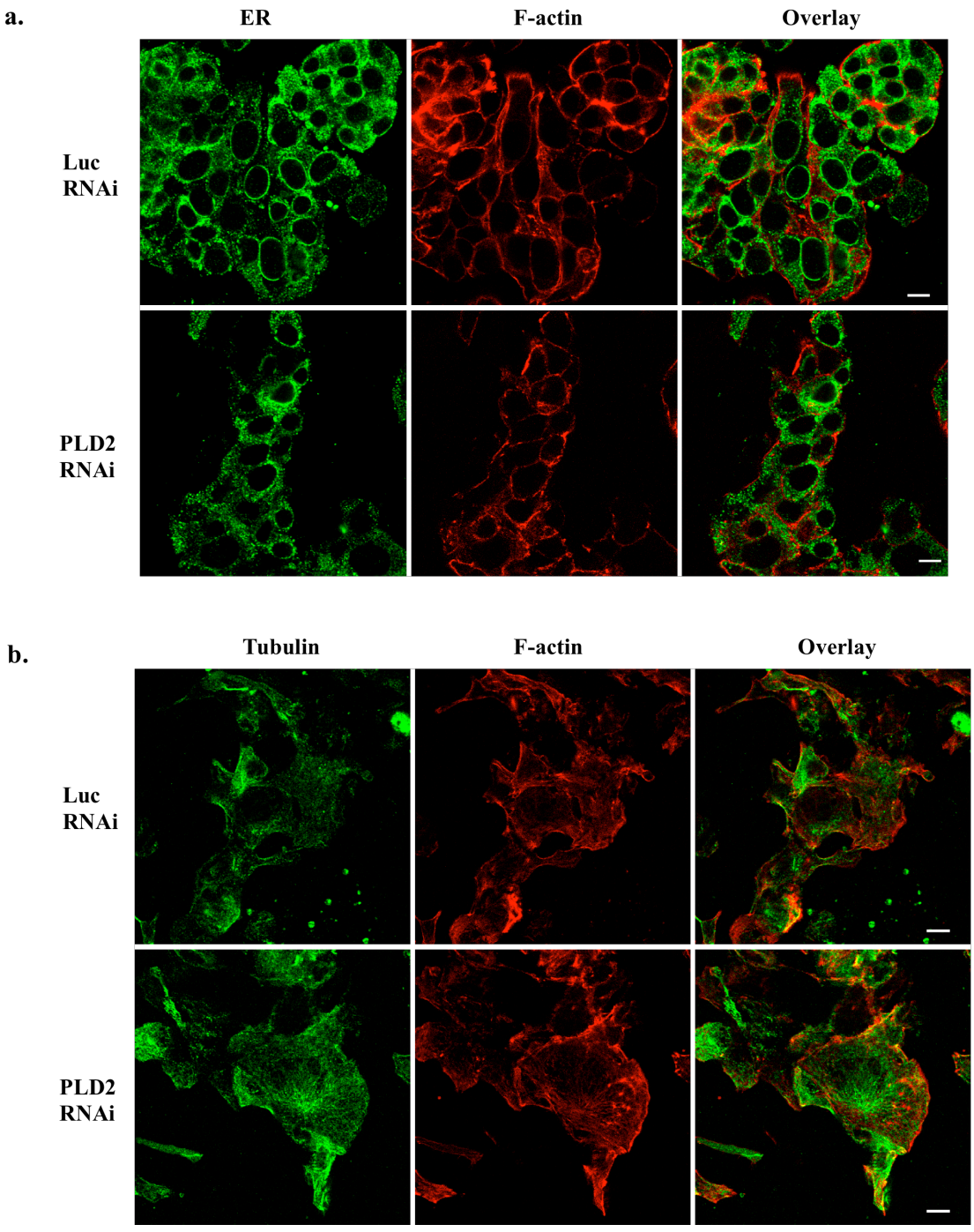
a.
ER
F-actin
Overlay
Luc RNAi
PLD2 RNAi
b.
Tubulin
F-actin
Overlay
Luc RNAi
PLD2 RNAi

Figure 3-4. PITPNM3 silencing leads to *cis*-golgi tubulation. (a) NIT-1 cells were treated with 50 nM of control or two different siRNA (O1 and O3) directed against PITPNM3. After 48 hrs, cells were fixed and stained with anti-GM130 and anti-insulin antibodies. White arrow points to tubulated golgi. (b). Quantification of golgi tubulation on PITPMN3-silenced cells (see methods for quantification methods) ($n = 15$. *, $p < 0.03$). Results are representative of 3 experiments. (c). Control and PITPMN3-silenced cells were stimulated with 2.5 mM and 20 mM glucose 48 hrs post-transfection and secreted insulin measured. $n = 5$. 100 ng of total RNA isolated from NIT-1 cells transfected with PITPNM3-silencing oligo1 and oligo3 was subjected to RT-PCR (see methods).

Figure 3-4

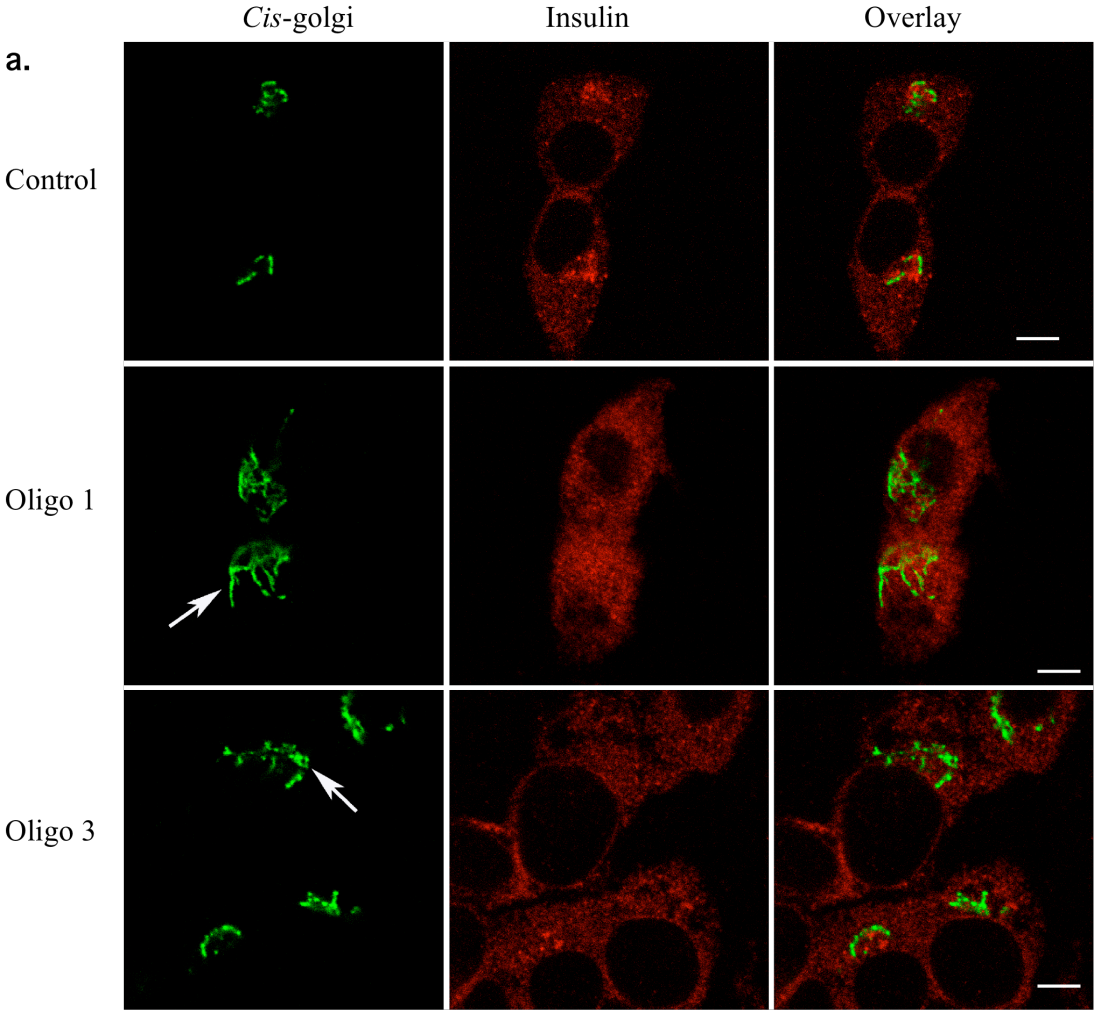
Cis-golgi
Insulin
Overlay
a.
Control
Oligo 1
Oligo 3

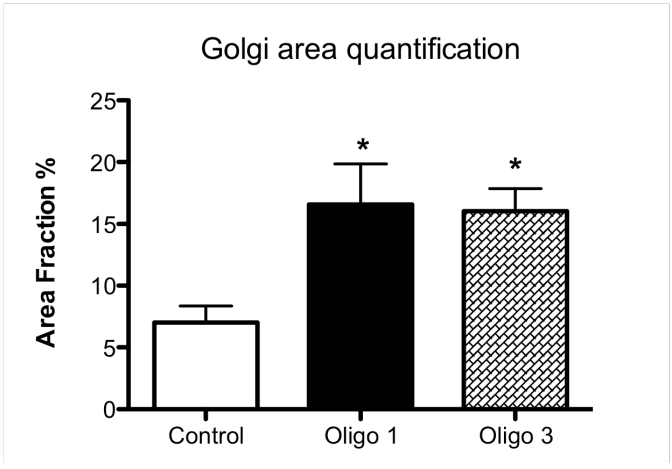
b.
Golgi area quantification
Area Fraction %
25
20
15
10
5
0
*
*
Control
Oligo 1
Oligo 3

Figure 3-4

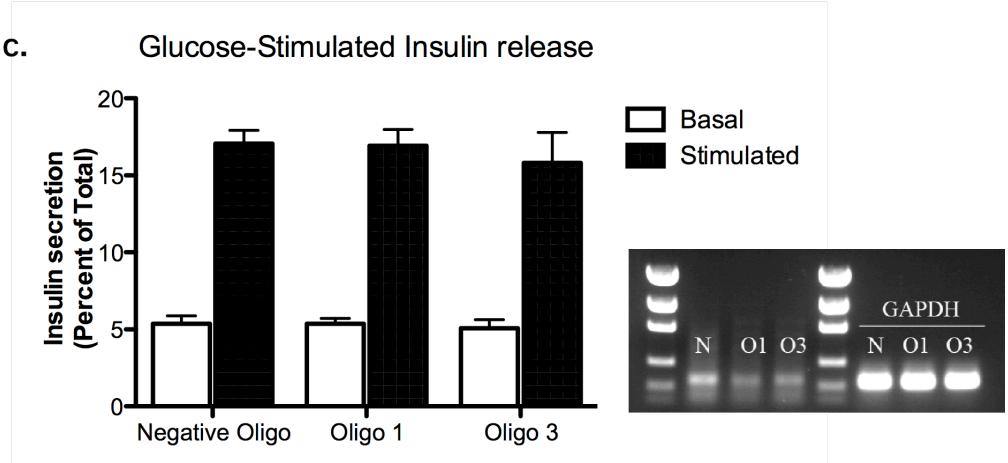
c.
Glucose-Stimulated Insulin release
Insulin secretion (Percent of Total)
20
15
10
5
0
Negative Oligo
Oligo 1
Oligo 3
Basal
Stimulated
GAPDH
N
O1
O3
N
O1
O3

Figure 3-5. PLD overexpression leads to tubulated *cis*-golgi.
(a). NIT-1 cells were transfected with PLD1 or PLD2 expression plasmids (or an empty vector control) for 48 hrs and stimulated with 100 ng/ml PMA for 1 hr. Cells were subsequently fixed and stained for *cis*-golgi and actin. White arrow points to tubulated golgi (b). Quantification of *cis*-golgi from (a). n = 29 .*, $p < 0.05$.

Figure 3-5

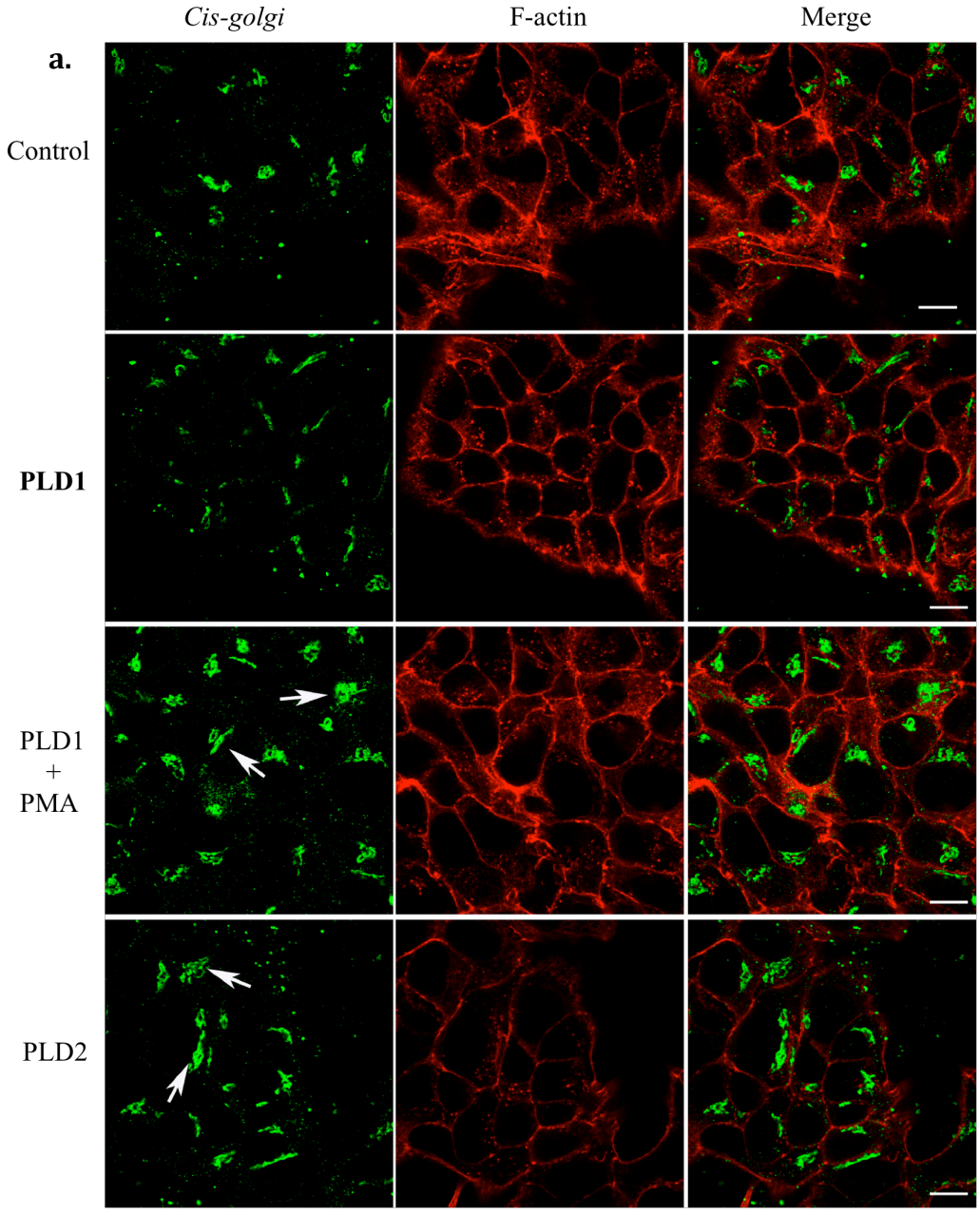
Cis-golgi
F-actin
Merge
a.
Control
PLD1
PLD1
+
PMA
PLD2

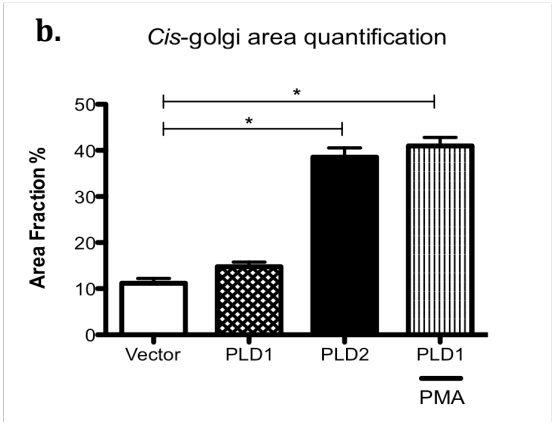
b.
Cis-golgi area quantification
Area Fraction %
50
40
30
20
10
0
*
*
Vector
PLD1
PLD2
PLD1
PMA

Figure 3-6. Overexpression of PITPNM3 rescues the PLD2 knockdown tubulation phenotype.
(a). NIT-1 insulinoma cells were transfected with PITPNM3-GFP, PITPNM3-mut-GFP, or PLD2 RNAi and PITPNM3-GFP/ mut at a 1:1 ratio and incubated for 48 hours. After the indicated time, the cells were fixed and stained for *cis*-golgi and actin. White asterisk indicates compact golgi in PITPNM3-GFP cells, white arrow points to tubulated golgi in PITPNM3-mut cell. (b). Quantification of *cis*-golgi for (a). $n = 14$. *, $p < 0.05$.

Figure 3-6

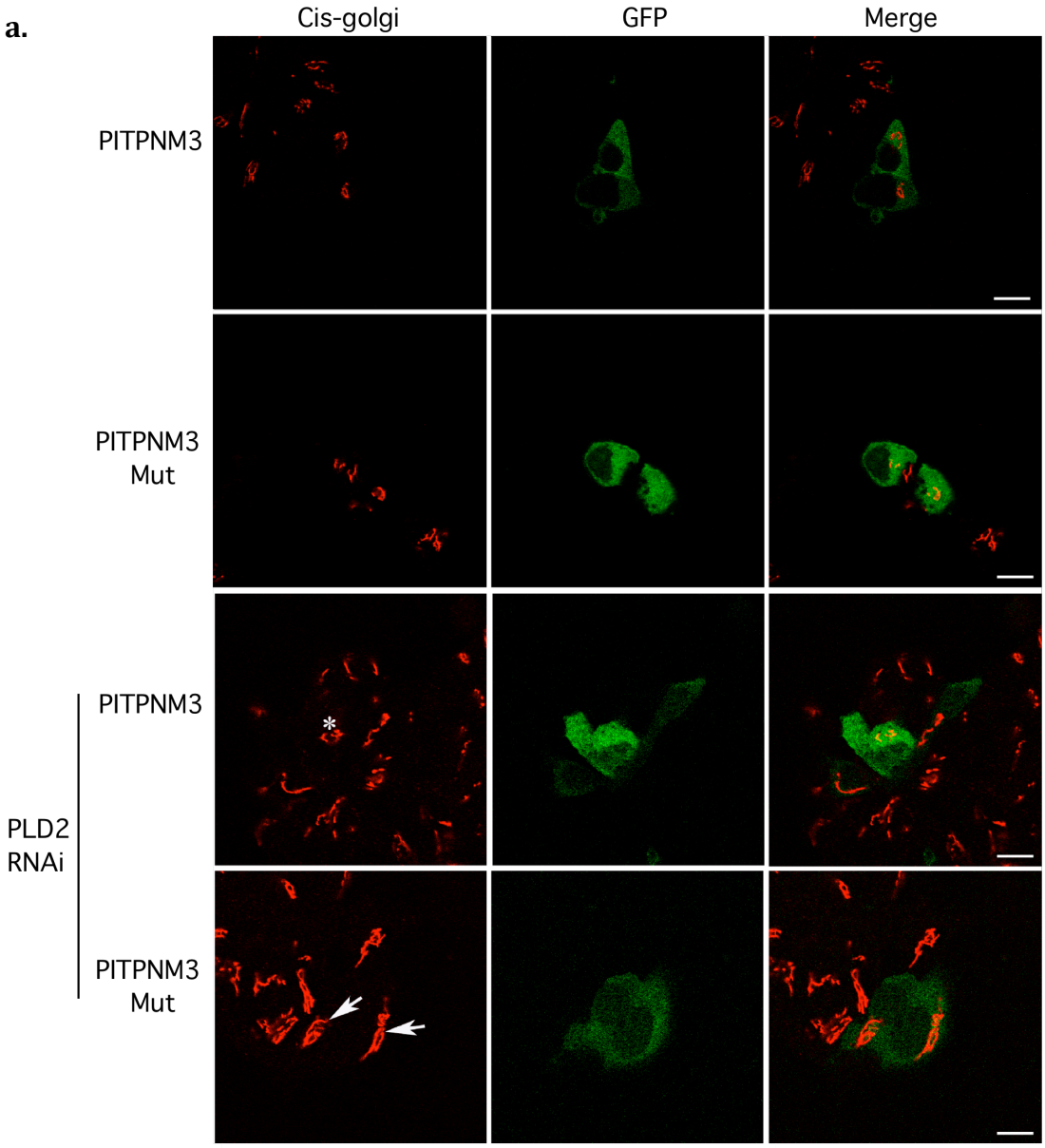
a.
Cis-golgi
GFP
Merge
PITPNM3
PITPNM3 Mut
PLD2 RNAi
PITPNM3
PITPNM3 Mut
b.
Golgi area quantification
Area Fraction %
80
60
40
20
0
N.S
N.S
*
*
PITP
Luc RNAi
PITP mut
PLD2 RNAi
PITP
PITP mut
PLD2 RNAi

Chapter 4

PLD1 and PLD2 play opposing roles in GSIR and Golgi architecture maintenance

Much of the work delineating the roles of PLD1 and PLD2 have relied on 1-butanol, a pan PLD inhibitor with potential off-target effects (Su et al., 2009). This has led to difficulty assigning individual roles to each isoform. In immune cells where PLD has been extensively studied, PA has been shown to be a chemoattractant (Frondorf et al., 2010) but the PLD isoform responsible for this PA generation was more difficult to pin down. Similarly, a role for PLD1 in phagocyte adhesion (Iyer et al., 2006) has also been identified but the function of PLD2 in this system was largely unaddressed. Overexpression studies identified a role for PLD2 in LPS-induced nitric oxide synthesis in macrophage cell lines (Park et al.). Cooperative roles for both PLD1 and PLD2 (Choi et al., 2002; Lehman et al., 2006) have been described in phagocyte migration and mast cell degranulation, respectively. In β-cells, PLD1 was shown to be critical for secretagogue-mediated insulin release (Hughes et al., 2004) but PLD2 was reportedly not expressed in the MIN6 cell line used for this study. Another study suggested a role for PLD2 in EGF (a secretagogue)-mediated insulin release in primary islets (Lee et al., 2008b). While independent and cooperative roles for PLD1 and PLD2 have been reported, antagonistic roles for both isoforms have yet to be documented. Earlier work from our lab replicated 1-butanol inhibition of GSIR in β-cells (Su et al., 2009) previously published by other groups (Hughes et al., 2004; Lee et al., 2008b). Surprisingly, treatment with FIPI (also a pan-PLD inhibitor) did not lead to significant changes in GSIR. This suggested to us that the PLD isoforms playing opposing roles in

β-cells, such that simultaneous inhibition of both isoforms leads to a lack of change in GSIR.

Materials and Methods

Antibodies, inhibitors and general reagents

cis-golgi antibody GM-130, and *Trans*-golgi antibody TGN38 were purchased from ABCAM. Mouse and rabbit alexia fluorescently conjugated secondary antibodies and rhodamine-conjugated Alexa phalloidin were purchased from Invitrogen. FIPI, a pan PLD inhibitor was developed by a collaborator and isoform-specific PLD inhibitors were purchased from Cayman Chemicals.

Intraperitoneal glucose tolerance test

8-12 week old male WT and PLD2$^{-/-}$ mice were weighed and injected with 1 mg/kg FIPI. The following morning, fasting serum glucose was measured from tail bleeds using a glucometer (One Touch) and then injected again with 1 mg/kg FIPI. 60 min later, the animals were injected i.p with 1 g/kg of 25% D-glucose. Tail blood was then collected at various time points for glucose measurement. WT and PLD2$^{-/-}$ mice were also injected with an equal volume of vehicle. Experiment was repeated 3 times for each condition.

Insulin secretion via static incubation

NIT-1 cells seeded overnight in 12- well plates were transfected with either luc RNAi or PLD2 RNAi for 48 hrs. Subsequently, all wells were incubated in 250 μL of KRBH buffer (KCl: 4.74 mmol/L, NaCl: 125 mmol/L, NaHCO3: 5 mmol/L, MgSO4: 1.2 mmol/L, CaCl2: 1 mmol/L, HEPES: 25 mmol/L, KH2PO4: 1.2 mmol/L, BSA: 0.10%) containing 2.5 mM D-glucose and ± 750 nM FIPI for 60 min at 37°C. Subsequently, the buffer was removed and fresh KRBH media containing 2.5 mM D-glucose and ± 750 nM

FIPI was added and placed at 37°C for 60 min. The buffer was collected, briefly centrifuged and the supernatant was collected as basal insulin secretion. For "stimulated" insulin secretion, the buffer was replaced with KRBH containing ± 750 nM FIPI and 20 mM glucose and incubated for 60 min at 37°C. The collected buffer was centrifuged and the supernatant preserved. All insulin-containing samples were placed on ice immediately after collection or stored at 20°C. To determine total insulin content, the islets were dissolved in 70% ethanol and 0.18 M HCl overnight, sonicated and centrifuged before samples were taken for ELISA measurements. ELISA measurements to determine basal, stimulated and total insulin concentrations were done with an ultrasensitive mouse insulin ELISA (Mercodia: 10115010) and BioRad plate reader. Each experimental condition was repeated 3 times.

Golgi quantification

Golgi images were analyzed using image J software. For each cell, the Golgi was highlighted and the fluorescence threshold was set and "Area fraction" analysis was used. Cells were counted over the course of 3 independent experiments.

Immunocytochemistry

NIT-1 cells were seeded on coverslips overnight. Cells were fixed in 4% paraformaldehyde for 10 min and rinsed with room temperature PBS. Cells were then permeabilized with 0.1% triton X-100 for 10 min. After rinsing with PBS, cells were then probed with primary antibody for 60 min, followed by 60 min incubation with fluorescently labeled secondary antibodies.

Results

PLD1 inhibition relieves the PLD2 GSIR phenotype

In a previously published report (Su et al., 2009), I explored the effect of PLD inhibition using a pan-PLD inhibitor on GSIR. To my surprise, I found no difference in insulin secretion for cells treated with FIPI, a pan-PLD inhibitor. Inhibition of PLD activity with 1-butanol, the current gold standard, showed robust depression of GSIR in agreement with published literature (Hughes et al., 2004; Lee et al., 2008b). I concluded that inhibition with butanol produced off-target effects. I further hypothesized that PLD1 and PLD2 performed opposing functions in β-cells. I investigated if FIPI treatment would affect GSIR in PLD2 knockdown cells (Fig. 4-1a). PLD2 knockdown cells secreted greater amounts of insulin upon low and high glucose stimulation relative to wild-type cells, as shown in Chapter 2. PLD2 knockdown cells that had been treated with 750 nM FIPI showed decreased insulin secretion compared to PLD2 knockdown cells in both low (16% decrease) and high glucose (19% decrease) concentrations. This decrease did not quite reach levels secreted by control cells (basal: 0.7% luc RNAi vs 1.0% PLD2 RNAi + FIPI: stimulated: 4.2% luc RNAi vs 5.8% PLD2 RNAi + FIPI). Luc RNAi-transfected control cells treated with FIPI did not exhibit significant differences in insulin secretion compared to control cells without FIPI treatment. To test if I would see the same attenuation of insulin secretion *in vivo*, I injected $PLD2^{-/-}$ and WT mice with FIPI overnight and 1 hour before GTT (Fig. 4-1b) with 1 mg/kg. $PLD2^{-/-}$ mice treated with FIPI showed a partial reversal of the enhanced GTT observed in $PLD2^{-/-}$ mice. FIPI treatment did not significantly impact GTT in WT animals. Higher doses of FIPI up to 3 mg/kg did not mediate a stronger effect in $PLD2^{-/-}$ mice.

PLD1 inhibition relieves PLD2 *cis*-golgi tubulation phenotype

NIT-1 cells were transfected with luc or PLD2 RNAi and subsequently treated with FIPI overnight. After the treatment period, I examined the *cis*-golgi (Fig. 4-2a). In PLD2 knockdown cells, the *cis*-golgi was tubulated as expected. However, I found a 31% reduction in tubulation in PLD2 knockdown cells that were treated with FIPI (Fig. 4-2b). Use of an isoform-specific PLD2 inhibitor (PLD2i) (Scott et al., 2009) also led to golgi tubulation (Fig. 4-3a). Of note, no tubulation was observed when the PLD1 specific isoform (PLD1i) alone or a mixture of both PLD1 and PLD2 specific isoforms were used (supporting FIPI findings). Golgi tubulation in PLD2 knockdown cells was rescued with treatment with the PLD1i (Fig. 4-3b). Our microarray screen of $PLD2^{-/-}$ islets (Fig. 2-4) identified downregulated levels of PITPNM3, and subsequent experiments emphasized the role of PITPNM3 downstream of PA generation by PLD2 (chapter 3). I hypothesized that PITPNM3 was downstream of PLD2 and restoration of normal golgi architecture by PLD1 inhibition was in the context of PITPNM3 reduction. NIT-1 cells were transfected with PITPNM3 siRNA for 48 hours and then treated with FIPI for 1 hour. The cells were then fixed and stained for *cis*-golgi (Fig. 4-4). PITPNM3 silencing led to *cis*-golgi tubulation that was subsequently reversed with short term FIPI treatment.

Discussion

In contrast to PLD1, PLD2 has constitutive activity (Sung et al., 1999a), and it has been shown that PLD1 and PLD2 target to different organelles and could have distinct functions (Brown et al., 1998; Chen et al., 1997; Choi et al., 2002; Cockcroft, 2001; Freyberg et al., 2002; Laine et al., 2000; Pathre et al., 2003; Yang et al., 2008) despite the production of an identical signaling mediator (PA). Earlier data from our lab suggested the possibility that PLD1 and PLD2 played either no role in GSIR or functioned antagonistically (Su et al., 2009). Indeed, I found that subsequent inhibition of PLD1 in the background of PLD2 knockdown led to attenuation of the PLD2 phenotype. I found reductions in the severity of *cis*-golgi tubulation and reduction in both *in vitro* GSIR and *in vivo* GTT. This is a new paradigm in our understanding of PLD function. Constitutive activity by PLD2 could serve a gatekeeper function while stimulus-activated PLD1 could be needed to overcome PLD2 inhibition. The different subcellular localization for each isoform may also contribute to how they oppose each other's function. For instance, PLD1 localization to the ER facilitates anterograde traffic (Roth et al., 1999) while PLD2 localizes in part to the Golgi (Freyberg et al., 2002; Freyberg et al., 2003; Freyberg et al., 2001; Yang et al., 2008) and facilitates retrograde traffic from the *cis*-golgi back to the ER. In our model (Fig 4-5), inhibition of PLD2 activity would lead to delayed vesicle budding from the *cis*-golgi to the ER without any effect on anterograde transport from the ER to the *cis*-golgi. This would then lead to tubulated or distended *cis*-golgi architecture. In this context, inhibition of PLD1 activity (with FIPI or PLD1i or combined PLD1i and PLD2i) would lead to delayed trafficking in both directions resulting in a relatively normal appearing *cis*-golgi.

Figure 4-1. FIPI treatment attenuates GSIR and GTT in PLD2-silenced NIT-1 cells and PLD2$^{-/-}$ animals respectively. (a). NIT-1 cells transfected with PLD2 RNAi for 48 hours were treated with 75 nM FIPI overnight and stimulated with low (2.5 mM) and high glucose (20 mM) concentrations (n = 4 for all genotypes. *, $p < 0.03$. Experiment repeated twice). (b) WT and PLD2$^{-/-}$ animals were fasted and injected i.p with 1 mg/kg FIPI for 16 hours. Animals were again injected 1 hour before performing a GTT (n = 4. *, PLD2$^{-/-}$ + FIPI compared to WT. **, PLD2$^{-/-}$ compared to WT. $p< 0.04$. **, PLD2$^{-/-}$ compared to PLD2$^{-/-}$ + FIPI is only significant at t = 0. Experiment was repeated twice).

Figure 4-1

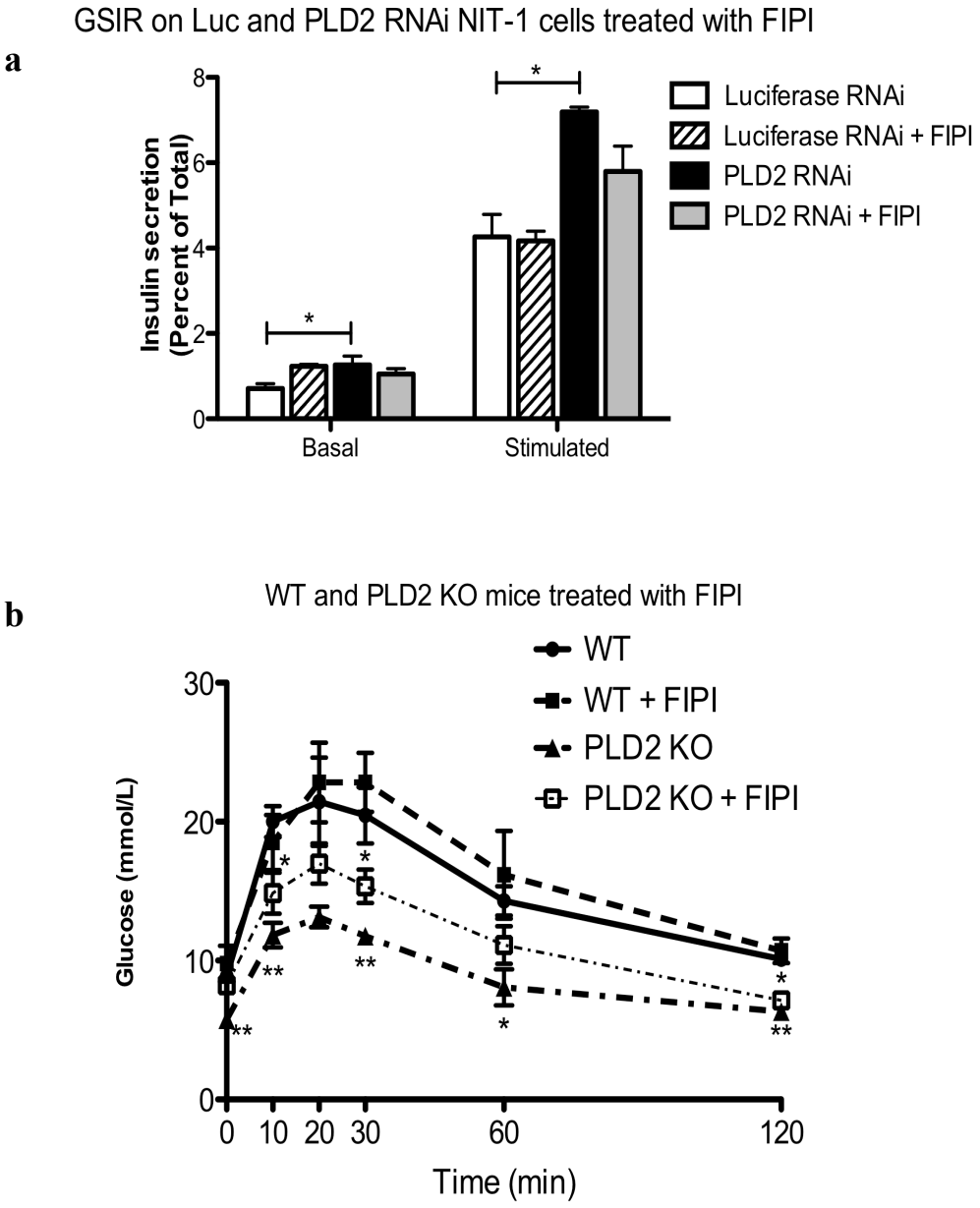
a
GSIR on Luc and PLD2 RNAi NIT-1 cells treated with FIPI
Insulin secretion (Percent of Total)
0
2
4
6
8
Basal
Stimulated
*
*
Luciferase RNAi
Luciferase RNAi + FIPI
PLD2 RNAi
PLD2 RNAi + FIPI
b
WT and PLD2 KO mice treated with FIPI
Glucose (mmol/L)
0
10
20
30
0
10
20
30
60
120
Time (min)
WT
WT + FIPI
PLD2 KO
PLD2 KO + FIPI

Figure 4-2. FIPI treatment of PLD2-silenced cells recues tubulated golgi morphology. (a). NIT-1 cells were transfected with either luciferase or PLD2 RNAi for 48 hours. A subset was then treated with 750 nM FIPI overnight and all samples stained with anti-GM130 and anti-insulin antibodies. (b). Quantification of golgi tubulation ($n = 14$. *, $p < 0.003$). White arrows point to tubulated golgi.

Figure 4-2

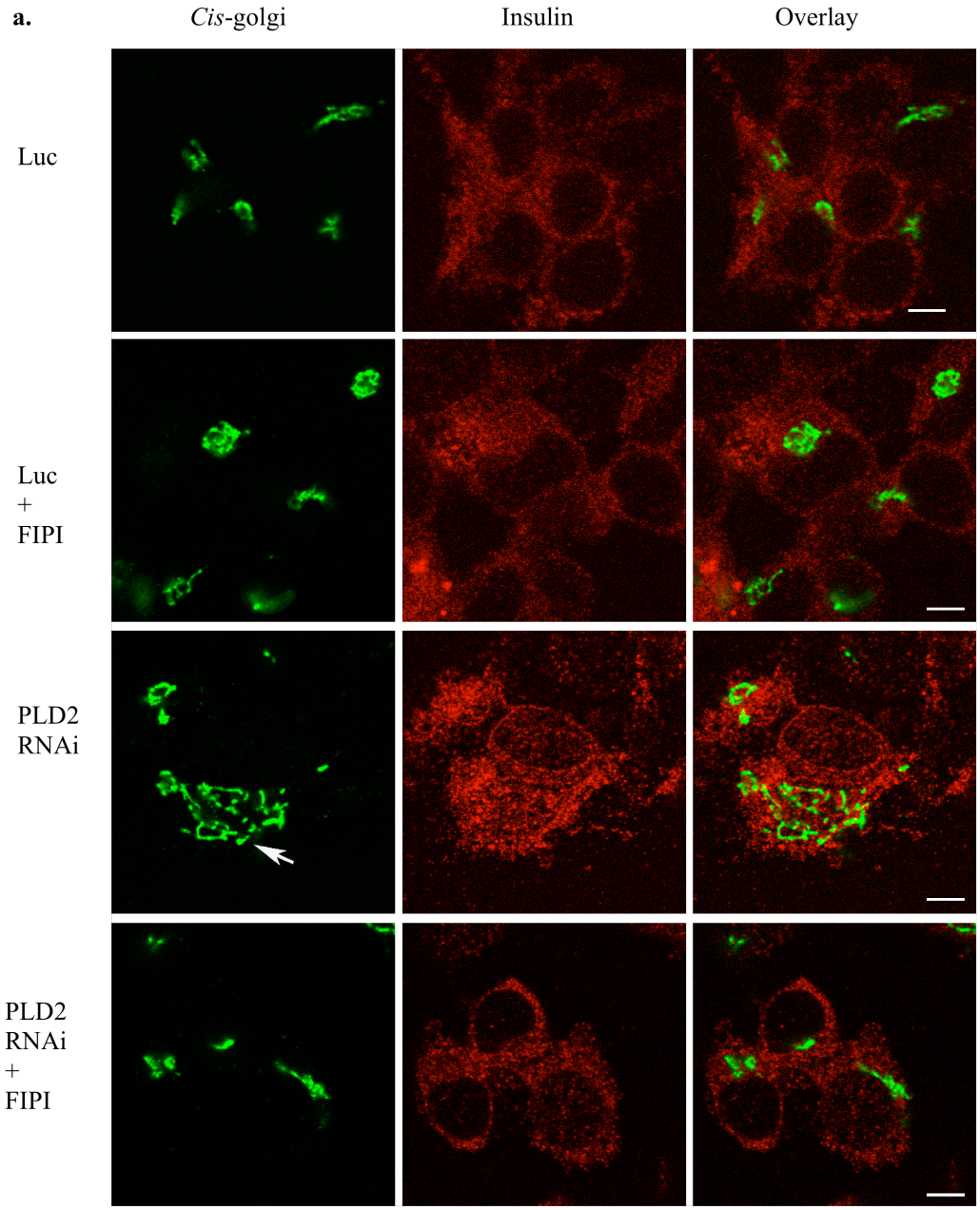
a.
Cis-golgi
Insulin
Overlay
Luc
Luc + FIPI
PLD2 RNAi
PLD2 RNAi + FIPI

Figure 4-2

b.

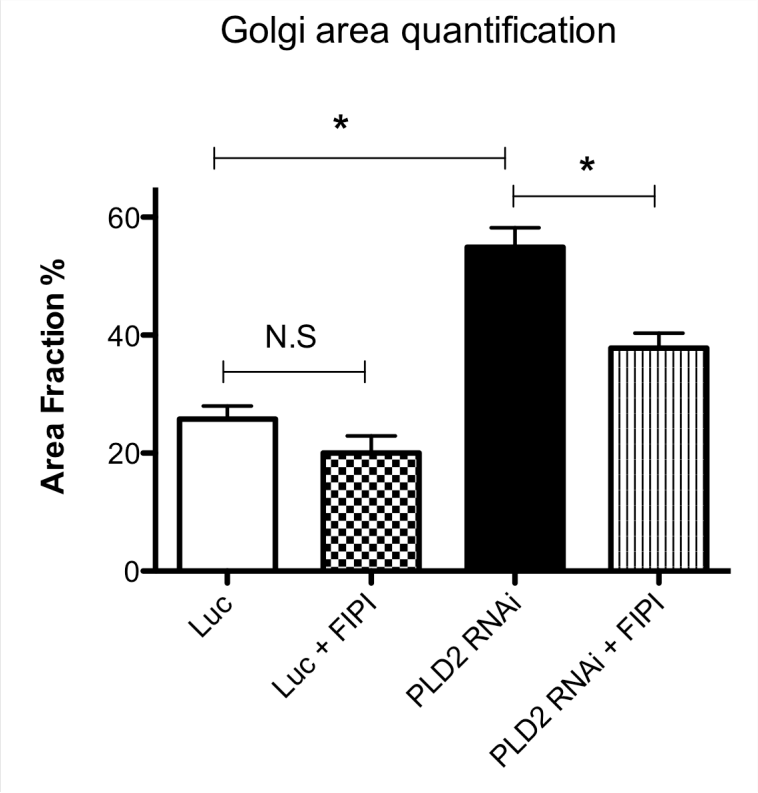
Golgi area quantification
*
*
N.S
Area Fraction %
60
40
20
0
Luc
Luc + FIPI
PLD2 RNAi
PLD2 RNAi + FIPI

Figure 4-3. Isoform specific PLD inhibitors support a role for PLD2 in golgi maintenance. (a). NIT-1 cells were treated with PLD1-specific (PLD1i, 10 μM), PLD2-specific (PLD2i, 10 μM) or a mixture of both PLD1i and PLD2i overnight (5 μM each). Cells were fixed and stained for *cis*-golgi. Quantification of golgi tubulation is shown below the image. (n = 16. *, $p < 0.003$) (b). Luciferase and PLD2-silenced cells were treated with PLD1i overnight and stained with *cis*-golgi antibody. (n = 15. *, $p < 0.003$). White arrows point to tubulated golgi.

Figure 4-3

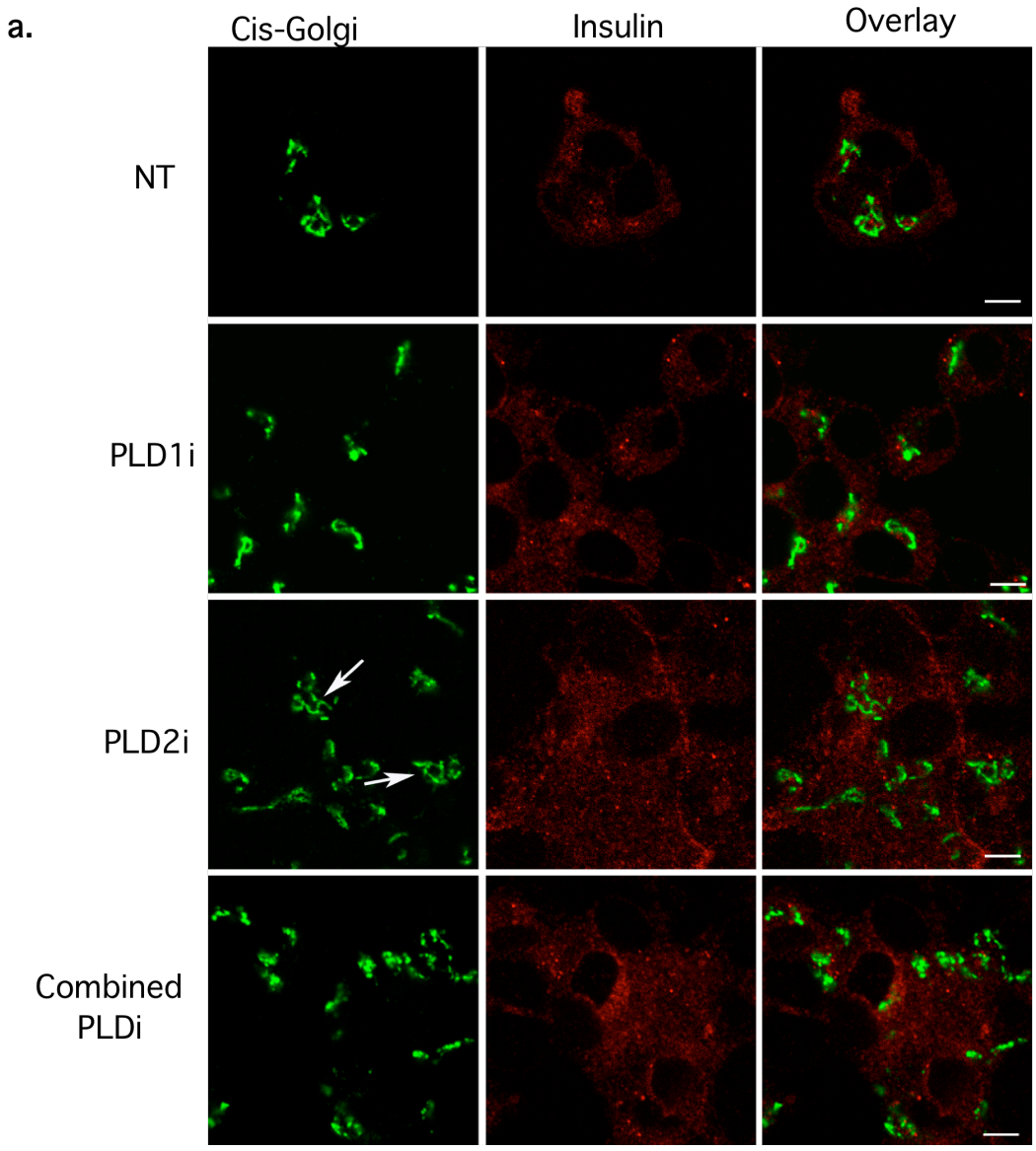
a.
Cis-Golgi
Insulin
Overlay
NT
PLD1i
PLD2i
Combined PLDi

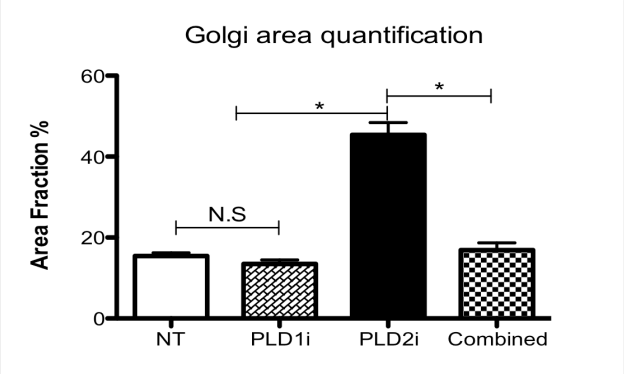
Golgi area quantification
Area Fraction %
60
40
20
0
N.S
*
*
NT
PLD1i
PLD2i
Combined

Figure 4-3

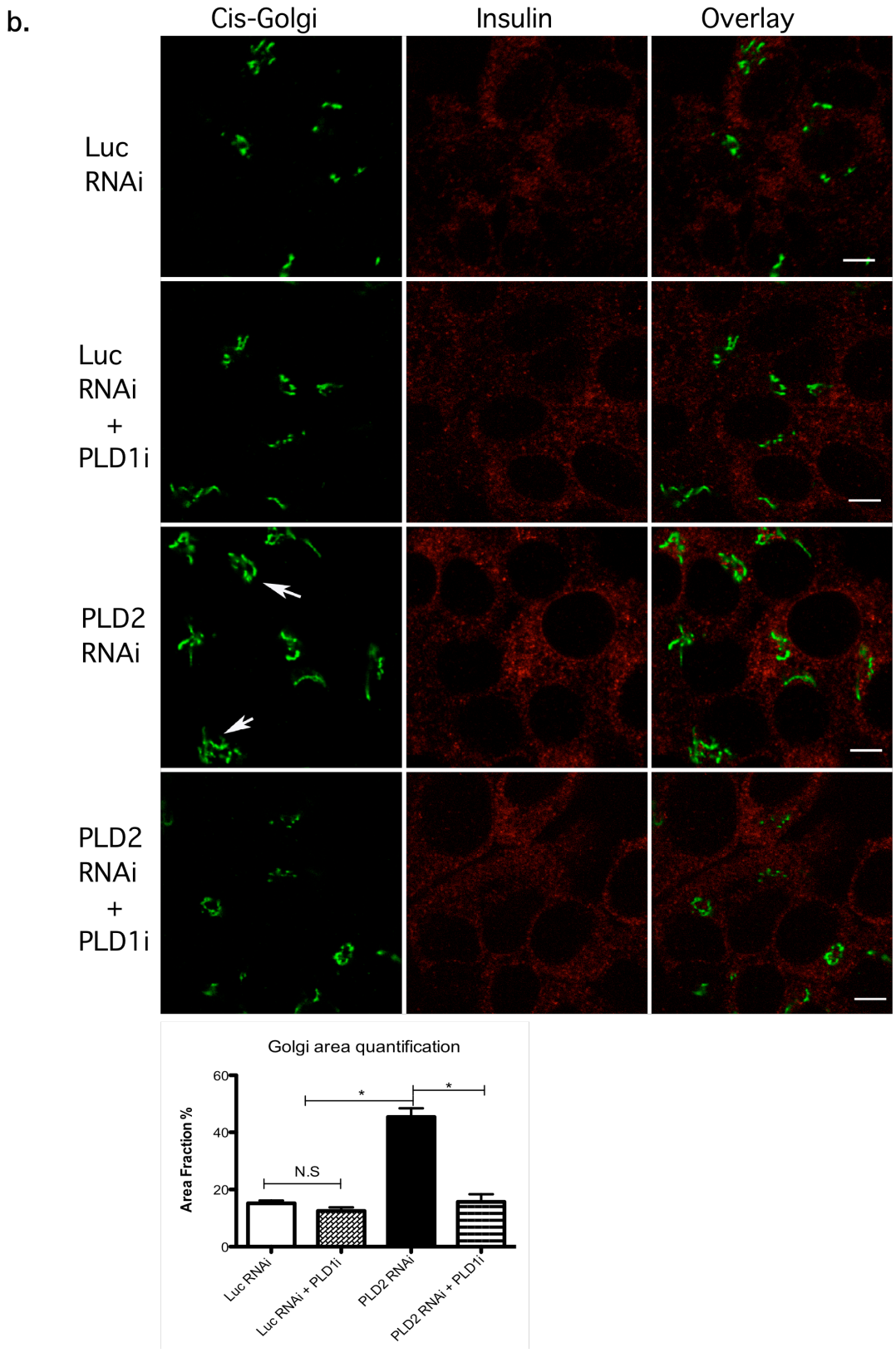
b.
Cis-Golgi
Insulin
Overlay
Luc RNAi
Luc RNAi + PLD1i
PLD2 RNAi
PLD2 RNAi + PLD1i
Golgi area quantification
Area Fraction %
60
40
20
0
N.S
*
*
Luc RNAi
Luc RNAi + PLD1i
PLD2 RNAi
PLD2 RNAi + PLD1i

Figure 4-4. FIPI treatment reverts PITPNM3-mediated *cis*-golgi tubulation.

(a). NIT-1 cells were transfected with 50 nM control and PITPNM3 siRNA for 48 hours. They were then treated with 750 nM FIPI for 1 hour, fixed and stained with a *cis*-golgi marker (GM130). ($n = 15$. *, $p < 0.05$). White arrows point to tubulated golgi.

Figure 4-4

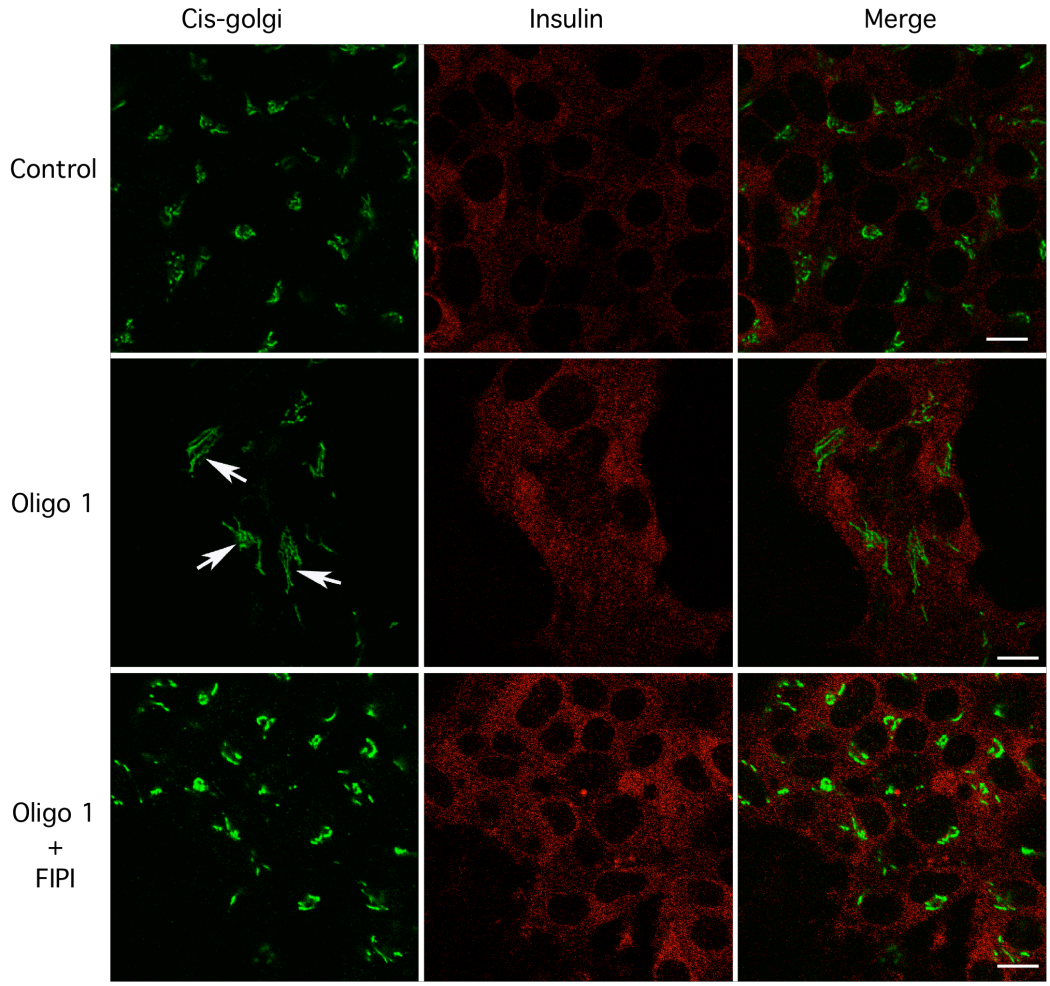
Cis-golgi
Insulin
Merge
Control
Oligo 1
Oligo 1
+
FIPI

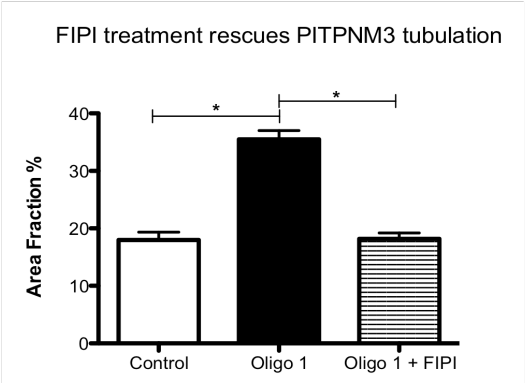
FIPI treatment rescues PITPNM3 tubulation
Area Fraction %
40
30
20
10
0
*
*
Control
Oligo 1
Oligo 1 + FIPI

Figure 4-5. Proposed model describing the roles of PLD1 and PLD2 in vesicular trafficking. (a) Figure summarizing the roles of PLD1 and PLD2 in anterograde and retrograde vesicular trafficking from the ER to the golgi to the plasma membrane (PM). (b). In the absence of PLD2 activity, there is attenuated retrograde transport from the *cis*-golgi to the ER. Anterograde (PLD1-mediated) is unaffected. Eventually, the trafficking imbalance will lead to tubulated *cis*-golgi. (c). Addition of FIPI, leads to an attenuation of PLD1 and PLD2, slowing both anterograde and retrograde trafficking, leading to an attenuation of the tubulated *cis*-golgi phenotype.

Figure 4-5

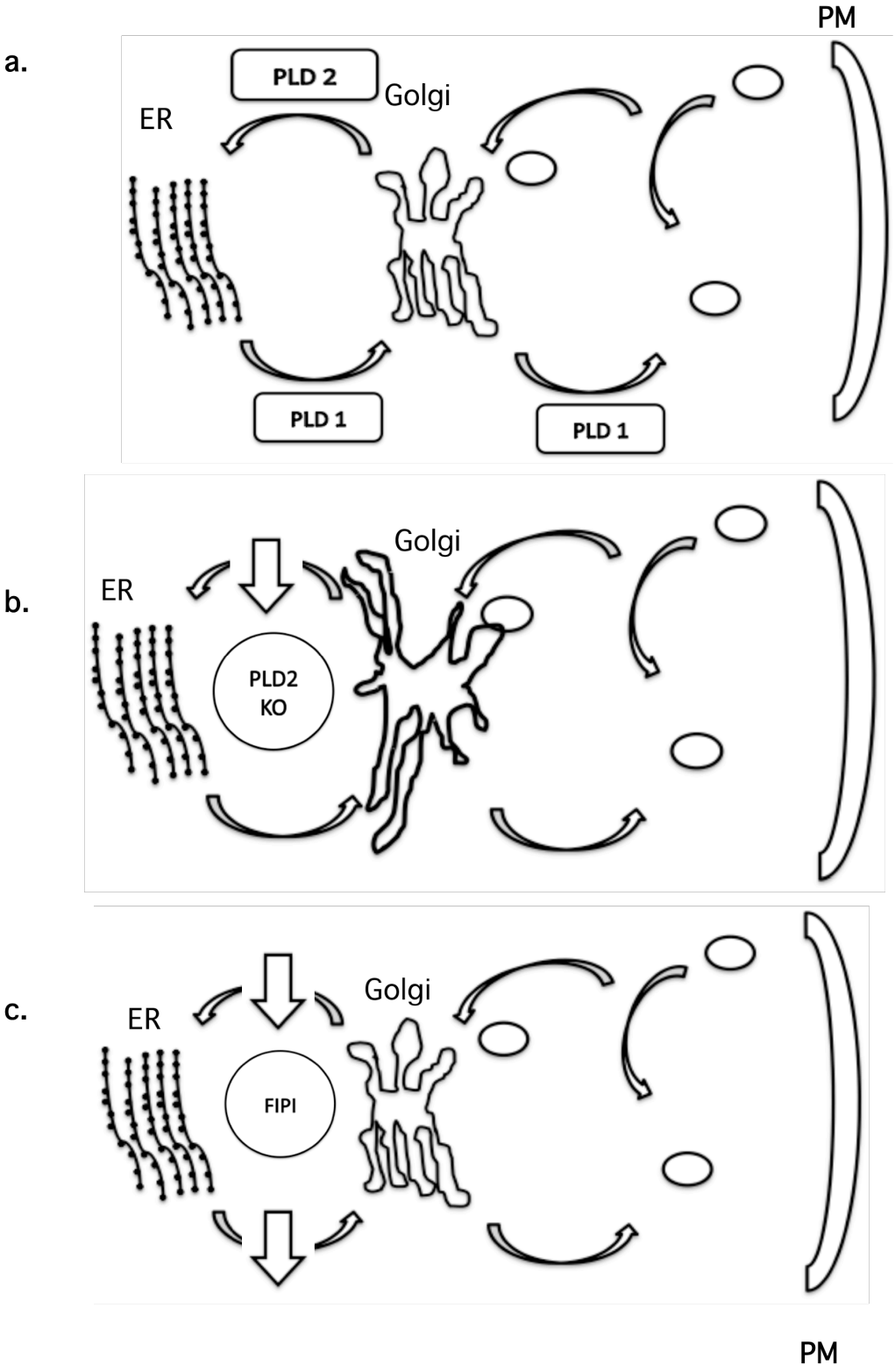
PM
a.
PLD 2
Golgi
ER
PLD 1
PLD 1
b.
Golgi
ER
PLD2
KO
c.
ER
Golgi
FIPI
PM

Chapter 5

Role of PLD2 in vacuolar nephropathy

Renal tubule epithelial cells are an excellent model for the study of vesicular trafficking. Because of their central role in acid/base homeostasis, and body fluid regulation, renal epithelial cells must maintain an apical-basal polarity and traffic various channels and pumps in response to stimuli. For example, the aquaporin 2 (AQP2) channel is a critical water channel used to maintain urine osmolarity. Upon vasopressin stimulation, AQP2 channels are phosphorylated and trafficked from the cytosol to the plasma membrane (Brown, 2003; Sasaki and Noda, 2007; Valenti et al., 2005). Failure of this relatively straightforward trafficking event leads to diabetes insipidus (Bichet, 2008; Loonen et al., 2008). Recycling of endocytosed vesicles and receptors is also a critical function of renal epithelial cells. The target of vasopressin, the vasopressin type 2 receptor is a G-protein coupled receptor (GPCR) that recycles slowly (Madziva and Birnbaumer, 2006) and much of the internalized receptor is degraded by lysosomes (Robben et al., 2006; Yi et al., 2007). Since some GPCR have been shown to signal from intracellular compartments such as the golgi and the ER (Boivin et al., 2008), V2R signaling from recycling endosomes is currently an area of intense investigation (Hanyaloglu and von Zastrow, 2008; Shenoy and Lefkowitz, 2005; Tzafriri and Edelman, 2007). Besides GPCRs, the extensive endosomal networks in renal epithelial cells are required for the degradation of several other membrane proteins via the endosomal/lysosomal pathway (Christensen and Birn, 2002; Marshansky et al., 2002). Reduced endosomal acidification in renal epithelial cells has been shown to lead to

albumin and other small proteins wasting into the urine (Marshansky et al., 2002) further underscoring the importance of endosomal/lysosomal trafficking.

PLD is expressed in a variety of tissues including kidneys (Kim et al., 2007). The function of either isoform in kidney organogenesis and function is currently unknown. ARF-stimulated PLD activity has been shown to be important for lysosomal and endosomal recycling (Jovanovic et al., 2006; Toda et al., 1999). Because of the importance of cargo sorting (Ellis et al., 2006), vesicular trafficking (Nokes et al., 2008) and lysosomal degradation and processing of endocytosed vesicles (van Balkom et al., 2009) in renal epithelial cells, I hypothesized that PLD2 might play a role in vesicular trafficking in kidney epithelial cells.

Materials and Methods

Antibodies and general reagents

AQP2 and Na^+/K^+ ATPase antibodies were purchased from Abcam. GM130 antibodies were purchased from BD Transduction Laboratories. Oil Red O was purchased from Sigma Aldrich. Serum LDL and HDL kits were purchased from Biovision. Glucose oxidase test for urine glucose measurement was purchased from Pointe Scientific. The QuantiChrome creatinine assay kit was purchased from BioAssay Systems. The albumin ELISA kit was purchased from Exocell. Anti-LAMP1, LC-3 and EEA1 antibodies were purchased from BD Transduction Laboratories.

Immunocytochemistry and Immunohistochemistry

MDCK3 cells (ATCC) were fixed in 4% paraformaldehyde or 10% formalin for 10 min and rinsed with room temperature PBS. Cells were then permeabilized with 0.1% triton X-100 for 10 min. After rinsing with PBS, cells were then probed with indicated primary antibody for 60 min, followed by a 60 min incubation with fluorescently labeled secondary antibodies. Knockdown was achieved in cells using either luciferase RNAi, PLD2 RNAi or luciferase/ PLD2 RNAi also expressing dsRed. For immunohistochemistry, freshly dissected kidneys were weighed and immediately fixed in either 4% paraformaldehyde or 10% formalin. 2 μm sections of WT and $PLD2^{-/-}$ paraffin embedded kidneys were probed with the various antibodies as indicated, followed by biotinylated secondary antibodies.

Oil Red O staining

MDCK cells were transfected with luciferase or PLD2 RNAi for 48 hrs and fixed with 10% formalin for 10 min. Cells were then washed with distilled H_2O twice and 60% isopropanol added to the cells for 5 min. The isopropanol was removed completely and Oil Red O was added for 10 min, followed by washing four times with distilled H_2O and imaging using light microscopy.

Serum collection for cholesterol and albumin measurements

Animals were anesthetized with isoflurane for 5-10 min. A fine capillary tube was then inserted behind the eye to draw blood. Collected blood was incubated at 37^{o}C for 60 min to allow for clotting and then briefly centrifuged to separate serum. LDL and HDL levels were measured using the appropriate kit (Biovision) according to the manufacturers instructions.

Urinalysis

Age-matched male mice were placed in a urine collection chamber overnight with unrestricted access to food and water. The following morning, pooled urine from each animal was examined under the microscope (for hematuria) and then centrifuged. The supernatant was then transferred to a fresh tube and used for measurements as described according to manufacturers instructions.

Results

PLD2$^{-/-}$ mice have vacuolated kidney tubules

Kidneys from WT and PLD2$^{-/-}$ mice were collected and fixed. PLD2$^{-/-}$ mice had slightly higher raw kidney weight (WT: 0.2487 g ± 0.056, PLD2$^{-/-}$: 0.2948 g ± 0.027) (fig. 5-1a), but because the animals weighed 26% more (WT: 29.2 g ± 2.2, PLD2$^{-/-}$: 39.66 g ± 2.5) (fig. 5-1b), kidney weight as a fraction of body weight was not significantly different compared to WT animals (fig. 5-1c). H&E sections of the kidney showed large vacuoles in the PLD2$^{-/-}$ kidneys (fig. 5-2a). Some apoptotic cells could be identified by their pyknotic nuclei and some regions showed cells that had sloughed into the tubule lumen. There were no differences in glomerular size, frequency or distribution by light microscope analysis. Vacuolar pathology was observed throughout the PLD2$^{-/-}$ kidneys, but to determine the cell type most affected, I performed a PAS stain. PAS staining highlights brush-border cells, which are mostly prevalent in the proximal tubules of the kidney. I found extensive vacuolization in brush border-containing regions in PLD2$^{-/-}$ kidneys, suggesting extensive proximal tubule damage (fig. 5-2b).

PLD2$^{-/-}$ pathology does not involve golgi, Na^+/K^+ ATPase or AQP2 distribution

Because of other ongoing studies in our laboratory, I had reason to suspect dysregulation of the golgi apparatus in PLD2$^{-/-}$ mice. Dysregulation of the *cis*-golgi would provide a ready explanation for disrupted vesicle trafficking, which could in-turn lead to vacuolization and eventually apoptosis. Fixed histological samples from PLD2$^{-/-}$ and WT kidneys were probed with a *cis*-golgi antibody. The *cis*-golgi was punctate and cytoplasmic in both control and PLD2$^{-/-}$ cells. I found no differences in *cis*-golgi staining

localization or intensity between both genotypes (fig. 5-3a). Next I examined the localization and distribution of the Na^+/K^+ ATPase channel responsible for proper water balance. Our hypothesis was that mislocalized or mistrafficked Na^+/K^+ ATPase channels could lead to the formation of fluid-filled cysts. Immunohistochemical staining did not show any differences in Na^+/K^+ ATPase staining (fig. 5-3b). In both cases, Na^+/K^+ ATPase localized to the plasma membrane. I then directly checked AQP2 channel localization, which has been shown to be mistrafficked in many human vacuolar nephropathies (Moon et al., 2009). AQP2 was diffusely distributed with some localization to the plasma membrane in both control and PLD2-silenced cells. I did not find any differences in AQP2 channel distribution and localization (fig. 5-3c).

PLD2$^{-/-}$ mice do not exhibit declined renal function

In order to probe the correlation between renal function and vacuolar nephropathy in PLD2$^{-/-}$ mice, I subjected the animals to overnight urine collection. Urine volume was similar between both genotypes and no blood or cloudiness was found in PLD2$^{-/-}$ urine (not shown). To directly test filtration function, I measured urine creatinine and found no difference in PLD2$^{-/-}$ mice (fig. 5-4a). Albumin is an abundant serum protein that is typically spilled into the urine when there is kidney damage (Tojo et al., 2001). There were no differences in serum albumin (fig. 5-4b) in PLD2$^{-/-}$ mice but there was a slight but non-significant reduction in urine albumin (fig. 5-4c). Finally, I measured urine glucose, which also leaks into the urine when the kidney is not able to properly reabsorb it from urine. I found lower urine glucose in PLD2$^{-/-}$ mice compared to WT mice (fig. 5-

4d). This was not surprising considering the hyperinsulinimic (hypoglycemic) phenotype of PLD2$^{-/-}$ mice (see chapter 2).

PLD2$^{-/-}$ mice have lower serum LDL

LDL cholesterol is one of the lipids that is metabolized and recycled in the proximal tubules of the kidney (Birn et al., 2000; Chatterjee et al., 1986; Saito et al., 2010). Measurement of serum HDL and LDL in WT and PLD2$^{-/-}$ mice showed a 58% decrease in LDL levels in the PLD2$^{-/-}$ serum samples (Fig 5-5a), however, this reduction was not statistically significant. No differences in HDL levels were observed (fig. 5-5b).

PLD2 knockdown *in vitro* shows accumulation of lipid and dysregulated vesicular trafficking

Due to the differences in serum LDL in PLD2$^{-/-}$ mice, I became interested in cholesterol homeostasis in renal epithelial cells. In control MDCK (kidney) epithelial cell lines, the cytoplasm contained relatively few vesicles. Knockdown of PLD using RNAi showed accumulation of tiny vesicles in MDCK cells compared to luc RNAi controls (Fig. 5-6a). To determine if these vesicles contained any lipids, they were subjected to Oil Red O staining. Oil Red O selectively binds to lipids and displays a deep red stain. There was no retention of Oil-red-o in control cells while PLD2-silenced cells displayed weak retention of the stain (Fig. 5-6b). This suggested to us that the content in these vesicles was not oil (because of the weak staining).

Lysosomes are critical organelles for cholesterol metabolism and homeostasis in cells (Saftig and Klumperman, 2009). Lysosomal staining of PLD2 RNAi cells showed

very large lysosomal vesicles (fig. 5-7a) that were not present in control cells. Early endosomes, which later on mature to become lysosomes (Saftig and Klumperman, 2009) were much smaller in PLD2 knockdown cells compared to control cells (fig. 5-7b) further supporting the hypothesis of a vesicular trafficking defect in PLD2 mutants. To determine whether caveolae and autophagosomes are also affected, I examined caveolin-1 (fig. 5-7c) and LC3 (fig. 5-7d) distribution between control and PLD2 RNAi cells but found no differences. Analysis of the *cis*-golgi in these cells showed micro-fragmentation (fig. 5-7e), and this was verified in mouse embryonic fibroblasts (MEF) isolated from $PLD2^{-/-}$ mice (fig. 5-7f).

Discussion

Vesicle trafficking is a critical component of cellular homeostasis. Endocytosis of receptors and vesicles leads to materials being targeted to the trans golgi, multivesicular bodies, or lysosomes for degradation. The consequences of a defect in any of these pathways vary in different cell types. Failure to properly traffic vesicles to lysosomes in macrophages leads to an increase infection susceptibility while failure to recycle GLUT4 receptors to the cell surface leads to insulin resistance (Lauritzen, 2009; Pieters, 2008).

PLD2 localizes to the plasma membrane and translocates to sub-membranous vesicles and membrane ruffles upon stimulation (Choi et al., 2002; Du et al., 2004; Honda et al., 1999). The importance of PLD activity to endosomal recycling has already been described (Jovanovic et al., 2006) but its role in intracellular lipid homeostasis, particularly in renal epithelial cells, has not been explored. Here I find that PLD2 knockdown leads to abnormal lysosomes. It is not yet clear if the lysosomes are functional or not. Lysosomal hydrolases and organelle pH studies would be required to further characterize PLD2$^{-/-}$ lysosomes. Endosomal changes in PLD2$^{-/-}$ cells further suggest that the downstream block in lysosomal activity/maturation is affecting proper endosomal trafficking. Our finding of fragmented *cis*-golgi in epithelial and fibroblast cells was surprising at first. I had found tubulated *cis*-golgi in insulin secreting cells (chapter 3). The finding of fragmented *cis*-golgi is actually corroborated by 1-butanol studies showing similar effects on golgi morphology (Freyberg et al., 2003). However, since insulin-secreting cells are functionally different from resting epithelial cells and fibroblasts, PLD2 dysfunction might result in different phenotypes. What I have yet to explore is the phenotypic importance of fragmented *cis*-golgi in renal epithelial cells.

Specifically I would be interested in following the trafficking of proteins synthesized in the golgi that need to be targeted to various organelles in order for them to function properly. For example, mannose-6-phosphate receptors are trafficked from the golgi to lysosomes and are critical for lysosomal function (Nadimpalli and Amancha, 2009). A key question that needs to be addressed is the functional capacity of lysosomes in PLD2 knockdown cells.

Despite the gross cytopathological findings in $PLD2^{-/-}$ kidneys, it is not entirely surprising that there is little or no renal function decline. Kidneys often need to suffer a large amount of persistent damage for frank renal failure to occur and since the $PLD2^{-/-}$ mice have probably gradually developed this phenotype over time, there would have been plenty of opportunity for their kidneys to adapt. It would still be interesting to see what would result if these animals were placed in a salt-loading or high fat diet. Acute stressors such as the ones mentioned might overcome any chronic adaptation in the $PLD2^{-/-}$ mice and help elucidate the physiological consequences of the PLD2 knock out.

Figure 5-1. PLD2$^{-/-}$ mice kidney weight.
(a). Age-matched male WT and PLD2$^{-/-}$ mice were sacrificed and their kidneys were immediately surgically removed and weighed. n = 4 (b). Body weight of WT and PLD2$^{-/-}$ mice used for the kidney studies. n = 6, * $p < 0.05$. (c). Kidney weight of WT and PLD2$^{-/-}$ mice represented as raw kidney weight divided by body weight. n = 4.

Figure 5-1

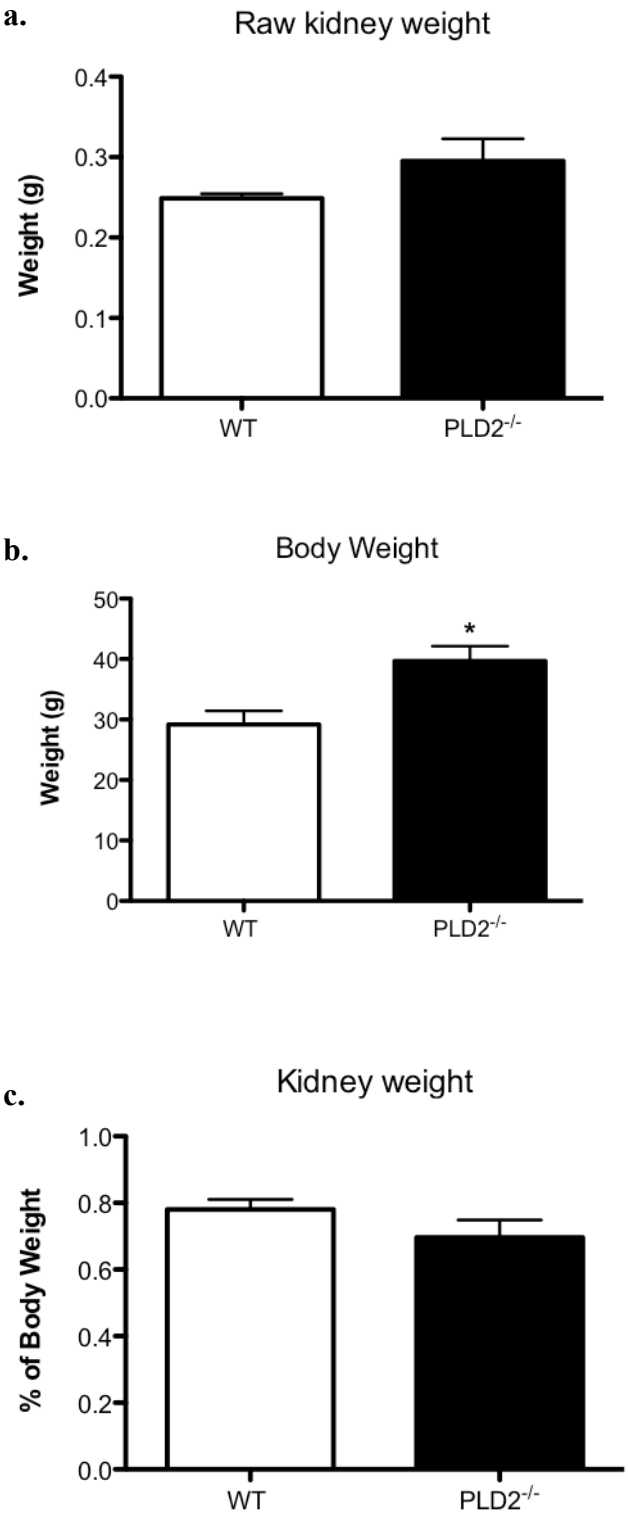
a.
Raw kidney weight
Weight (g)
0.4
0.3
0.2
0.1
0.0
WT
PLD2-/-
b.
Body Weight
Weight (g)
50
40
30
20
10
0
*
WT
PLD2-/-
c.
Kidney weight
% of Body Weight
1.0
0.8
0.6
0.4
0.2
0.0
WT
PLD2-/-

Figure 5-2. Vacuolated proximal tubules Kidney in PLD2$^{-/-}$ mice kidneys.
(a). Kidneys from WT and PLD2$^{-/-}$ mice were fixed, embedded in paraffin and 2 μm sections were stained with hematoxylin and eosin. (b). PAS stain of WT and PLD2$^{-/-}$ kidneys. Brush borders in proximal tubules retain deep pink stain. Black arrows point to vacuoles.

Figure 5-2

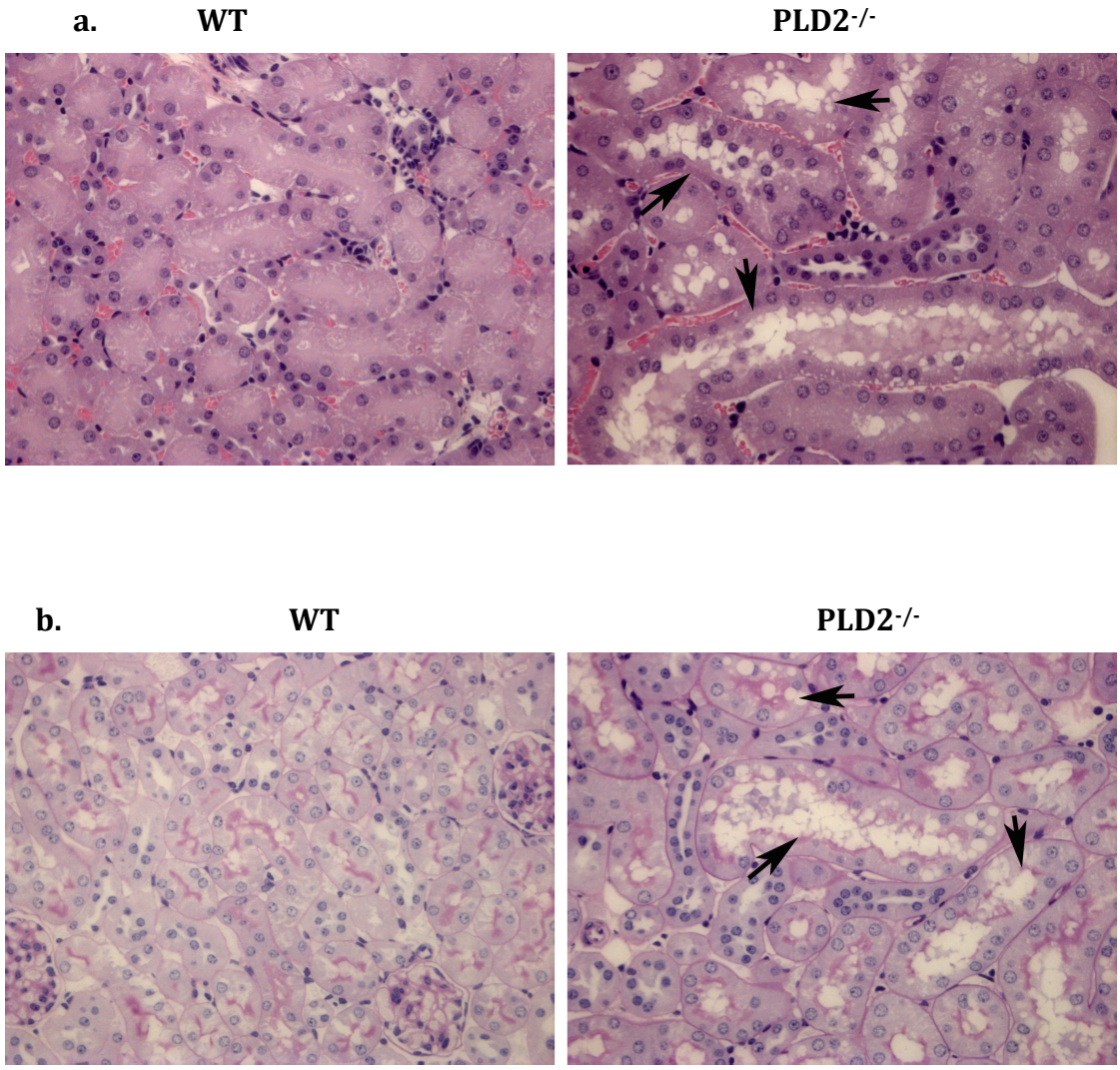

Figure 5-3. Expression and localization of *cis*-golgi, Na^+/K^+ ATPase and AQP2 in PLD2$^{-/-}$ kidneys.
(a). Immunohistochemical stain of the *cis*-golgi using GM130, a cis-golgi antibody in WT and PLD2$^{-/-}$ kidneys. (b). Na^+/K^+ ATPase immunohistochemical stain of WT and PLD2$^{-/-}$ kidneys. (c). WT and PLD2$^{-/-}$ kidneys probed with AQP2 antibodies.

Figure 5-3

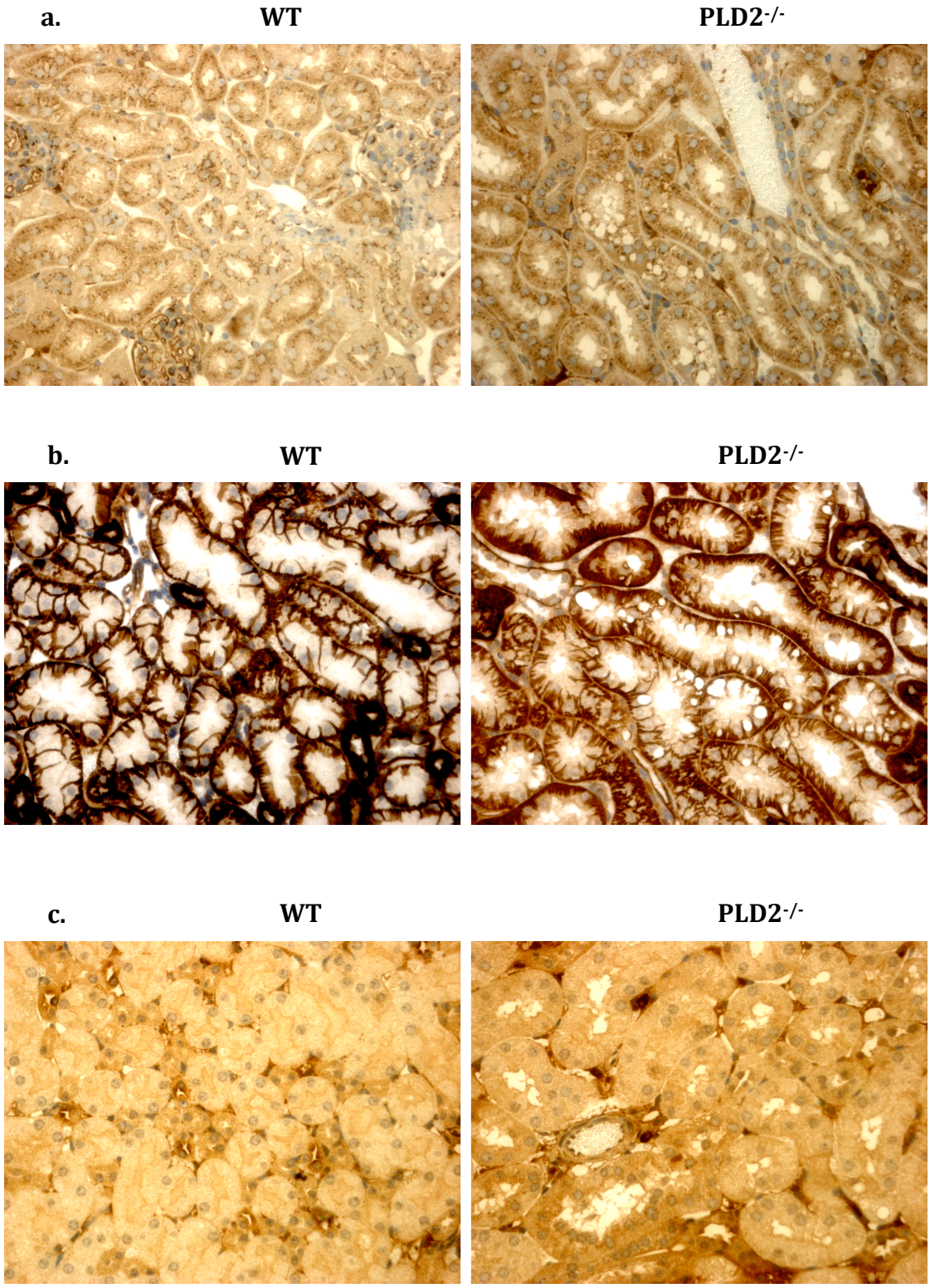

Figure 5-4. PLD2$^{-/-}$ mouse urinalysis.
(a). Urine creatinine levels were measured from overnight urine collections from WT and PLD2$^{-/-}$ mice. n = 4 (b). Albumin was measured from serum collected from retro-orbital bleeds from WT and PLD2$^{-/-}$ mice. n = 4 (c). Overnight urine albumin concentrations in WT and PLD2$^{-/-}$ mice urine. n = 6 (d). Glucose levels were measured in WT and PLD2$^{-/-}$ urine. n = 4 * $p < 0.05$. All results are representative of 3 independent experiments.

Figure 5-4

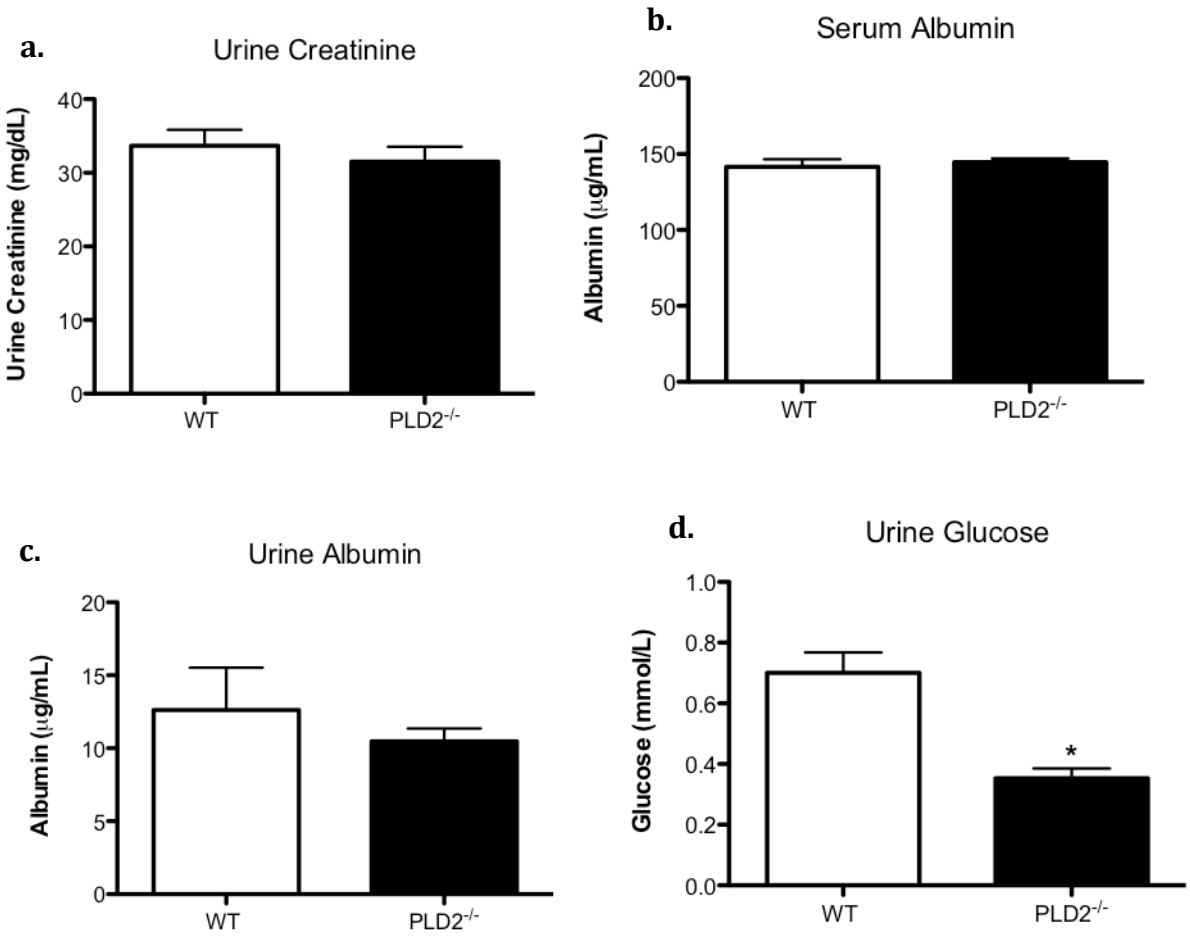
a.
Urine Creatinine
Urine Creatinine (mg/dL)
40
30
20
10
0
WT
PLD2-/-
b.
Serum Albumin
Albumin (µg/mL)
200
150
100
50
0
WT
PLD2-/-
c.
Urine Albumin
Albumin (µg/mL)
20
15
10
5
0
WT
PLD2-/-
d.
Urine Glucose
Glucose (mmol/L)
1.0
0.8
0.6
0.4
0.2
0.0
*
WT
PLD2-/-

Figure 5-5. PLD2$^{-/-}$ mice have lower serum LDL cholesterol.
(a). Serum LDL was measured from blood collected from WT and PLD2$^{-/-}$ mouse retro-orbital bleeds. n = 7 (b). Serum HDL measurements from WT and PLD2$^{-/-}$ mice. n = 7. All results are representative of 3 independent experiments.

Figure 5-5

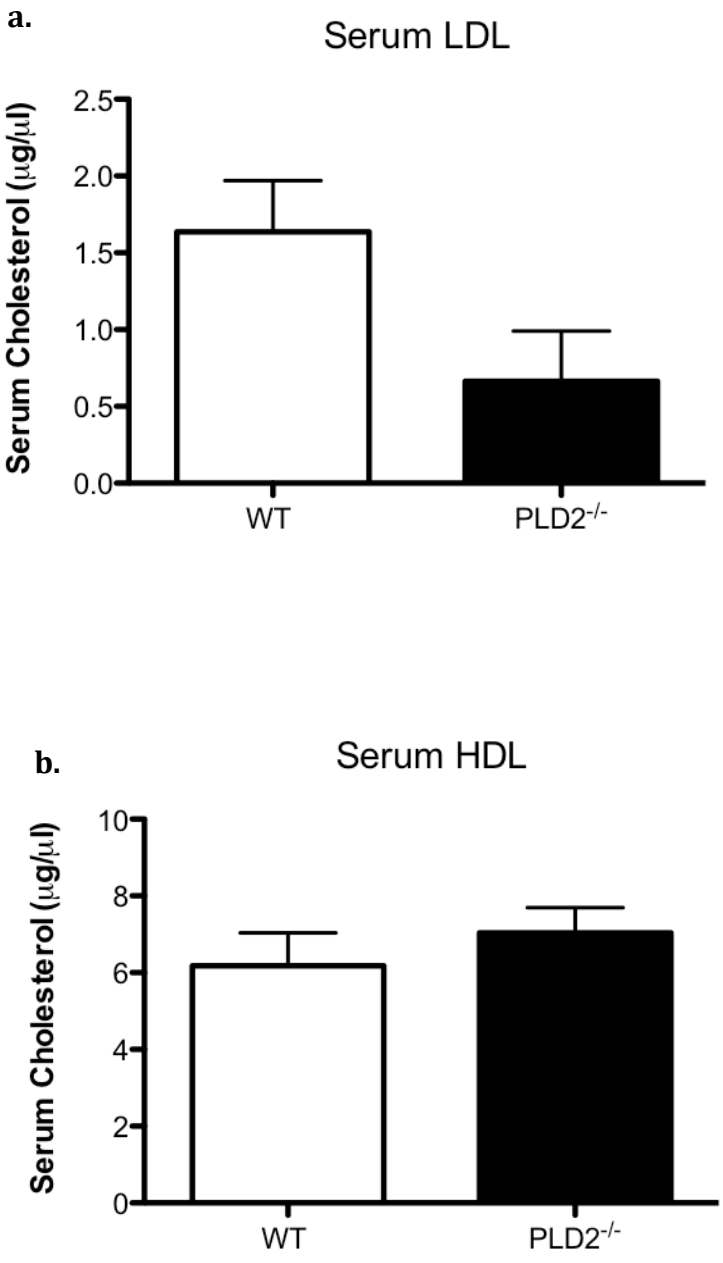
a.
Serum LDL
Serum Cholesterol (μg/μl)
2.5
2.0
1.5
1.0
0.5
0.0
WT
PLD2-/-
b.
Serum HDL
Serum Cholesterol (μg/μl)
10
8
6
4
2
0
WT
PLD2-/-

Figure 5-6. Lipid droplets in PLD2 RNAi MDCK cells.
(a). Bright-field images of MDCK cells transfected with either luciferase or PLD2 RNAi for 48 hours. Black arrows point to vesicles. (b) Luciferase or PLD2 RNAi transfected MDCK cells stained with Oil Red O. Enlarged region showed inset. Black arrows point to droplets. Results are representative of 2 experiments.

Figure 5-6

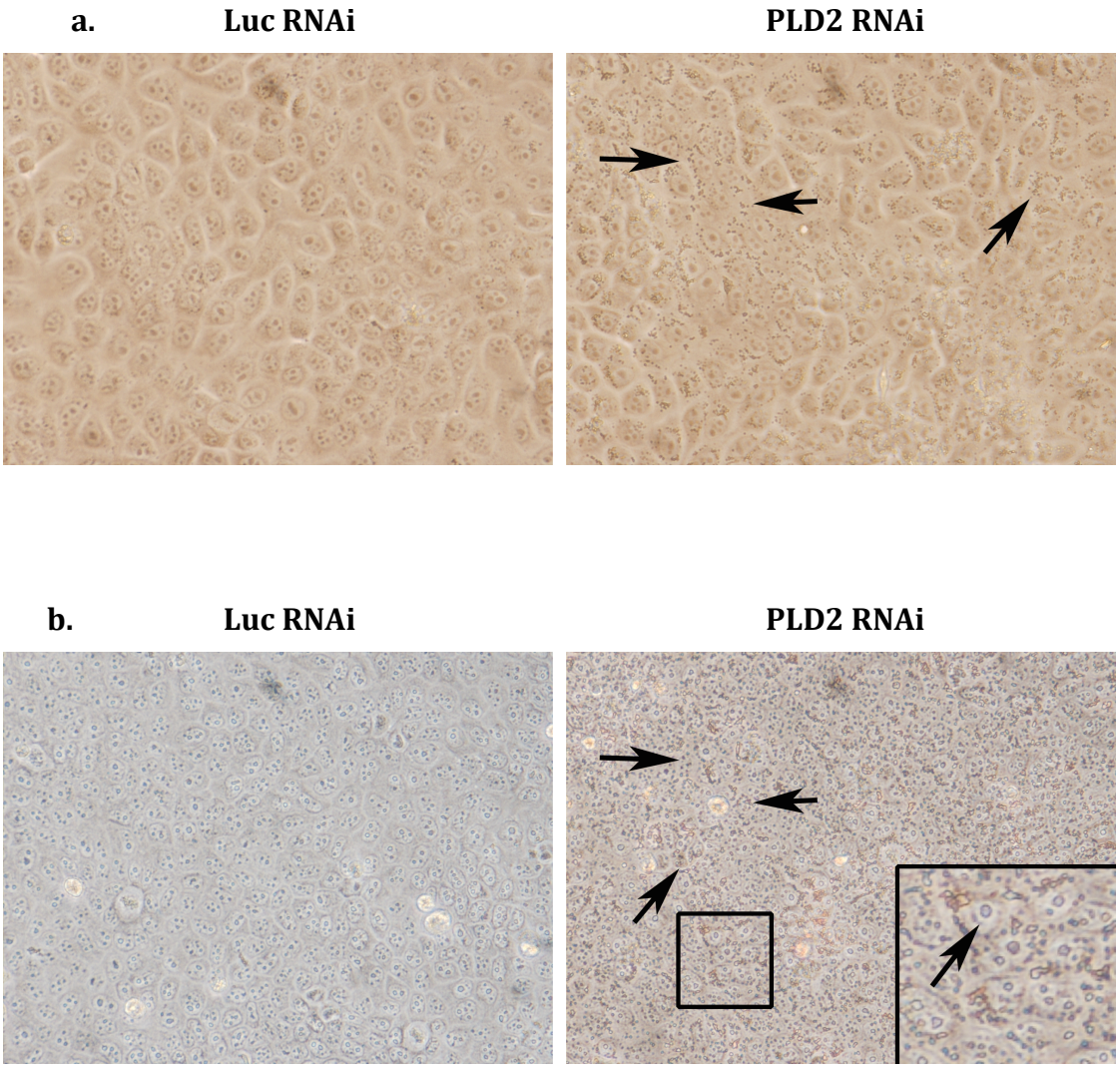

Figure 5-7. Trafficking defects in PLD2-silenced MDCK cells.
(a). Luciferase or PLD2 RNAi silenced cells were fixed and stained with LAMP-1, a lysosomal marker. PLD2 and Luciferase plasmids contain a dsRed marker to identify transfected cells. White arrow points to an enlarged lysosome (b). MDCK3 cells were transfected with PLD2 or Luciferase RNAi for 48 hours and then fixed and stained with EEA-1. White arrow indicates enlarged endosome. (c). Luciferase and PLD2-silenced cells stained with caveolin-1 antibody. (d). Autophagosome staining of luciferase and PLD2 RNAi –transfected cells. (e). MDCK3 cells transfected with luciferase or PLD2 RNAi for 48 hours and stained with *cis*- golgi antibody GM130. White arrows point to fragmented golgi (f). WT and PLD2$^{-/-}$ MEF's fixed and stained with *cis*- golgi antibody. White arrows point to fragmented golgi.

Figure 5-7

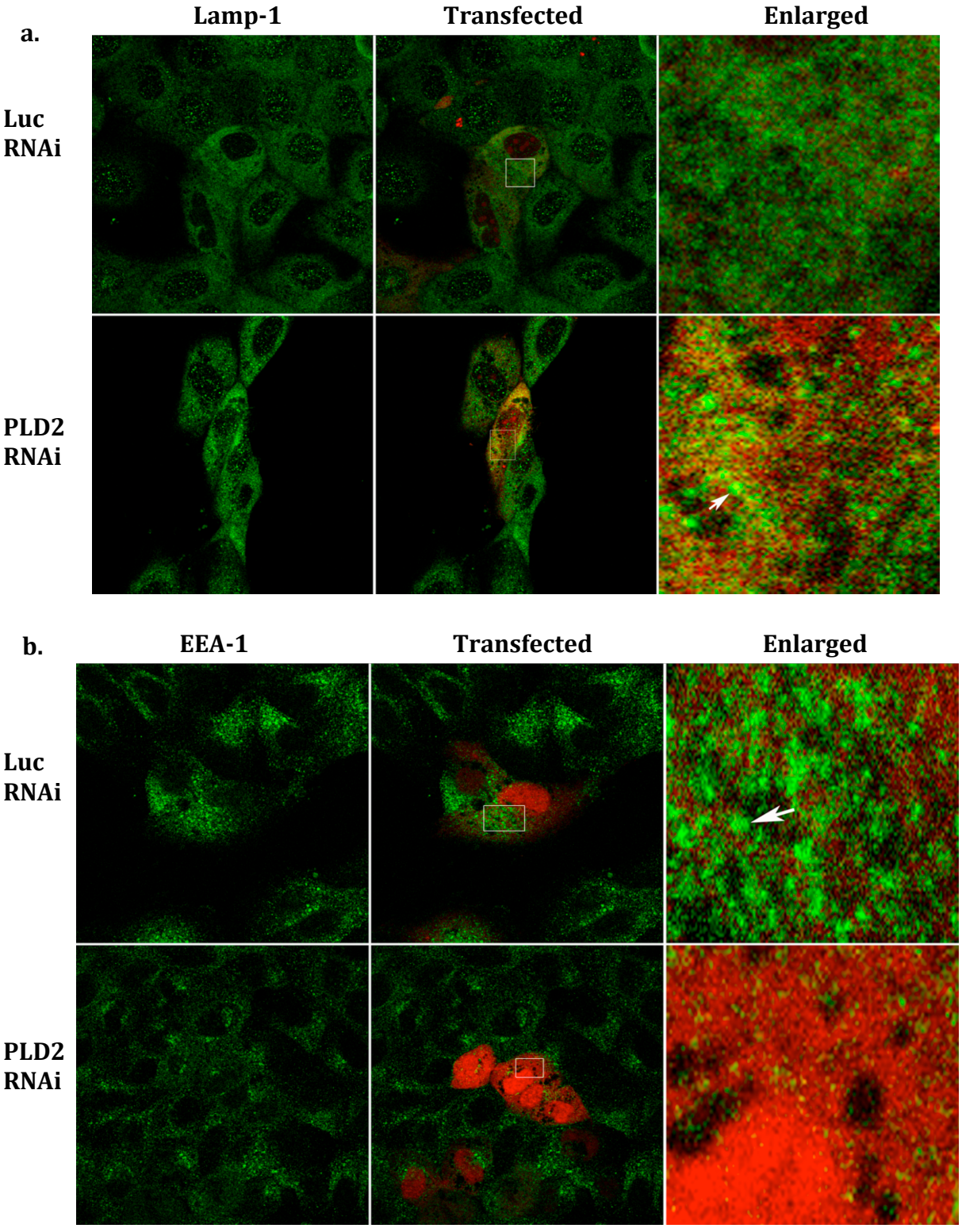
a.
Lamp-1
Transfected
Enlarged
Luc RNAi
PLD2 RNAi
b.
EEA-1
Transfected
Enlarged
Luc RNAi
PLD2 RNAi

Figure 5-7

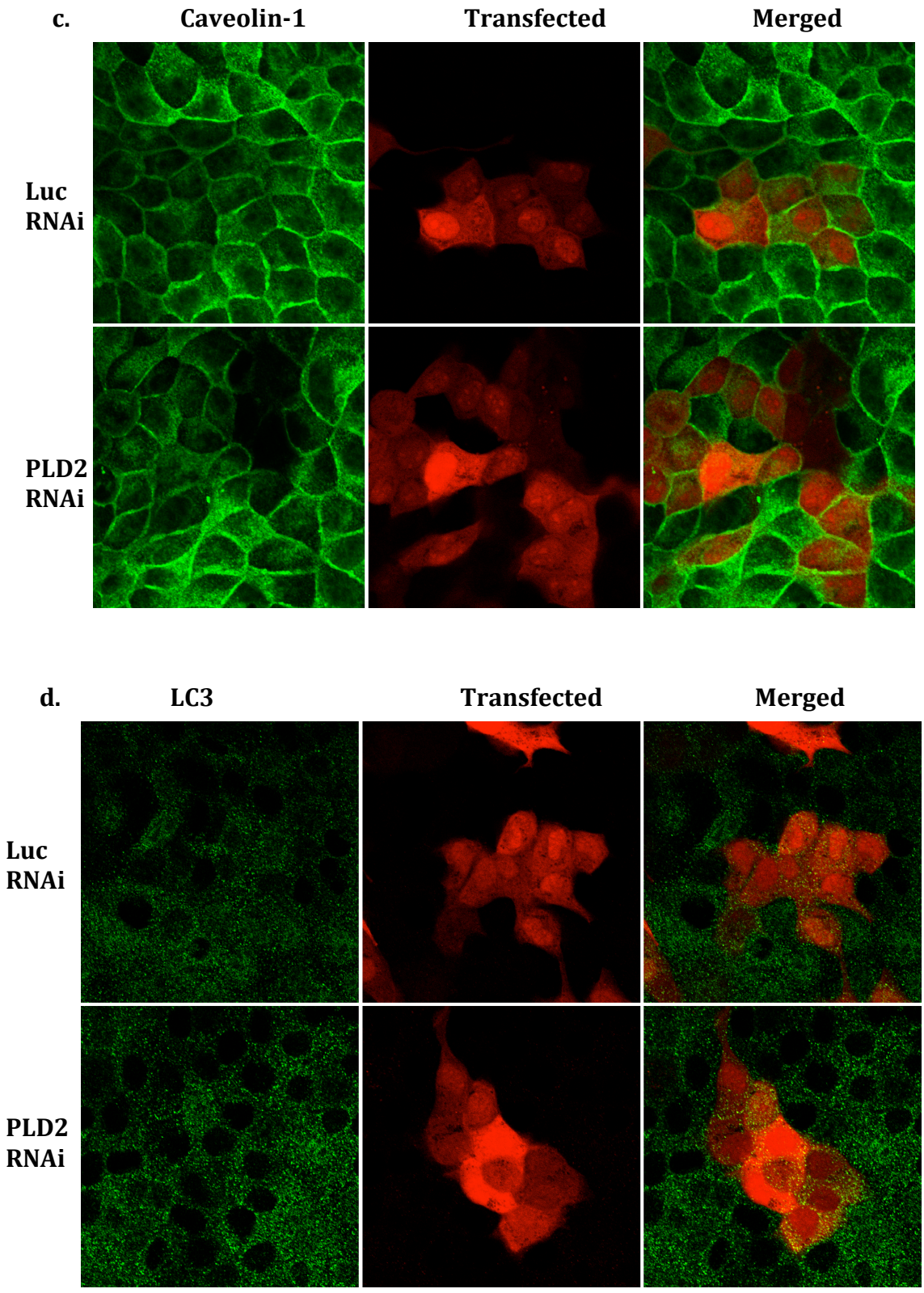
c.
Caveolin-1
Transfected
Merged
Luc RNAi
PLD2 RNAi
d.
LC3
Transfected
Merged
Luc RNAi
PLD2 RNAi

Figure 5-7

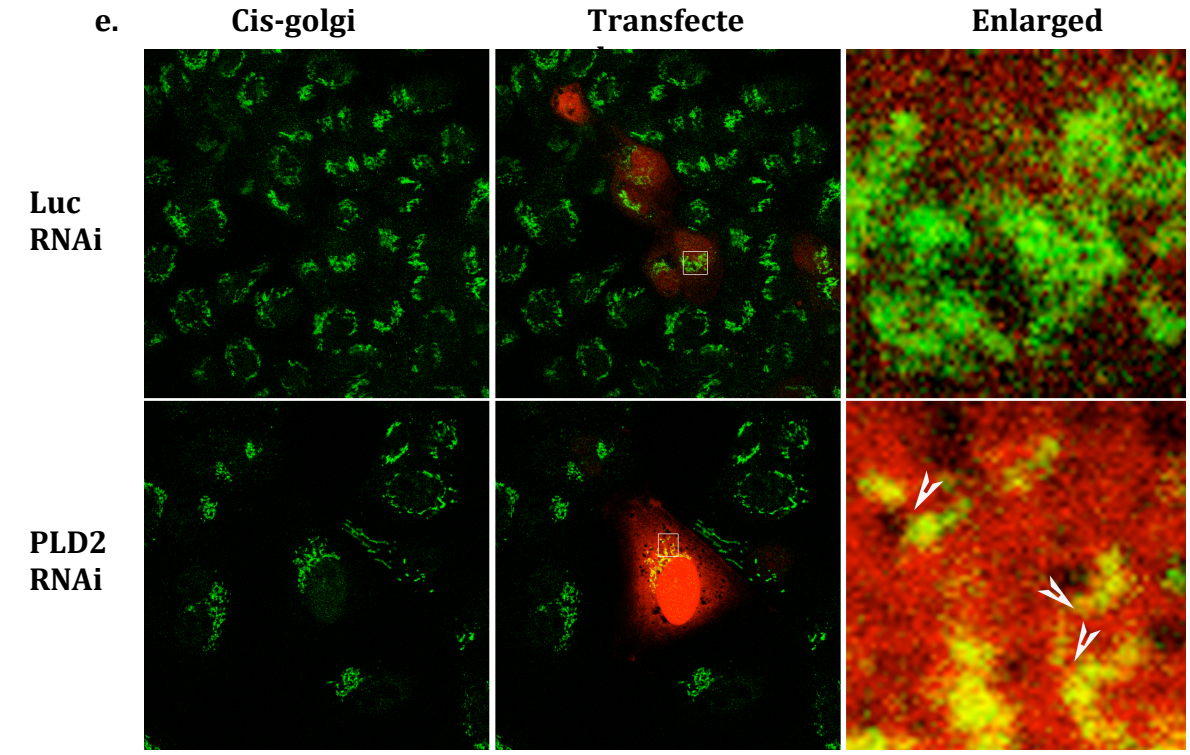
e.
Cis-golgi
Transfecte
Enlarged
Luc RNAi
PLD2 RNAi

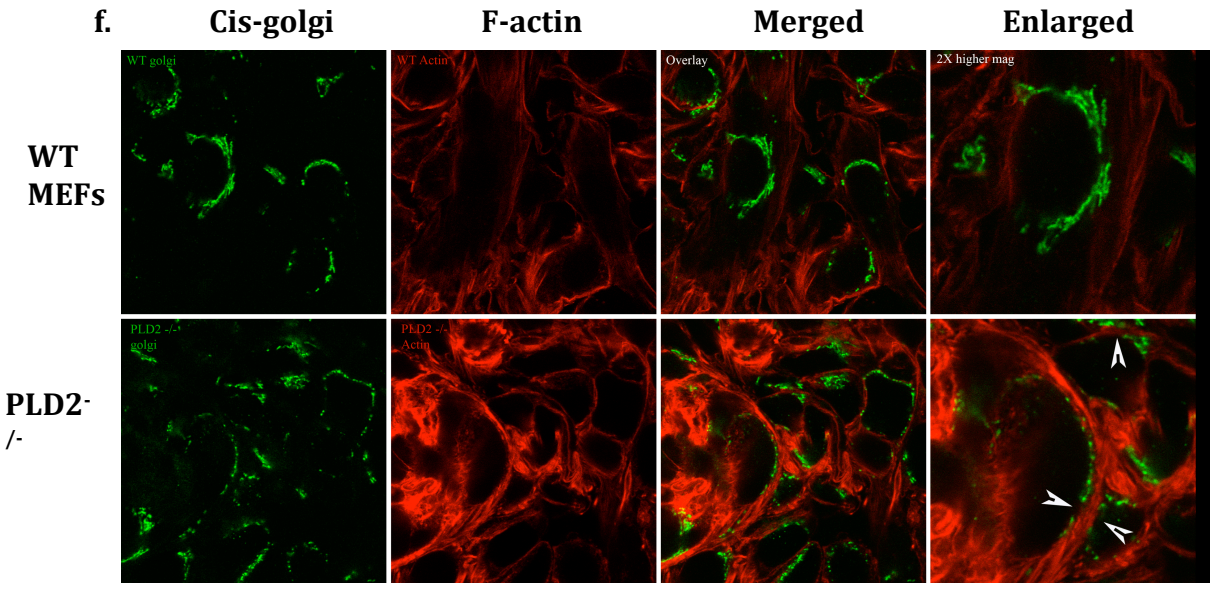
f.
Cis-golgi
F-actin
Merged
Enlarged
WT MEFs
PLD2-/-
WT golgi
WT Actin
Overlay
2X higher mag
PLD2 -/- golgi
PLD2 -/- Actin

Chapter 6

Imaging the pancreatic β-cell using NMR

Type I diabetes is a disease characterized by complete failure of β-cells to secrete insulin. Despite a strong genetic link, it is often difficult to predict when the disease will develop in susceptible individuals. Furthermore, the course of the disease is also difficult to predict in patients who have become symptomatic (Lin et al., 2008; Souza et al., 2006). This has significant therapeutic ramifications because patients need to be switched from secretagogues and sensitizers like metformin to insulin when there is significant β-cell failure. Detection of serum anti-glutamic acid decarboxylase (GAD), anti-islet and anti-insulin (IA2) antibodies have been utilized with limited success to determine β-cell destruction. However, these assays reveal evidence of on-going or prior autoimmunity, but provide limited ability to predict disease progression or severity. Because there is no direct way to image and assess functional β-cell mass, frequent monitoring of serum glucose levels is the current gold standard of treatment. The same challenges are encountered in patients who are undergoing therapy to preserve β-cells or those who have just received β-cell transplantation.

Current efforts to image β-cell mass involve PET scanning (Simpson et al., 2006; Wangler et al., 2004), SPECT imaging using radioactive ligands (Moore et al., 2001) or MRI with Mn^{2+} (Medarova and Moore, 2009). All these approaches are sensitive enough to detect large β-cell loss, but by this time the patient is usually symptomatic, so the utility of these approaches in the clinic is questionable. Also, since these methods often require repeated administration of radioactive or other contrast agents (Hampe et al.,

2005) their utility for monitoring the progress of treatment is not without risk, especially in pediatric populations where this disease is most devastating. Following the discovery that neural precursor cells (NPCs) posses unique metabolomic signals that could be identified by proton NMR (^{1}H-NMR) *in vitro* and MRS (^{1}H-MRS) *in vivo* (Manganas et al., 2007), I hypothesized that pancreatic β-cells could also be identified using ^{1}H-NMR and ^{1}H-MRS. This study further showed that increases in NPCs induced by electroconvulsive shock were detectable by ^{1}H-MRS suggesting that this approach was sensitive enough to detect low levels of a specific NPC metabolite and also detect changes in metabolite level that correlated with the number of NPCs present (Manganas et al., 2007). I decided to explore ^{1}H-NMR and ^{1}H-MRS as a non-invasive and quantitative approach to image β-cell mass.

Materials and methods

Cell lines and primary cells

Insulin-secreting β-cell lines; NIT-1, MIN6 and TC-β6 were purchased from ATCC. NIT-1 cells were cultured in F12 media + 10% fetal bovine serum (FBS) and MIN6 and TC-β6 were cultured in RPMI + 10% FBS. The alpha cell line α1 was also purchased from ATCC and cultured in DMEM + 10% calf serum. Fibroblast (3T3) and neuroendocrine (PC12) cell lines were purchased from ATCC and cultured in DMEM + 10% calf serum. Primary Islets were isolated as described in chapter 2. Briefly, Animals were sacrificed by CO_2 asphyxiation and the pancreas was removed. Mouse pancreata was then incubated in collagenase dissolved in HBSS buffer for 50 min. The digestion was terminated by washing with ice-cold HBSS containing 5% FBS three times. After the final wash, individual islets were hand picked under a dissecting microscope. The remaining cells are primary pancreatic acinar cells and were used for certain experiments. To dissociate islets into individual β-cells, islets were washed in PBS and incubated in trypsin for 15 min at 37^{o}. Complete media was added and the solution was passed through a 25G needle a few times to mechanically dissociate the islets to β-cells.

Homogenates

Freshly dissected whole pancreas was briefly rinsed in ice-cold PBS and then suspended in ice-cold PBS. The tissue was then briefly blended with a tissue homogenizer until no more solid tissue could be identified. This was regarded as 100%. Aliquots were then taken out and diluted in PBS at the percentages described for each experiment.

^{1}H-NMR scans

For adherent cells, cells were rinsed with PBS and briefly trypsinized. The trypsinization was stopped by adding complete media, centrifuged and resuspended in PBS. The cells were counted and the final amount used for each experiment was resuspended in 500 μL PBS. Homogenates, β-cells, acinar cells and islets were similarly resuspended in 500 μL PBS. For certain experiments, 5 μL TMS was added to the solution containing cells/homogenate. 100 μL of deuterium was added right before each scan. The entire solution was briefly mixed added to a cuvette and placed in a 16-Tesla NMR.

Results

Different cell lines possess different ^{1}H-NMR spectral scans

Our hypothesis that β-cell mass could be identified and quantified using NMR hinged on the emerging data that cells posses unique metabolites that can be readily identified by NMR. To test this in our system, I prepared and scanned 3 classes of cells. Insulinoma cell lines NIT-1, TC-β6 and MIN6 were used to represent insulin-secreting β-cells. I used PC12 cell lines to represent neuroendocrine cells. Similar to insulinoma cells, neuroendocrine cells also exhibit regulated exocytosis and need to be distinguished from β-cells. Additionally, neuroendocrine cells are chromaffin cells on the superior pole of the left kidney, inferior to the pancreas so signals generated from these cells need to be distinguished from signals generated by β-cells. I also included 3T3 cells (fibroblasts) because these signals should be readily distinguishable from insulinoma and neuroendocrine cells because they do not have the same agonist-stimulated exocytotic machinery. Signals emanating from fibroblasts also need to be distinguished from β-cells. First, I scanned PBS (not shown), which is the diluent for all our scans, and the spectrum for PBS is flat except the peak between 4.5 and 5.0, which represents H_2O. Scans of NIT-1, TC-β6 and MIN6 showed no differences among these cell lines (NIT-1 and TC-β6 shown Fig. 6-1a). The green spectrum corresponds to TC-β6 and the red spectrum corresponds to NIT-1. Close-ups of region 3.0 - 4.0 ppm (Fig. 6-1b) and 5.0 - 6.0 ppm (Fig. 6-1c) show similar peaks between NIT-1 and TC-β6 cell lines (note the black peaks represent PBS). Next I compared 3T3 to PC12 cells and found that they were significantly different from each other (Fig. 6-2). The blue peaks represent PC12 and the purple peaks correspond to 3T3 spectra. 3T3 cells compared to TC-β6 cell also showed

significant differences (Fig. 6-3a). For example, a higher resolution examination of the region between 3.0 - 4.0 ppm highlights several of the differences between 3T3 cells and TC-β6 cells (Fig. 6-3b). All the same scans were performed using NIT-1 and MIN6 cells using all the comparisons discussed above with the same results (not shown).

β-cell scans are different from alpha cells.

The functional pancreatic islet is composed largely of β-cells (85% - 90%), a small percentage of α-cells (~8%) and an even smaller amount of δ-cells (> 2%). Because of the close juxtaposition of β and α-cells I needed to scan and compare spectra from both cell lines. Scans of NIT-1 and α-1 cell lines show significant difference between the two (Fig. 6-4a). Closer examination of regions 2.0 – 3.0 ppm (Fig. 6-4b) and 3.0 – 4.0 ppm (fig. 6-4c) highlights the differences between both species of cells. Based on these results, I have proof of principle that cells of different lineages are different from one another and can be visually distinguished by ^{1}H-NMR. Further, closely apposed β and α-cells are easily distinguished by ^{1}H-NMR.

Unique spectral peaks are not a result of cell-culture media

The different cell lines used in our experiments were cultured in different media and I wondered if the media made any contribution to the spectral scans I was observing. I performed spectral scans on the 3 media types I use for the culturing the cell lines. I found minor differences among spectral scans conducted on F12, DMEM and RPMI media (Fig. 6-5a), but they were mostly similar. I then cultured 3T3 cells in each of the media for 48 hours and scanned the cells (Fig. 6-5b). I did not find any differenced

among 3T3 cells cultured in F12, DMEM or RPMI media. Hence, differences in spectra among different cell lines was not due to contamination or metabolites unique to the media they were cultured in.

Primary β-cells posses different scans from primary acinar cells

The majority of the pancreas is composed of the exocrine pancreas. These acinar cells secrete digestive enzymes and are present in overwhelming numbers compared to endocrine (β-cells) pancreatic cells. Distinguishing the signal generated from acinar cells is extremely important in the development of any *in situ* β-cell quantification method. An overwhelming signal from acinar cells could potentially drown-out β-cell signals. To address this issue, I purified primary β-cells and acinar cells from mice. ^{1}H-NMR scanning revealed that β-cells generated a unique spectra and was visually distinguishable from acinar cells (Fig. 6-6a-c).

^{1}H-NMR can distinguish pancreatic homogenates from WT and type-I diabetic animals.

Ultimately, ^{1}H-NMR should not only be able to distinguish different cell types from one another but it should be able to quantitate functional pancreatic β-cell mass. In the first step towards this goal, I switched to using whole pancreatic homogenates for β-cell spectral scans. Since our earlier studies with cell lines and primary cells suggested that β-cell spectra was sufficiently unique enough from acinar and other contaminating cell types, I felt confident proceeding in this direction. I used the pharmacological agent streptozocin (STZ) to induce type-I diabetes in mice. STZ is a toxin that selectively

induces apoptosis in Glut-2 positive cells (β-cells). I injected C57 black mice with 200 mg/Kg STZ for 1 day, 3 days or 7 days. At the 7-day time point, all animals (including "no-injection" controls) were sacrificed and their entire pancreas was homogenized and subjected to ^{1}H-NMR analysis. Overview of the entire spectra did not show any immediate difference because of the overall low resolution (Fig. 6-7a). However, when individual sections are compared, differences in the amplitude of several spectra are obvious. The interval 1.0 – 2.5 ppm shows a gradual decrease in the peak at approximately 2.4 ppm. This peak is prominent in the control, 1-day and 3-day post- STZ but is notably absent 7-day post STZ treatment (Fig. 6-7b). The region between 2.5 – 3.5 ppm also shows a peak at approximately 3.04 ppm that gradually decreases with the length of STZ treatment (Fig. 6-7c). The region between 3.5 – 4.5 ppm (Fig. 6-7d) does not show any apparent differences. The study has been repeated multiple times and all the groups show consistency between scans taken months apart on different animals. Scans on control animals (Fig. 6-8a), 1-day post-STZ (Fig. 6-8b), 3-day post-STZ (Fig. 6-8c) and 7-day post-STZ (Fig. 6-8d) all show remarkable consistency.

PCA mathematical categorization differentiates healthy from diabetic animals

In collaboration with Dr. Petar Djuric (Stony Brook University) of the Engineering department, healthy and diabetic animals that had been treated with STZ for varying amounts of time were mathematically modeled and distinguished using Principal Component Analysis (PCA). Mathematical characterization and classification is important because it eliminates human error and it also takes the entire spectrum into consideration instead of individual peaks.

Discussion

I have undertaken and successfully completed the prerequisite *in vitro* studies required for *in vivo* quantification of β-cell mass using ^{1}H-NMR. Here I show that different cell lines can be distinguished from each other using ^{1}H-NMR. Insulinoma cells are visually distinguishable from fibroblasts and neuroendocrine cells. I further demonstrate that primary β-cells can be distinguished from primary acinar cells which constitute the majority of pancreatic cell mass. Finally, I show quantitative differences between control and an experimental type-I diabetes mouse model. Animals injected with STZ, a β-cell toxin, showed identifiable decreases in unique spectral peaks. A peak at 3.04 ppm is a prominent example but there are also a few other peaks that can be visually scored. Animals that had been treated with the toxin the longest (i.e. 7 days) showed the most significant deceases in signal amplitude and mice treated for shorter periods showed less reduction compared to control mice.

Since visual inspection of peaks can be subject to experimenter bias, I collaborated with signal analysis experts who were able to convert the spectral scans to unique mathematical models that described control, 1-day, 3-day and 7-day diabetic mice. These models could automatically identify which scan belonged to which treatment paradigm without human intervention. This approach provides a more powerful approach to visual spectra characterization. Visual characterization depends on identification of individual peaks, some of which might to too small to distinguish. Deconstructing each spectrum to individual points and then mathematically modeling its constituent points can describe the whole spectrum. This promotes automatic classification and removes experimenter bias.

The next step in this research is to move to *in vivo* ^{1}H-MRS (the *in vivo* cognate of ^{1}H-NMR). In this approach, live animals will have their panaceas scanned *in situ*. The resulting spectrum will then be compared to STZ-injected mice and other genetic models of diabetes. These scans can then be subjected to PCA or equivalent mathematical analysis and a predictive model that quantifies the degree of β-cell destruction can be generated. These studies will set the stage for non-invasive ^{1}H-MRS scanning of people with the hope of early type-I diabetes detection, especially in pediatric populations. This technology will enable physicians to follow islet-transplant patients to monitor rejection and patients undergoing therapy to preserve endogenous β-cell function.

Figure 6-1. Insulinoma cell lines have similar NMR spectra.
(a). NIT-1 (red) and TC-β6 (green) cell lines were subjected to NMR scanning. Spectra shown covers 0.0 ppm – 7.0 ppm. Water peak is located between 4.5 ppm – 5.0 ppm. (b). Region 3.0 ppm – 4.0 ppm of NIT-1 and TC-β6 spectra shown. Note PBS (black plot) spectra also plotted in this graph. (c). Region 5.0 ppm – 6.0 ppm of NIT-1 and TC-β6 spectra.

Figure 6-1

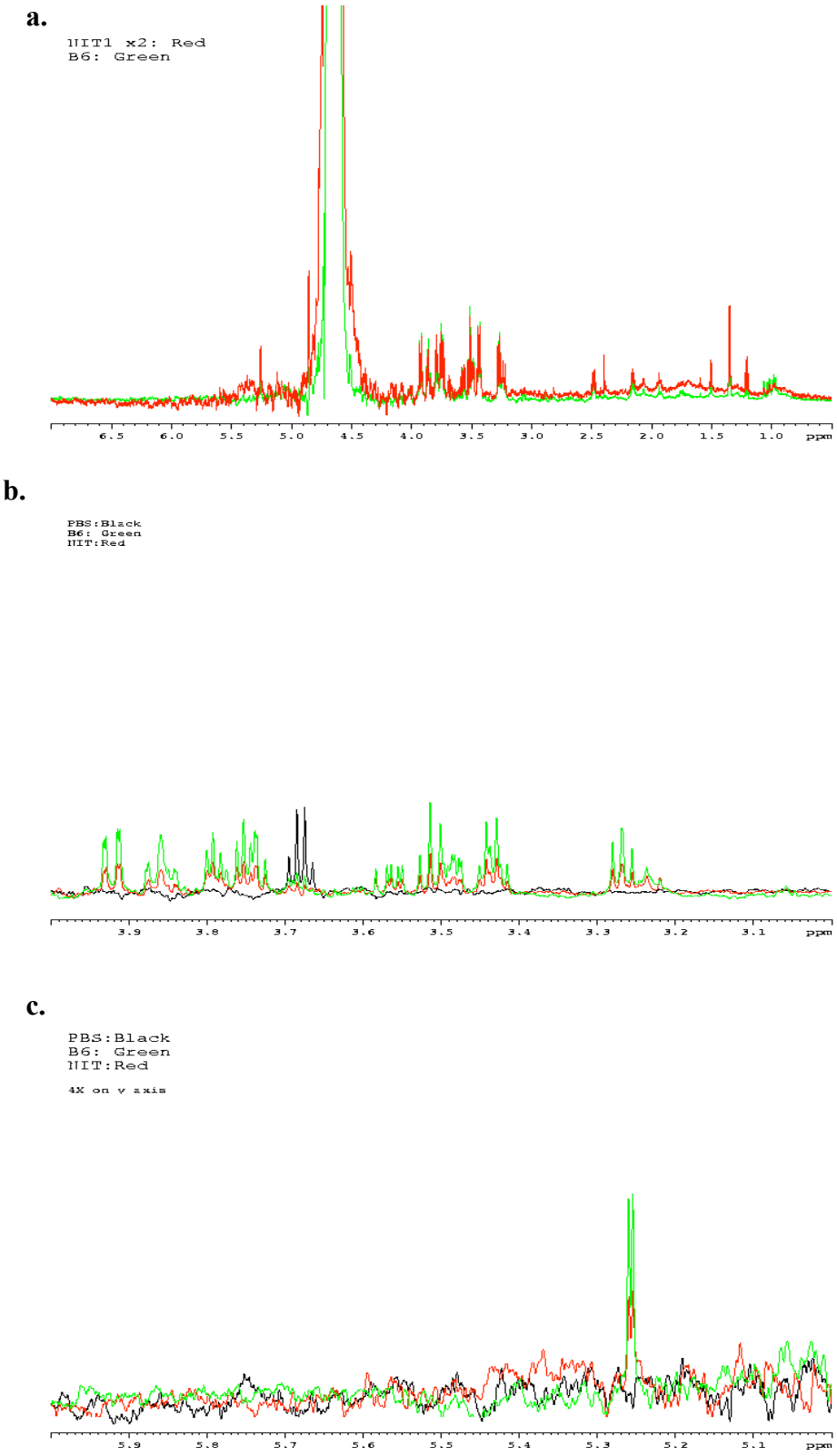
a.
HIT1 x2: Red
B6: Green
6.5 6.0 5.5 5.0 4.5 4.0 3.5 3.0 2.5 2.0 1.5 1.0 ppm
b.
PBS:Black
B6: Green
HIT:Red
3.9 3.8 3.7 3.6 3.5 3.4 3.3 3.2 3.1 ppm
c.
PBS:Black
B6: Green
HIT:Red
4X on y axis
5.9 5.8 5.7 5.6 5.5 5.4 5.3 5.2 5.1 ppm

Figure 6-2. Other cell lines are different from one another.
Neuroendocrine PC12 (blue) and fibroblast 3T3 (purple) cell lines were scanned and the spectrum plotted from 0.0 ppm – 10.0 ppm.

Figure 6-2

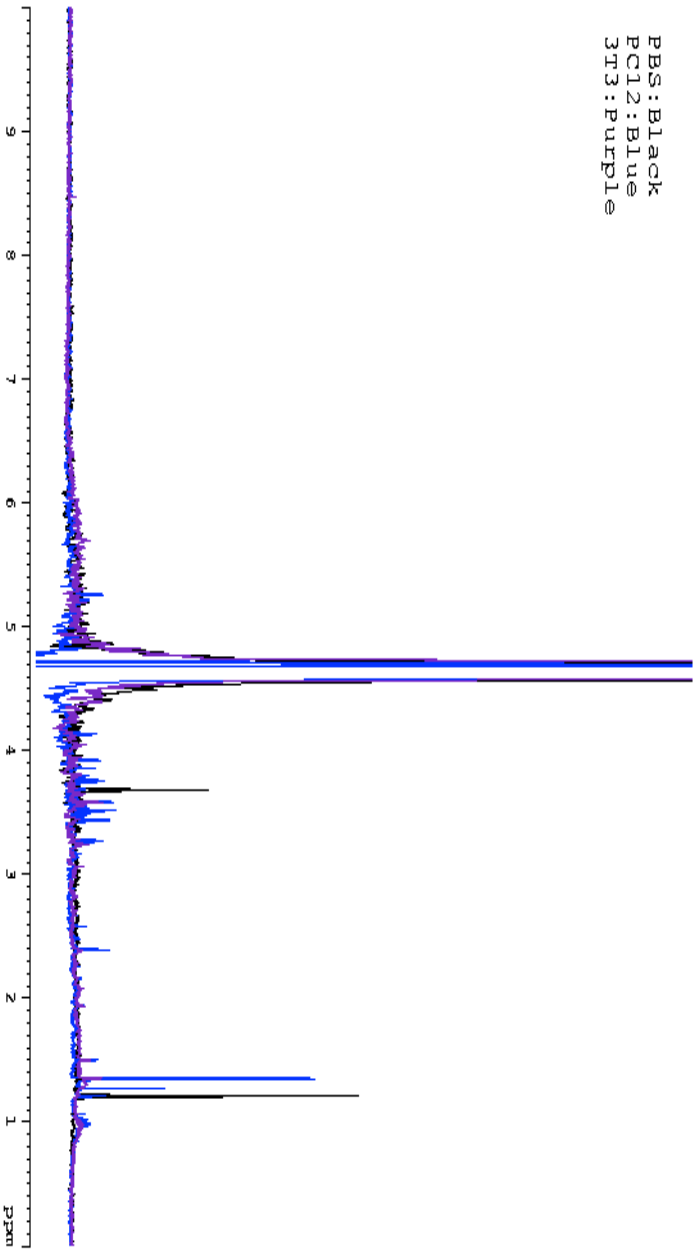

Figure 6-3. Insulinoma cells can be differentiated from fibroblasts by NMR.
(a). NMR plot of TC-β6 (green) and 3T3 (purple) cell lines over the range of 0.0 ppm – 10.0 ppm. (b). Spectrum of TC-β6 (green) and 3T3 (purple) between 3.0 ppm – 4.0 ppm. In both cases, PBS spectrum is also plotted in black.

Figure 6-3

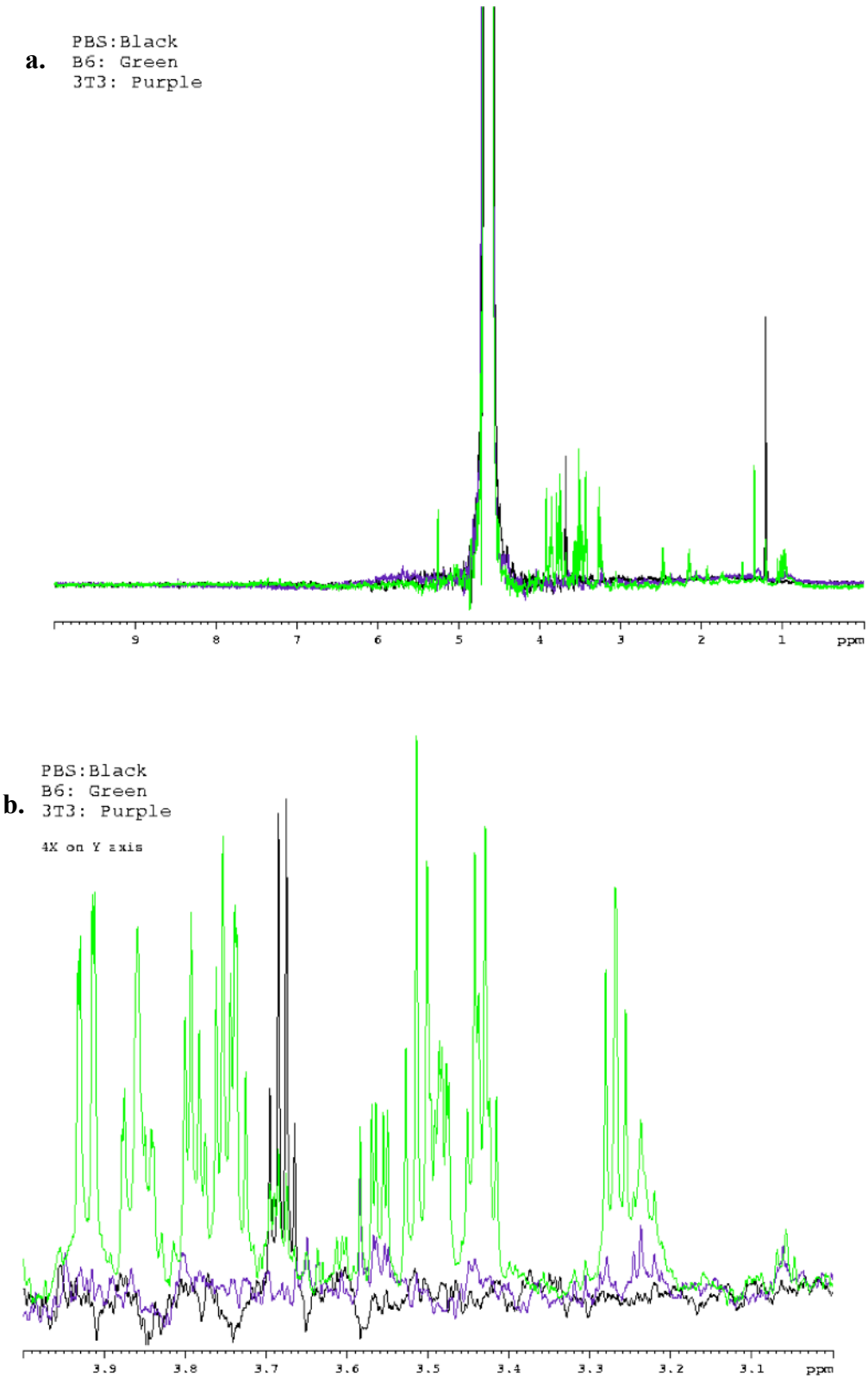
a.
PBS:Black
B6: Green
3T3: Purple
9
8
7
6
5
4
3
2
1
ppm
b.
PBS:Black
B6: Green
3T3: Purple
4X on Y axis
3.9
3.8
3.7
3.6
3.5
3.4
3.3
3.2
3.1
ppm

Figure 6-4. Insulin secreting β-cells can de distinguished from α-cells by NMR.
(a). β-cell line NIT1 (red) and α-cell line α-1 (brown) NMR scans plotted between 0.0 ppm – 2.0 ppm. (b). NIT1 and α-1 scans representing regions 2.0 ppm – 3.0 ppm shown. (c). Regions 3.0 ppm – 4.0 ppm of NIT1 and α-1 NMR scans.

Figure 6-4

a.

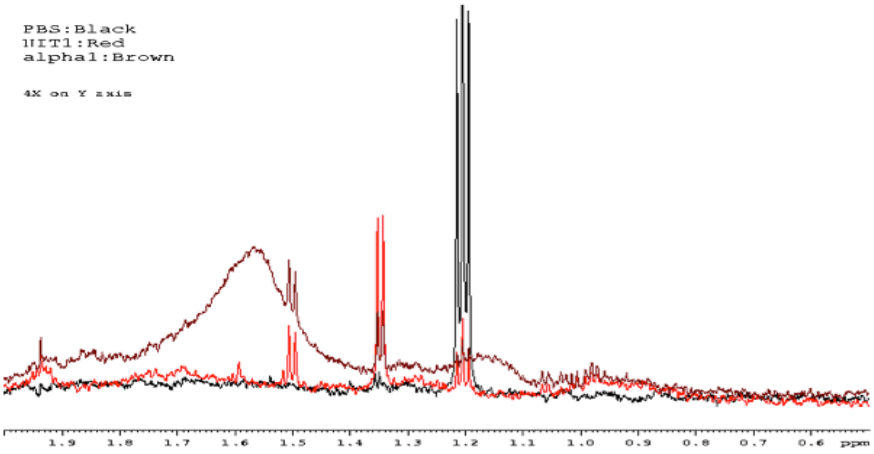

b.

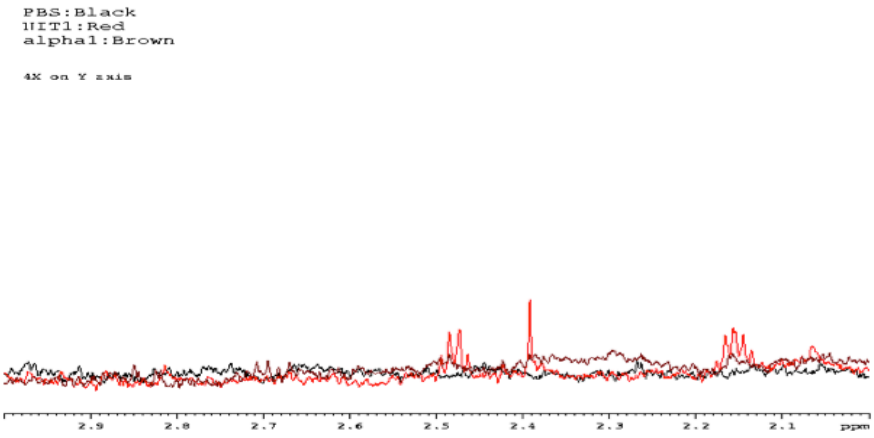

c.

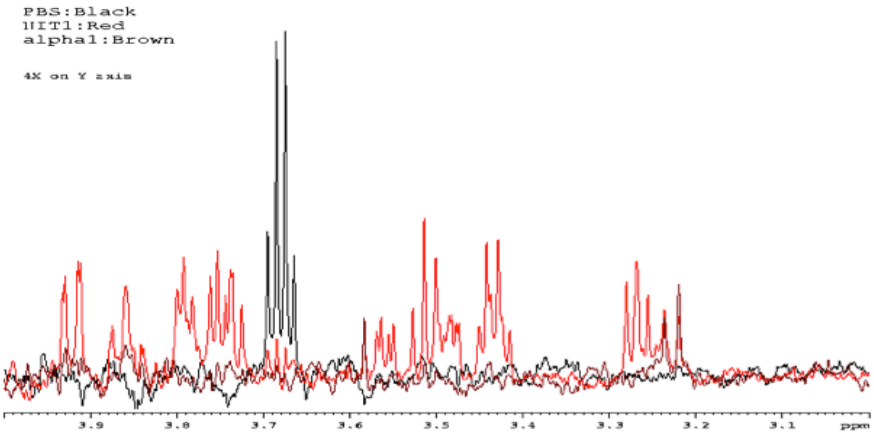

Figure 6-5. Culture media does not affect Cell-line NMR scans.
(a). NMR scans of different culture media used in NMR experiments. DMEM (black), RPMI (red) and F12 (blue). Regions 0.0 ppm – 10.0 ppm plotted. (b). NMR scans of 3T3 cells cultured for 48 hours in either DMEM (black), RPMI (red) or F12 (blue) media. Regions 0.0 ppm – 10.0 ppm plotted.

Figure 6-5

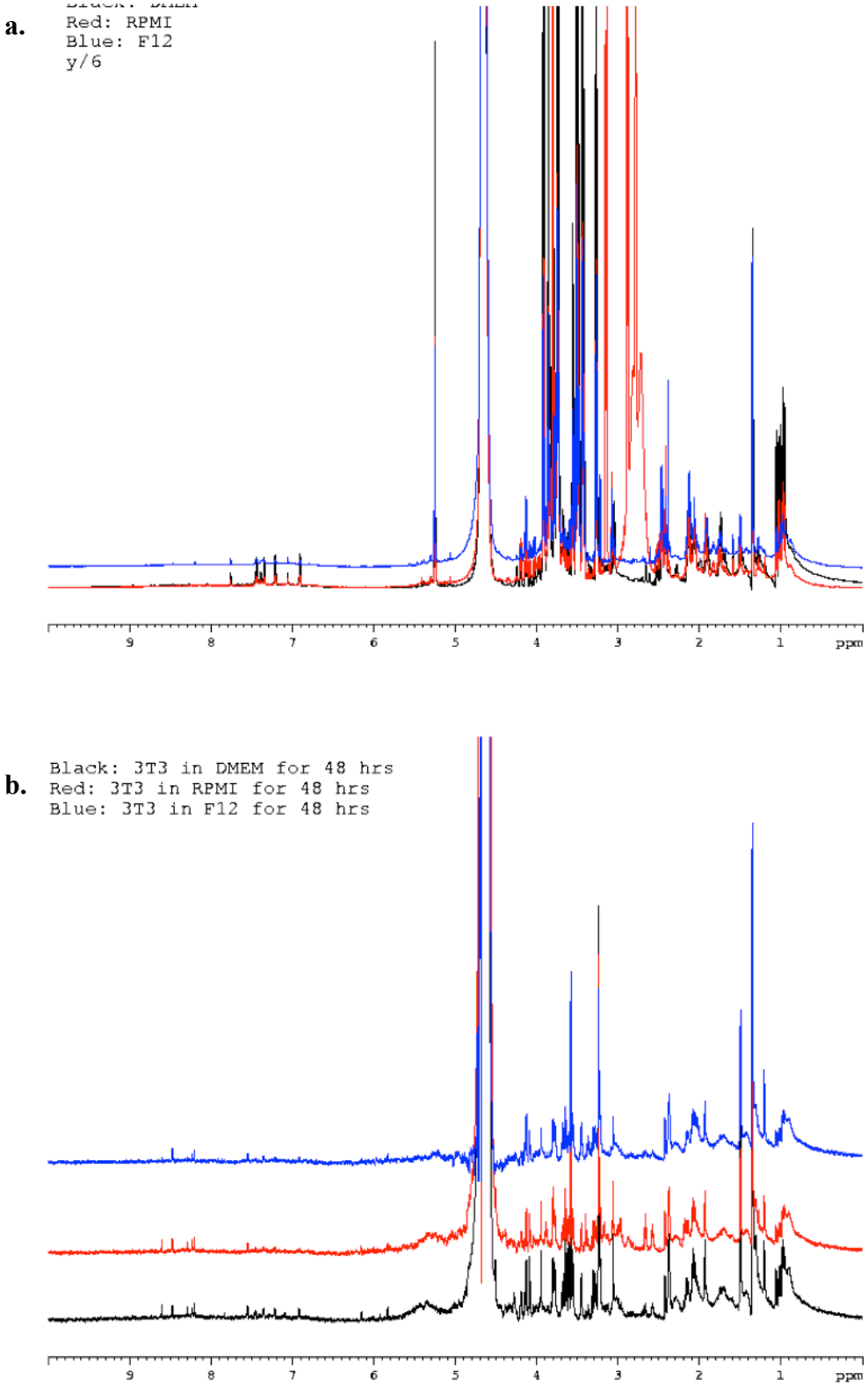
a.
Red: RPMI
Blue: F12
y/6
9
8
7
6
5
4
3
2
1
ppm
b.
Black: 3T3 in DMEM for 48 hrs
Red: 3T3 in RPMI for 48 hrs
Blue: 3T3 in F12 for 48 hrs
9
8
7
6
5
4
3
2
1
ppm

Figure 6-6. Primary β-cells posses different scans from primary acinar cells.
(a). Isolated primary β-cells and primary acinar cells were scanned by NMR. β-cell spectrum (red) and acinar cell spectrum (black) are plotted from 0.0 ppm – 2.0 ppm. (b). β-cell and acinar cell spectrum plotted from 2.0 ppm – 3.5 ppm. (c). β-cell and acinar cell spectrum plotted from 3.5 ppm – 4.5 ppm.

Figure 6-6

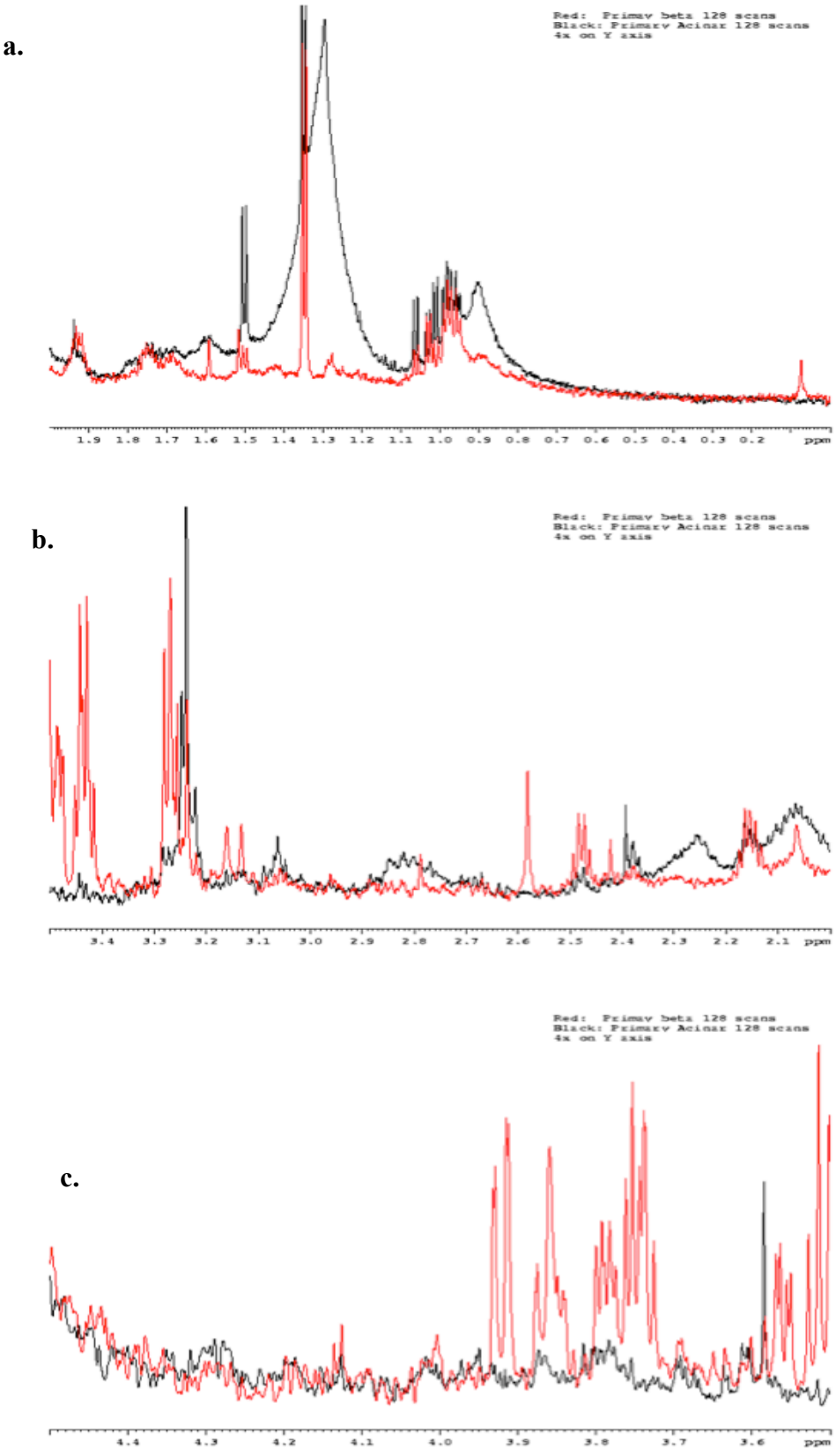
a.
Red: Primav beta 128 scans
Black: Primary Acinar 128 scans
4x on Y axis
1.9 1.8 1.7 1.6 1.5 1.4 1.3 1.2 1.1 1.0 0.9 0.8 0.7 0.6 0.5 0.4 0.3 0.2 ppm
b.
Red: Primav beta 128 scans
Black: Primary Acinar 128 scans
4x on Y axis
3.4 3.3 3.2 3.1 3.0 2.9 2.8 2.7 2.6 2.5 2.4 2.3 2.2 2.1 ppm
Red: Primav beta 128 scans
Black: Primary Acinar 128 scans
4x on Y axis
c.
4.4 4.3 4.2 4.1 4.0 3.9 3.8 3.7 3.6 ppm

Figure 6-7. Homogenate scans of WT and diabetic animals reveal differences by NMR.
(a). Pancreatic homogenates from WT and STZ-treated animals were prepared and scanned by NMR. Homogenates from control (black), 1-day post- STZ treatment (blue), 3-day post-STZ treatment (red) and 7- day post STZ treatment (green) scans from region 0.0 ppm – 10.0 ppm shown. (b). Regions 0.0 ppm – 2.5 ppm of STZ treated animals. (c). 2.5 ppm – 3.5 ppm sections and (d). 3.5 ppm – 4.5 ppm regions of pancreatic homogenates prepared from STZ treated animals. Diabetes was confirmed in treated animals and defined as plasma glucose > 20 mmol/L.

Figure 6-7

a.

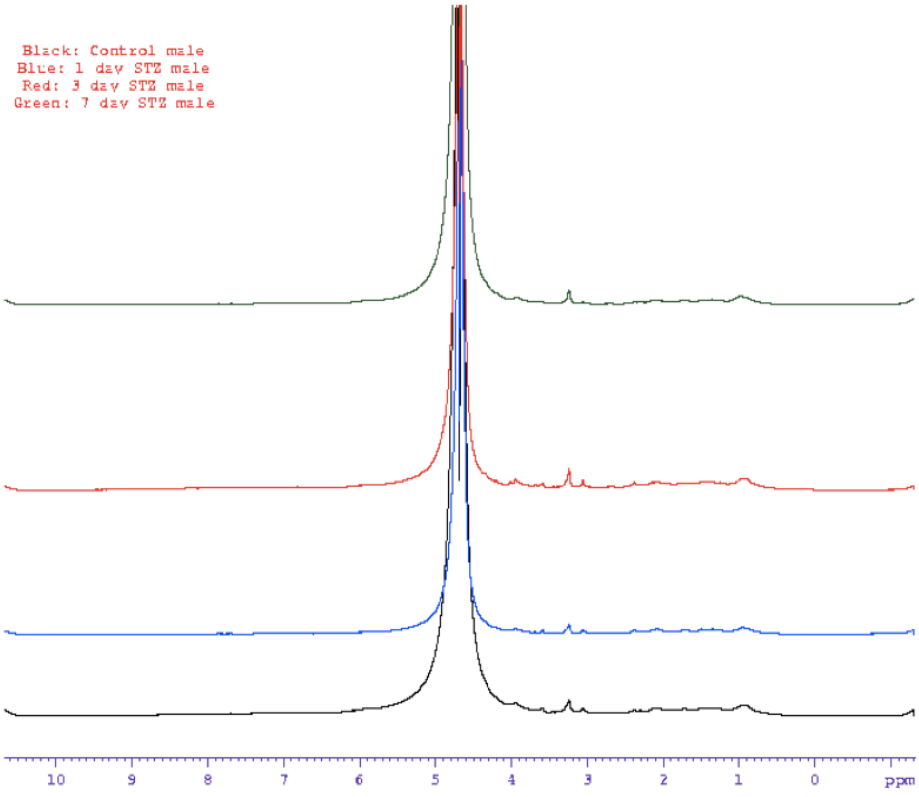
Black: Control male
Blue: 1 day STZ male
Red: 3 day STZ male
Green: 7 day STZ male
10
9
8
7
6
5
4
3
2
1
0
ppm

Figure 6-7

b.

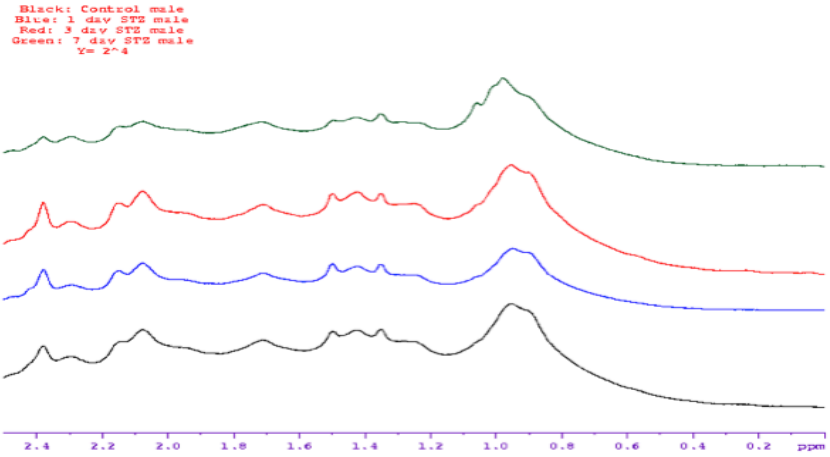

c.

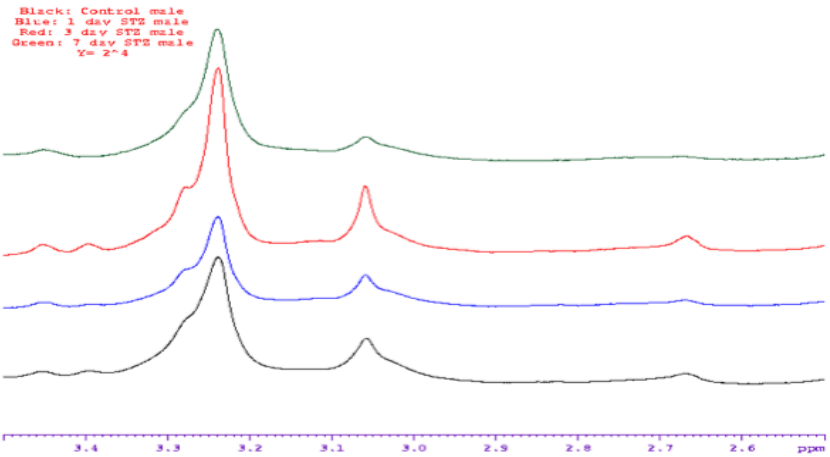

d.

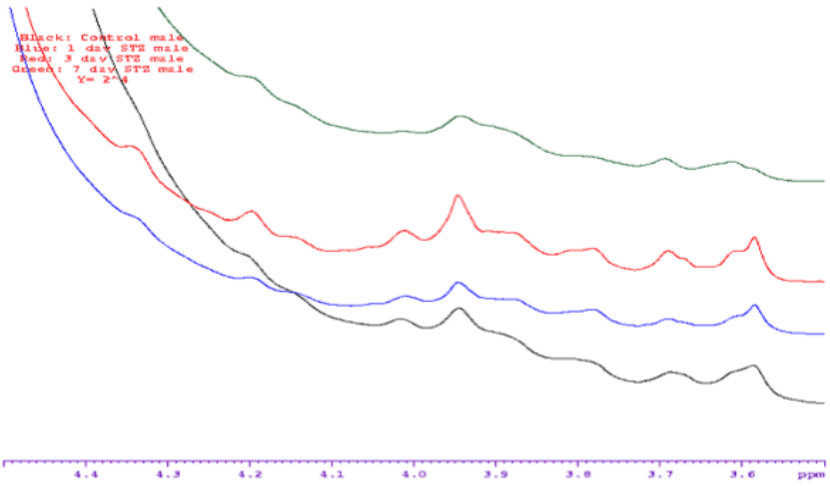

Figure 6-8. NMR scans of pancreatic homogenates are consistent between various animals.
(a). Scans of 4 different non-STZ treated control animals. Regions 0.0 ppm – 10.0 ppm shown. (b). Scans of 2 different animals treated with STZ and scanned 1 day later, regions 2.5 ppm – 4.5 ppm. (c). Scans of 3 different animals treated with STZ and scanned 3 days later, regions 0.0 ppm – 10 .0 ppm shown and (d). 2 animals treated with STZ ad scanned 7 days later. Regions 0.0 ppm - 10.0 ppm shown.

Figure 6-8

a.

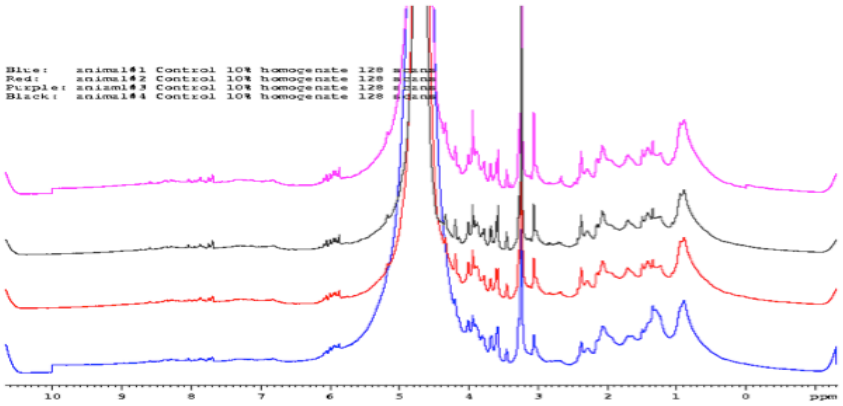

b.

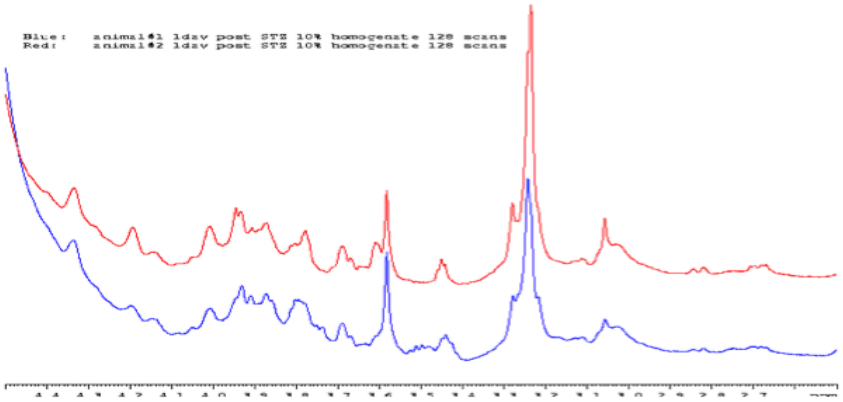

c.

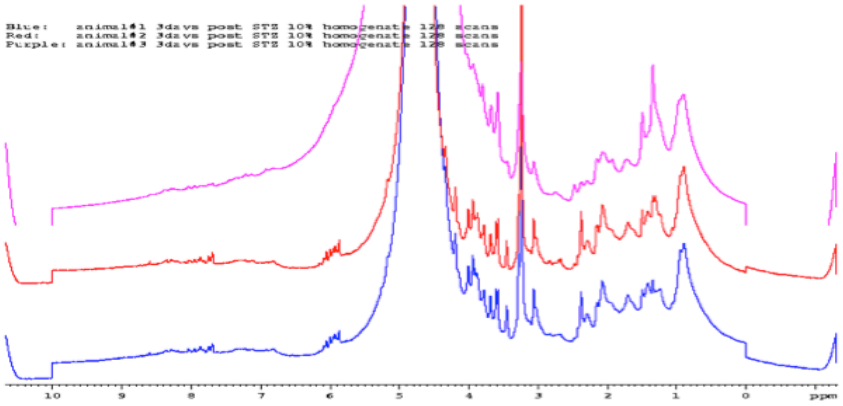

d.

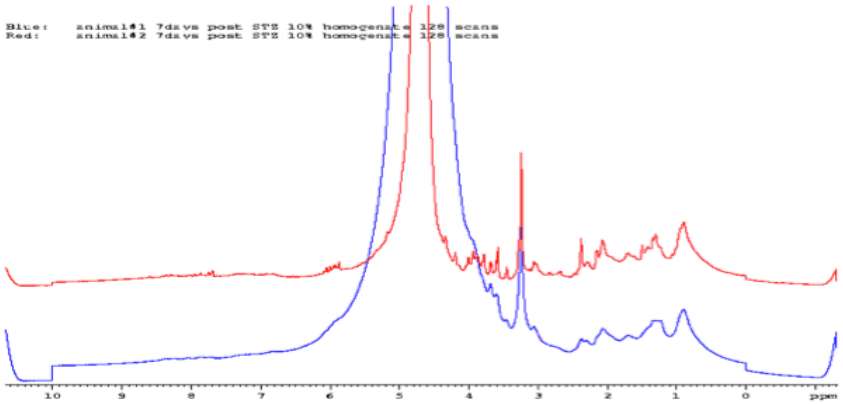

Chapter 7

Conclusion

PLD2, insulin secretion and disease

Diabetes is a disease characterized by failure of β-cells to secrete insulin, insensitivity of peripheral tissue to insulin, or both. In insulin-resistant type-II diabetes, peripheral tissue insensitivity to insulin leads to increased insulin secretion by β-cells. To maintain euglycemia, β-cells secrete ever-increasing amounts of insulin over time eventually leading to β-cell burnout. At this point, β-cells paradoxically secrete less insulin and the patient has to take exogenous insulin for survival. In non-insulin resistant forms of type-II diabetes, β-cells secrete inadequate amounts of insulin to maintain euglycemia. This form of diabetes is very similar to early stages of type-I diabetes where gradual failure of β-cell function is manifest as worsening hyperglycemia. An important class of drugs used for the management of early type-I and type-II diabetes are sulfonylureas. Glipizide is an example of this class of drugs and it functions primarily by inhibiting β-cell K^+ channels leading to increased Ca^{2+} influx and insulin release. One of the major drawbacks of this class of drugs is their propensity to facilitate too much insulin secretion and cause hypoglycemia.

In this study I demonstrate that $PLD2^{-/-}$ mice have resting and fasting hypoglycemia. $PLD2^{-/-}$ mice also have enhanced GTT, clearing glucose more rapidly than WT animals. Insulin tolerance tests strongly suggest that the effect of PLD2 is in the β-cell and this is confirmed by *ex vivo* islet stimulation with glucose. Islets isolated from $PLD2^{-/-}$ mice secrete more insulin when stimulated with low and high glucose concentrations compared to WT islets. Microarray analysis of WT and $PLD2^{-/-}$ islets

show down-regulation of an IP_3R inhibitor. Further studies using IP_3R, PLC, and VDCC inhibitors show that PLD2 hypersecretory phenotype is primarily due to increased influx of Ca^{2+} upon stimulation leading to increased insulin release. This is what happens downstream of glipizide activity, albeit via a different mechanism. Cursory behavioral monitoring of $PLD2^{-/-}$ mice does not yield any signs of pathological hypoglycemia. For instance, sluggish activity, withdrawal or seizures have not been observed in these animals, even after fasting. More stringent behavioral studies, including stressful situations will be required in order to fully characterize the consequences of hypoglycemia in the $PLD2^{-/-}$ mice. The possibility of PLD2 as a therapeutic target in the management of diabetes is still very appealing. I already have an orally bioavailable pan-PLD inhibitor with no documented adverse effects (Monovich et al., 2007; Su et al., 2009). Isoform-specific inhibitors are now available (Scott et al., 2009) but they still require optimization for animal pharmacodynamics and pharmacokinetics. Animals with dominant negative Kir6.2 channel expression (mimicking glipizide treatment) have severe hypoglycemia, high resting membrane potential and intracellular Ca^{2+} (Miki et al., 1997). Animals with complete knockout of the Kir6.2 channel are paradoxically diabetic (Miki et al., 1998), indicating the requirement of functional K^+ channels that can close in response to rising ATP levels and trigger Ca^{2+} influx. Comparatively, $PLD2^{-/-}$ mice exhibit increased insulin release without excessive hypoglycemia or neurological deficit (as far I can tell). This suggests that carefully titrated pharmacological inhibition of PLD2 might be beneficial in diabetes management. I would also be very curious to see if PLD2 inhibition delays onset or severity of diabetes in mouse genetic diabetes models such as db/db mice.

PLD2, golgi apparatus and disease

Golgi structural and functional integrity is critical for cell homeostasis. Various proteins are trafficked from the ER via the Golgi to the plasma membrane and various organelles. Failure of this trafficking process is an underlying cause of several diseases including lysosomal storage disorders (Nadimpalli and Amancha, 2009) and diabetes insipidus (Savelkoul et al., 2009). The role of PLD in the regulation of golgi trafficking is not yet fully understood. Inhibition of both PLD isoforms using 1-butanol leads to golgi fragmentation (Freyberg et al., 2003). However, treatment of insulinoma cells with FIPI, a more specific pan-PLD inhibitor does not lead to the same effect. PLD1 has been proposed to localize to the ER where it facilitates Sar1p recruitment of COPII proteins (Roth et al., 1999). Cells exhibiting increased PLD1 activity were further shown to have accelerated anterograde and retrograde trafficking. Experiments on reconstituted golgi membranes *in vitro* have suggested a role for PLD2 in COPI coatomer recruitment and retrograde trafficking (Yang et al., 2008). In all these cases, PA has been suggested to be the main effector of PLD activity but high levels of DAG have also been found on golgi membranes with high PLD activity (Roth et al., 1999), suggesting a second player involved in metabolizing PA to DAG on the membrane surface.

Other studies using insulinoma cell lines and primary β-cells support a role for PLD2 in the maintenance of *cis*-golgi architecture. While PLD2 has been shown to associate with the golgi (Freyberg et al., 2002; Yang et al., 2008), its exact role *in vivo* has yet to be characterized. Our studies show that PLD2 might facilitate *cis*-golgi vesicle budding. Knockout and knockdown of PLD2 leads to tubulated *cis*-golgi, suggesting a failure of vesicles to bud off a growing *cis*-golgi surface. However, overexpression of

PLD2 or stimulation of endogenous PLD activity with PMA also led to *cis*-golgi tubulation. This seemingly contradictory result would suggest that while generation of PA is important for fission, there is another factor downstream that is also playing a role in vesicle fission. Microarray screen of PLD2$^{-/-}$ islets showed down-regulation of PITPNM3, a transmembrane protein that I show is an enzyme with hypothetical PAP activity. This finding hints at a role for the conversion of PA to DAG for proper golgi function. Too little PA leads to down-regulation of PITPNM3 and too little DAG in our PLD2$^{-/-}$ scenario, while overexpression of PLD2 also leads to *cis*-golgi tubulation. To our knowledge, this is the first report of the golgi surface serving as a lipid signaling platform where dysregulation of PA metabolism leads to tubulation.

While I have not directly assessed the role of PLD1 in golgi architecture maintenance, I have shown data that suggests that it plays an apposed role to PLD2. Golgi tubulation caused by PLD2 inhibition was rescued by PLD1 inhibition. I have proposed a model that could account for these findings (Fig. 4-5). PLD2 could potentially be facilitating retrograde traffic while PLD1 facilitates anterograde traffic. Inhibition of PLD2 leads to a defect in retrograde trafficking while anterograde traffic is unperturbed. Over time, increased forward flow without adequate return of content to the ER would lead to tubulation. Inhibition of PLD1 in this context would slow forward traffic leading to a rescue of the PLD2 phenotype. However, more work needs to be done on the role of both PLD isoforms in golgi trafficking before a clearer picture can emerge.

Emerging role for PLD2 in vesicle trafficking and disease

Thus far, I have explored the role of PLD2 in both specialized secretory (chapter 2-4) and non-secretory cells (chapter 5). The consequences of defective vesicle trafficking and disease are obvious. I have just set out to investigate instances where defective signaling might prevent disease. For instance, budding viral particles depend on intact ER and golgi vesicle transport pathways to transport their proteins to the cell surface. I hypothesize that interruption of this pathway would lead to a reduction in viral particle infectivity, entry, or replication. Recently, a genome wide screen of RNAi targets required for influenza virus replication in human cells showed PLD2 as a possible candidate (Karlas et al., 2010). With this in mind, I examined if pan-PLD inhibition using FIPI had any effect on the transport of HA, an important influenza virus protein. Work by Bi *et al* (Bi et al., 1997) had demonstrated that PLD-generated PA was required for ER to golgi transport, a critical step for HA transport to the plasma membrane. Excitingly, I found that treatment of MDCK cells with FIPI inhibited translocation of HA to the plasma membrane (not shown), with the majority of the HA found to be localized to the cytoplasm.

This and our other studies mark the beginning of the re-exploration of the roles of PLD using more specific and sensitive tools. Bearing in mind that PLD1 and PLD2 might play different roles in different cell types, context-specific exploration of PLD1 and PLD2 will also yield new insight into their roles in health and disease.

References

Aguilar-Bryan, L., J. Bryan, and M. Nakazaki. 2001. Of mice and men: K(ATP) channels and insulin secretion. Recent Prog Horm Res 56:47-68.

Asp, L., C. Claesson, J. Boren, and S. O. Olofsson. 2000. ADP-ribosylation factor 1 and its activation of phospholipase D are important for the assembly of very low density lipoproteins. J Biol Chem 275:26285-92.

Balboa, M. A., J. Balsinde, E. A. Dennis, and P. A. Insel. 1995. A phospholipase D-mediated pathway for generating diacylglycerol in nuclei from Madin-Darby canine kidney cells. J Biol Chem 270:11738-40.

Bankaitis, V. A. 2009. The Cirque du Soleil of Golgi membrane dynamics. J Cell Biol 186:169-71.

Bankaitis, V. A., D. E. Malehorn, S. D. Emr, and R. Greene. 1989. The Saccharomyces cerevisiae SEC14 gene encodes a cytosolic factor that is required for transport of secretory proteins from the yeast Golgi complex. J Cell Biol 108:1271-81.

Bankaitis, V. A., S. Phillips, L. Yanagisawa, X. Li, S. Routt, and Z. Xie. 2005. Phosphatidylinositol transfer protein function in the yeast Saccharomyces cerevisiae. Adv Enzyme Regul 45:155-70.

Barlowe, C., L. Orci, T. Yeung, M. Hosobuchi, S. Hamamoto, N. Salama, M. F. Rexach, M. Ravazzola, M. Amherdt, and R. Schekman. 1994. COPII: a membrane coat formed by Sec proteins that drive vesicle budding from the endoplasmic reticulum. Cell 77:895-907.

Baron, C. L., and V. Malhotra. 2002. Role of diacylglycerol in PKD recruitment to the TGN and protein transport to the plasma membrane. Science 295:325-8.

Bi, K., M. G. Roth, and N. T. Ktistakis. 1997. Phosphatidic acid formation by phospholipase D is required for transport from the endoplasmic reticulum to the Golgi complex. Curr Biol 7:301-7.

Bichet, D. G. 2008. Vasopressin receptor mutations in nephrogenic diabetes insipidus. Semin Nephrol 28:245-51.

Birn, H., H. Vorum, P. J. Verroust, S. K. Moestrup, and E. I. Christensen. 2000. Receptor-associated protein is important for normal processing of megalin in kidney proximal tubules. J Am Soc Nephrol 11:191-202.

Boivin, B., G. Vaniotis, B. G. Allen, and T. E. Hebert. 2008. G protein-coupled receptors in and on the cell nucleus: a new signaling paradigm? J Recept Signal Transduct Res 28:15-28.

Brindley, D. N., and D. W. Waggoner. 1996. Phosphatidate phosphohydrolase and signal transduction. Chem Phys Lipids 80:45-57.

Brown, D. 2003. The ins and outs of aquaporin-2 trafficking. Am J Physiol Renal Physiol 284:F893-901.

Brown, F. D., N. Thompson, K. M. Saqib, J. M. Clark, D. Powner, N. T. Thompson, R. Solari, and M. J. Wakelam. 1998. Phospholipase D1 localizes to secretory granules and lysosomes and is plasma-membrane translocated on cellular stimulation. Curr Biol 8:835-8.

Brown, H. A., S. Gutowski, R. A. Kahn, and P. C. Sternweis. 1995. Partial purification and characterization of Arf-sensitive phospholipase D from porcine brain. J Biol Chem 270:14935-43.

Brown, H. A., S. Gutowski, C. R. Moomaw, C. Slaughter, and P. C. Sternweis. 1993. ADP-ribosylation factor, a small GTP-dependent regulatory protein, stimulates phospholipase D activity. Cell 75:1137-44.

Caumont, A. S., M. C. Galas, N. Vitale, D. Aunis, and M. F. Bader. 1998. Regulated exocytosis in chromaffin cells. Translocation of ARF6 stimulates a plasma membrane-associated phospholipase D. J Biol Chem 273:1373-9.

Chatterjee, S., K. S. Clarke, and P. O. Kwiterovich, Jr. 1986. Uptake and metabolism of lactosylceramide on low density lipoproteins in cultured proximal tubular cells from normal and familial hypercholesterolemic homozygotes. J Biol Chem 261:13480-6.

Chen, Y. G., A. Siddhanta, C. D. Austin, S. M. Hammond, T. C. Sung, M. A. Frohman, A. J. Morris, and D. Shields. 1997. Phospholipase D stimulates release of nascent secretory vesicles from the trans-Golgi network. J Cell Biol 138:495-504.

Cheng, H., S. G. Straub, and G. W. Sharp. 2007. Inhibitory role of Src family tyrosine kinases on Ca2+-dependent insulin release. Am J Physiol Endocrinol Metab 292:E845-52.

Choi, S. Y., P. Huang, G. M. Jenkins, D. C. Chan, J. Schiller, and M. A. Frohman. 2006. A common lipid links Mfn-mediated mitochondrial fusion and SNARE-regulated exocytosis. Nat Cell Biol 8:1255-62.

Choi, W. S., Y. M. Kim, C. Combs, M. A. Frohman, and M. A. Beaven. 2002. Phospholipases D1 and D2 regulate different phases of exocytosis in mast cells. J Immunol 168:5682-9.

Christensen, E. I., and H. Birn. 2002. Megalin and cubilin: multifunctional endocytic receptors. Nat Rev Mol Cell Biol 3:256-66.

Cockcroft, S. 2001. Signaling roles of mammalian phospholipase D1 and D2. Cell Mol Life Sci 58:1674-87.

Cockcroft, S., G. M. Thomas, A. Fensome, B. Geny, E. Cunningham, I. Gout, I. Hiles, N. F. Totty, O. Truong, and J. J. Hsuan. 1994. Phospholipase D: a downstream effector of ARF in granulocytes. Science 263:523-6.

Colley, W. C., Y. M. Altshuller, C. K. Sue-Ling, N. G. Copeland, D. J. Gilbert, N. A. Jenkins, K. D. Branch, S. E. Tsirka, R. J. Bollag, W. B. Bollag, and M. A. Frohman. 1997a. Cloning and expression analysis of murine phospholipase D1. Biochem J 326 (Pt 3):745-53.

Colley, W. C., T. C. Sung, R. Roll, J. Jenco, S. M. Hammond, Y. Altshuller, D. Bar-Sagi, A. J. Morris, and M. A. Frohman. 1997b. Phospholipase D2, a distinct phospholipase D isoform with novel regulatory properties that provokes cytoskeletal reorganization. Curr Biol 7:191-201.

Cross, M. J., S. Roberts, A. J. Ridley, M. N. Hodgkin, A. Stewart, L. Claesson-Welsh, and M. J. Wakelam. 1996. Stimulation of actin stress fibre formation mediated by activation of phospholipase D. Curr Biol 6:588-97.

Diaz Anel, A. M. 2007. Phospholipase C beta3 is a key component in the Gbetagamma/PKCeta/PKD-mediated regulation of trans-Golgi network to plasma membrane transport. Biochem J 406:157-65.

Du, G., Y. M. Altshuller, N. Vitale, P. Huang, S. Chasserot-Golaz, A. J. Morris, M. F. Bader, and M. A. Frohman. 2003. Regulation of phospholipase D1 subcellular cycling through coordination of multiple membrane association motifs. J Cell Biol 162:305-15.

Du, G., P. Huang, B. T. Liang, and M. A. Frohman. 2004. Phospholipase D2 localizes to the plasma membrane and regulates angiotensin II receptor endocytosis. Mol Biol Cell 15:1024-30.

Edwards, Y. S., and A. W. Murray. 1995. Accumulation of phosphatidylalcohol in cultured cells: use of subcellular fractionation to investigate phospholipase D activity during signal transduction. Biochem J 308 (Pt 2):473-80.

Ella, K. M., J. W. Dolan, and K. E. Meier. 1995. Characterization of a regulated form of phospholipase D in the yeast Saccharomyces cerevisiae. Biochem J 307 (Pt 3):799-805.

Ellis, M. A., B. A. Potter, K. O. Cresawn, and O. A. Weisz. 2006. Polarized biosynthetic traffic in renal epithelial cells: sorting, sorting, everywhere. Am J Physiol Renal Physiol 291:F707-13.

Emoto, M., J. K. Klarlund, S. B. Waters, V. Hu, J. M. Buxton, A. Chawla, and M. P. Czech. 2000. A role for phospholipase D in GLUT4 glucose transporter translocation. J Biol Chem 275:7144-51.

Fensome, A., E. Cunningham, S. Prosser, S. K. Tan, P. Swigart, G. Thomas, J. Hsuan, and S. Cockcroft. 1996. ARF and PITP restore GTP gamma S-stimulated protein secretion from cytosol-depleted HL60 cells by promoting PIP2 synthesis. Curr Biol 6:730-8.

Freyberg, Z., S. Bourgoin, and D. Shields. 2002. Phospholipase D2 is localized to the rims of the Golgi apparatus in mammalian cells. Mol Biol Cell 13:3930-42.

Freyberg, Z., A. Siddhanta, and D. Shields. 2003. "Slip, sliding away": phospholipase D and the Golgi apparatus. Trends Cell Biol 13:540-6.

Freyberg, Z., D. Sweeney, A. Siddhanta, S. Bourgoin, M. Frohman, and D. Shields. 2001. Intracellular localization of phospholipase D1 in mammalian cells. Mol Biol Cell 12:943-55.

Frondorf, K., K. M. Henkels, M. A. Frohman, and J. Gomez-Cambronero. 2010. Phosphatidic acid (PA) is a leukocyte chemoattractant that acts through S6 kinase signaling. J Biol Chem.

Gromada, J., J. Frokjaer-Jensen, and S. Dissing. 1996. Glucose stimulates voltage- and calcium-dependent inositol trisphosphate production and intracellular calcium mobilization in insulin-secreting beta TC3 cells. Biochem J 314 (Pt 1):339-45.

Guo, T., C. Gregg, T. Boukh-Viner, P. Kyryakov, A. Goldberg, S. Bourque, F. Banu, S. Haile, S. Milijevic, K. H. San, J. Solomon, V. Wong, and V. I. Titorenko. 2007. A signal from inside the peroxisome initiates its division by promoting the remodeling of the peroxisomal membrane. J Cell Biol 177:289-303.

Hammond, S. M., Y. M. Altshuller, T. C. Sung, S. A. Rudge, K. Rose, J. Engebrecht, A. J. Morris, and M. A. Frohman. 1995. Human ADP-ribosylation factor-activated phosphatidylcholine-specific phospholipase D defines a new and highly conserved gene family. J Biol Chem 270:29640-3.

Hammond, S. M., J. M. Jenco, S. Nakashima, K. Cadwallader, Q. Gu, S. Cook, Y. Nozawa, G. D. Prestwich, M. A. Frohman, and A. J. Morris. 1997.

Characterization of two alternately spliced forms of phospholipase D1. Activation of the purified enzymes by phosphatidylinositol 4,5-bisphosphate, ADP-ribosylation factor, and Rho family monomeric GTP-binding proteins and protein kinase C-alpha. J Biol Chem 272:3860-8.

Hampe, C. S., A. R. Wallen, M. Schlosser, M. Ziegler, and I. R. Sweet. 2005. Quantitative evaluation of a monoclonal antibody and its fragment as potential markers for pancreatic beta cell mass. Exp Clin Endocrinol Diabetes 113:381-7.

Han, G. S., S. Siniossoglou, and G. M. Carman. 2007. The cellular functions of the yeast lipin homolog PAH1p are dependent on its phosphatidate phosphatase activity. J Biol Chem 282:37026-35.

Hanyaloglu, A. C., and M. von Zastrow. 2008. Regulation of GPCRs by endocytic membrane trafficking and its potential implications. Annu Rev Pharmacol Toxicol 48:537-68.

Hirota, J., H. Ando, K. Hamada, and K. Mikoshiba. 2003. Carbonic anhydrase-related protein is a novel binding protein for inositol 1,4,5-trisphosphate receptor type 1. Biochem J 372:435-41.

Honda, A., M. Nogami, T. Yokozeki, M. Yamazaki, H. Nakamura, H. Watanabe, K. Kawamoto, K. Nakayama, A. J. Morris, M. A. Frohman, and Y. Kanaho. 1999. Phosphatidylinositol 4-phosphate 5-kinase alpha is a downstream effector of the small G protein ARF6 in membrane ruffle formation. Cell 99:521-32.

Huang, P., Y. M. Altshuller, J. C. Hou, J. E. Pessin, and M. A. Frohman. 2005. Insulin-stimulated plasma membrane fusion of Glut4 glucose transporter-containing vesicles is regulated by phospholipase D1. Mol Biol Cell 16:2614-23.

Hughes, W. E., Z. Elgundi, P. Huang, M. A. Frohman, and T. J. Biden. 2004. Phospholipase D1 regulates secretagogue-stimulated insulin release in pancreatic beta-cells. J Biol Chem 279:27534-41.

Hughes, W. E., and P. J. Parker. 2001. Endosomal localization of phospholipase D 1a and 1b is defined by the C-termini of the proteins, and is independent of activity. Biochem J 356:727-36.

Iyer, S. S., R. S. Agrawal, C. R. Thompson, S. Thompson, J. A. Barton, and D. J. Kusner. 2006. Phospholipase D1 regulates phagocyte adhesion. J Immunol 176:3686-96.

Jenkins, G. H., P. L. Fisette, and R. A. Anderson. 1994. Type I phosphatidylinositol 4-phosphate 5-kinase isoforms are specifically stimulated by phosphatidic acid. J Biol Chem 269:11547-54.

Jenkins, G. M., and M. A. Frohman. 2005. Phospholipase D: a lipid centric review. Cell Mol Life Sci 62:2305-16.

Jones, D. H., B. Bax, A. Fensome, and S. Cockcroft. 1999. ADP ribosylation factor 1 mutants identify a phospholipase D effector region and reveal that phospholipase D participates in lysosomal secretion but is not sufficient for recruitment of coatomer I. Biochem J 341 (Pt 1):185-92.

Jovanovic, O. A., F. D. Brown, and J. G. Donaldson. 2006. An effector domain mutant of Arf6 implicates phospholipase D in endosomal membrane recycling. Mol Biol Cell 17:327-35.

Karlas, A., N. Machuy, Y. Shin, K. P. Pleissner, A. Artarini, D. Heuer, D. Becker, H. Khalil, L. A. Ogilvie, S. Hess, A. P. Maurer, E. Muller, T. Wolff, T. Rudel, and T.

F. Meyer. 2010. Genome-wide RNAi screen identifies human host factors crucial for influenza virus replication. Nature 463:818-22.
Kim, H., J. Lee, S. Kim, M. K. Shin, S. Min do, and T. Shin. 2007. Differential expression of phospholipases D1 and D2 in mouse tissues. Cell Biol Int 31:148-55.
Kobayashi, M., and J. N. Kanfer. 1987. Phosphatidylethanol formation via transphosphatidylation by rat brain synaptosomal phospholipase D. J Neurochem 48:1597-603.
Ktistakis, N. T., H. A. Brown, M. G. Waters, P. C. Sternweis, and M. G. Roth. 1996. Evidence that phospholipase D mediates ADP ribosylation factor-dependent formation of Golgi coated vesicles. J Cell Biol 134:295-306.
Laine, J., S. Bourgoin, J. Bourassa, and J. Morisset. 2000. Subcellular distribution and characterization of rat pancreatic phospholipase D isoforms. Pancreas 20:323-36.
Lauritzen, H. P. 2009. In vivo imaging of GLUT4 translocation. Appl Physiol Nutr Metab 34:420-3.
Lee, H. Y., H. Jung, I. H. Jang, P. G. Suh, and S. H. Ryu. 2008a. Cdk5 phosphorylates PLD2 to mediate EGF-dependent insulin secretion. Cell Signal 20:1787-94.
Lee, H. Y., K. Yea, J. Kim, B. D. Lee, Y. C. Chae, H. S. Kim, D. W. Lee, S. H. Kim, J. H. Cho, C. J. Jin, D. S. Koh, K. S. Park, P. G. Suh, and S. H. Ryu. 2008b. Epidermal growth factor increases insulin secretion and lowers blood glucose in diabetic mice. J Cell Mol Med 12:1593-604.
Lehman, N., M. Di Fulvio, N. McCray, I. Campos, F. Tabatabaian, and J. Gomez-Cambronero. 2006. Phagocyte cell migration is mediated by phospholipases PLD1 and PLD2. Blood 108:3564-72.
Lev, S., J. Hernandez, R. Martinez, A. Chen, G. Plowman, and J. Schlessinger. 1999. Identification of a novel family of targets of PYK2 related to Drosophila retinal degeneration B (rdgB) protein. Mol Cell Biol 19:2278-88.
Li, X., S. M. Routt, Z. Xie, X. Cui, M. Fang, M. A. Kearns, M. Bard, D. R. Kirsch, and V. A. Bankaitis. 2000. Identification of a novel family of nonclassic yeast phosphatidylinositol transfer proteins whose function modulates phospholipase D activity and Sec14p-independent cell growth. Mol Biol Cell 11:1989-2005.
Lin, M., A. Lubag, M. J. McGuire, S. Y. Seliounine, E. N. Tsyganov, P. P. Antich, A. D. Sherry, K. C. Brown, and X. Sun. 2008. Advances in molecular imaging of pancreatic beta cells. Front Biosci 13:4558-75.
Liu, Z., P. B. Jeppesen, S. Gregersen, X. Chen, and K. Hermansen. 2008. Dose- and Glucose-Dependent Effects of Amino Acids on Insulin Secretion from Isolated Mouse Islets and Clonal INS-1E Beta-Cells. Rev Diabet Stud 5:232-44.
Loonen, A. J., N. V. Knoers, C. H. van Os, and P. M. Deen. 2008. Aquaporin 2 mutations in nephrogenic diabetes insipidus. Semin Nephrol 28:252-65.
Lopez, I., R. S. Arnold, and J. D. Lambeth. 1998. Cloning and initial characterization of a human phospholipase D2 (hPLD2). ADP-ribosylation factor regulates hPLD2. J Biol Chem 273:12846-52.
Lucocq, J., M. Manifava, K. Bi, M. G. Roth, and N. T. Ktistakis. 2001. Immunolocalisation of phospholipase D1 on tubular vesicular membranes of endocytic and secretory origin. Eur J Cell Biol 80:508-20.

MacDonald, M. J. 2007. Synergistic potent insulin release by combinations of weak secretagogues in pancreatic islets and INS-1 cells. J Biol Chem 282:6043-52.
Madesh, M., and K. A. Balasubramanian. 1997. Metal ion stimulation of phospholipase D-like activity of isolated rat intestinal mitochondria. Lipids 32:471-9.
Madziva, M. T., and M. Birnbaumer. 2006. A role for ADP-ribosylation factor 6 in the processing of G-protein-coupled receptors. J Biol Chem 281:12178-86.
Manganas, L. N., X. Zhang, Y. Li, R. D. Hazel, S. D. Smith, M. E. Wagshul, F. Henn, H. Benveniste, P. M. Djuric, G. Enikolopov, and M. Maletic-Savatic. 2007. Magnetic resonance spectroscopy identifies neural progenitor cells in the live human brain. Science 318:980-5.
Marshansky, V., D. A. Ausiello, and D. Brown. 2002. Physiological importance of endosomal acidification: potential role in proximal tubulopathies. Curr Opin Nephrol Hypertens 11:527-37.
Martin, A., F. D. Brown, M. N. Hodgkin, A. J. Bradwell, S. J. Cook, M. Hart, and M. J. Wakelam. 1996. Activation of phospholipase D and phosphatidylinositol 4-phosphate 5-kinase in HL60 membranes is mediated by endogenous Arf but not Rho. J Biol Chem 271:17397-403.
Medarova, Z., and A. Moore. 2009. MRI in diabetes: first results. AJR Am J Roentgenol 193:295-303.
Metz, S. A., and M. Dunlop. 1990. Stimulation of insulin release by phospholipase D. A potential role for endogenous phosphatidic acid in pancreatic islet function. Biochem J 270:427-35.
Miki, T., K. Nagashima, F. Tashiro, K. Kotake, H. Yoshitomi, A. Tamamoto, T. Gonoi, T. Iwanaga, J. Miyazaki, and S. Seino. 1998. Defective insulin secretion and enhanced insulin action in KATP channel-deficient mice. Proc Natl Acad Sci U S A 95:10402-6.
Miki, T., F. Tashiro, T. Iwanaga, K. Nagashima, H. Yoshitomi, H. Aihara, Y. Nitta, T. Gonoi, N. Inagaki, J. Miyazaki, and S. Seino. 1997. Abnormalities of pancreatic islets by targeted expression of a dominant-negative KATP channel. Proc Natl Acad Sci U S A 94:11969-73.
Monovich, L., B. Mugrage, E. Quadros, K. Toscano, R. Tommasi, S. LaVoie, E. Liu, Z. Du, D. LaSala, W. Boyar, and P. Steed. 2007. Optimization of halopemide for phospholipase D2 inhibition. Bioorg Med Chem Lett 17:2310-1.
Moon, S. S., H. J. Kim, Y. K. Choi, H. A. Seo, J. H. Jeon, J. E. Lee, J. Y. Lee, T. H. Kwon, J. G. Kim, B. W. Kim, and I. K. Lee. 2009. Novel mutation of aquaporin-2 gene in a patient with congenital nephrogenic diabetes insipidus. Endocr J 56:905-10.
Moore, A., S. Bonner-Weir, and R. Weissleder. 2001. Noninvasive in vivo measurement of beta-cell mass in mouse model of diabetes. Diabetes 50:2231-6.
Moritz, A., P. N. De Graan, W. H. Gispen, and K. W. Wirtz. 1992. Phosphatidic acid is a specific activator of phosphatidylinositol-4-phosphate kinase. J Biol Chem 267:7207-10.
Nadimpalli, S. K., and P. K. Amancha. 2009. Evolution of Mannose 6-Phosphate Receptors (MPR300 and 46): Lysosomal Enzyme Sorting Proteins. Curr Protein Pept Sci.

Nokes, R. L., I. C. Fields, R. N. Collins, and H. Folsch. 2008. Rab13 regulates membrane trafficking between TGN and recycling endosomes in polarized epithelial cells. J Cell Biol 182:845-53.
Novick, P., C. Field, and R. Schekman. 1980. Identification of 23 complementation groups required for post-translational events in the yeast secretory pathway. Cell 21:205-15.
Ohara-Imaizumi, M., T. Fujiwara, Y. Nakamichi, T. Okamura, Y. Akimoto, J. Kawai, S. Matsushima, H. Kawakami, T. Watanabe, K. Akagawa, and S. Nagamatsu. 2007. Imaging analysis reveals mechanistic differences between first- and second-phase insulin exocytosis. J Cell Biol 177:695-705.
Oka, T., and A. Nakano. 1994. Inhibition of GTP hydrolysis by Sar1p causes accumulation of vesicles that are a functional intermediate of the ER-to-Golgi transport in yeast. J Cell Biol 124:425-34.
Olofsson, S. O., L. Asp, and J. Boren. 1999. The assembly and secretion of apolipoprotein B-containing lipoproteins. Curr Opin Lipidol 10:341-6.
Park, S. Y., J. H. Cho, W. Ma, H. J. Choi, and J. S. Han. Phospholipase D2 acts as an important regulator in LPS-induced nitric oxide synthesis in Raw 264.7 cells. Cell Signal 22:619-28.
Pathre, P., K. Shome, A. Blumental-Perry, A. Bielli, C. J. Haney, S. Alber, S. C. Watkins, G. Romero, and M. Aridor. 2003. Activation of phospholipase D by the small GTPase Sar1p is required to support COPII assembly and ER export. EMBO J 22:4059-69.
Pieters, J. 2008. Mycobacterium tuberculosis and the macrophage: maintaining a balance. Cell Host Microbe 3:399-407.
Pinton, P., T. Pozzan, and R. Rizzuto. 1998. The Golgi apparatus is an inositol 1,4,5-trisphosphate-sensitive Ca2+ store, with functional properties distinct from those of the endoplasmic reticulum. EMBO J 17:5298-308.
Reue, K., and D. N. Brindley. 2008. Thematic Review Series: Glycerolipids. Multiple roles for lipins/phosphatidate phosphatase enzymes in lipid metabolism. J Lipid Res 49:2493-503.
Robben, J. H., N. V. Knoers, and P. M. Deen. 2006. Cell biological aspects of the vasopressin type-2 receptor and aquaporin 2 water channel in nephrogenic diabetes insipidus. Am J Physiol Renal Physiol 291:F257-70.
Rose, K., S. A. Rudge, M. A. Frohman, A. J. Morris, and J. Engebrecht. 1995. Phospholipase D signaling is essential for meiosis. Proc Natl Acad Sci U S A 92:12151-5.
Roth, M. G., K. Bi, N. T. Ktistakis, and S. Yu. 1999. Phospholipase D as an effector for ADP-ribosylation factor in the regulation of vesicular traffic. Chem Phys Lipids 98:141-52.
Saftig, P., and J. Klumperman. 2009. Lysosome biogenesis and lysosomal membrane proteins: trafficking meets function. Nat Rev Mol Cell Biol 10:623-35.
Saito, A., H. Sato, N. Iino, and T. Takeda. 2010. Molecular mechanisms of receptor-mediated endocytosis in the renal proximal tubular epithelium. J Biomed Biotechnol 2010:403272.
Saito, M., and J. Kanfer. 1975. Phosphatidohydrolase activity in a solubilized preparation from rat brain particulate fraction. Arch Biochem Biophys 169:318-23.

Sasaki, S., and Y. Noda. 2007. Aquaporin-2 protein dynamics within the cell. Curr Opin Nephrol Hypertens 16:348-52.
Savelkoul, P. J., F. De Mattia, Y. Li, E. J. Kamsteeg, I. B. Konings, P. van der Sluijs, and P. M. Deen. 2009. p.R254Q mutation in the aquaporin-2 water channel causing dominant nephrogenic diabetes insipidus is due to a lack of arginine vasopressin-induced phosphorylation. Hum Mutat 30:E891-903.
Schmidt, J. A., and W. J. Brown. 2009. Lysophosphatidic acid acyltransferase 3 regulates Golgi complex structure and function. J Cell Biol 186:211-8.
Sciorra, V. A., and A. J. Morris. 1999. Sequential actions of phospholipase D and phosphatidic acid phosphohydrolase 2b generate diglyceride in mammalian cells. Mol Biol Cell 10:3863-76.
Scott, S. A., P. E. Selvy, J. R. Buck, H. P. Cho, T. L. Criswell, A. L. Thomas, M. D. Armstrong, C. L. Arteaga, C. W. Lindsley, and H. A. Brown. 2009. Design of isoform-selective phospholipase D inhibitors that modulate cancer cell invasiveness. Nat Chem Biol 5:108-17.
Shenoy, S. K., and R. J. Lefkowitz. 2005. Receptor-specific ubiquitination of beta-arrestin directs assembly and targeting of seven-transmembrane receptor signalosomes. J Biol Chem 280:15315-24.
Siddhanta, A., J. M. Backer, and D. Shields. 2000. Inhibition of phosphatidic acid synthesis alters the structure of the Golgi apparatus and inhibits secretion in endocrine cells. J Biol Chem 275:12023-31.
Simpson, N. R., F. Souza, P. Witkowski, A. Maffei, A. Raffo, A. Herron, M. Kilbourn, A. Jurewicz, K. Herold, E. Liu, M. A. Hardy, R. Van Heertum, and P. E. Harris. 2006. Visualizing pancreatic beta-cell mass with [11C]DTBZ. Nucl Med Biol 33:855-64.
Souza, F., M. Freeby, K. Hultman, N. Simpson, A. Herron, P. Witkowsky, E. Liu, A. Maffei, and P. E. Harris. 2006. Current progress in non-invasive imaging of beta cell mass of the endocrine pancreas. Curr Med Chem 13:2761-73.
Sreenivas, A., J. L. Patton-Vogt, V. Bruno, P. Griac, and S. A. Henry. 1998. A role for phospholipase D (Pld1p) in growth, secretion, and regulation of membrane lipid synthesis in yeast. J Biol Chem 273:16635-8.
Srinivasan, M., R. Aalinkeel, F. Song, B. Lee, S. G. Laychock, and M. S. Patel. 2000. Adaptive changes in insulin secretion by islets from neonatal rats raised on a high-carbohydrate formula. Am J Physiol Endocrinol Metab 279:E1347-57.
Stuckey, J. A., and J. E. Dixon. 1999. Crystal structure of a phospholipase D family member. Nat Struct Biol 6:278-84.
Su, W., O. Yeku, S. Olepu, A. Genna, J. S. Park, H. Ren, G. Du, M. H. Gelb, A. J. Morris, and M. A. Frohman. 2009. 5-Fluoro-2-indolyl des-chlorohalopemide (FIPI), a phospholipase D pharmacological inhibitor that alters cell spreading and inhibits chemotaxis. Mol Pharmacol 75:437-46.
Sung, T. C., Y. M. Altshuller, A. J. Morris, and M. A. Frohman. 1999a. Molecular analysis of mammalian phospholipase D2. J Biol Chem 274:494-502.
Sung, T. C., R. L. Roper, Y. Zhang, S. A. Rudge, R. Temel, S. M. Hammond, A. J. Morris, B. Moss, J. Engebrecht, and M. A. Frohman. 1997. Mutagenesis of phospholipase D defines a superfamily including a trans-Golgi viral protein required for poxvirus pathogenicity. EMBO J 16:4519-30.

Sung, T. C., Y. Zhang, A. J. Morris, and M. A. Frohman. 1999b. Structural analysis of human phospholipase D1. J Biol Chem 274:3659-66.
Tang, Y. Z., D. Q. Li, F. J. Sun, L. Li, and D. M. Yu. 2009. P-glycoprotein regulating biphasic insulin secretion in rat pancreatic beta cells. Chin Med J (Engl) 122:2587-92.
Toda, K., M. Nogami, K. Murakami, Y. Kanaho, and K. Nakayama. 1999. Colocalization of phospholipase D1 and GTP-binding-defective mutant of ADP-ribosylation factor 6 to endosomes and lysosomes. FEBS Lett 442:221-5.
Tojo, A., M. L. Onozato, H. Ha, H. Kurihara, T. Sakai, A. Goto, T. Fujita, and H. Endou. 2001. Reduced albumin reabsorption in the proximal tubule of early-stage diabetic rats. Histochem Cell Biol 116:269-76.
Tzafriri, A. R., and E. R. Edelman. 2007. Endosomal receptor kinetics determine the stability of intracellular growth factor signaling complexes. Biochem J 402:537-49.
Vadakekalam, J., M. E. Rabaglia, Q. H. Chen, and S. A. Metz. 1996. Role for GTP in glucose-induced phospholipase C activation in pancreatic islets. Am J Physiol 271:E85-95.
Vadakekalam, J., M. E. Rabaglia, and S. A. Metz. 1997. Roles of GTP and phospholipase C in the potentiation of Ca(2+)-induced insulin secretion by glucose in rat pancreatic islets. J Endocrinol 153:61-71.
Valenti, G., G. Procino, G. Tamma, M. Carmosino, and M. Svelto. 2005. Minireview: aquaporin 2 trafficking. Endocrinology 146:5063-70.
van Balkom, B. W., M. Boone, G. Hendriks, E. J. Kamsteeg, J. H. Robben, H. C. Stronks, A. van der Voorde, F. van Herp, P. van der Sluijs, and P. M. Deen. 2009. LIP5 interacts with aquaporin 2 and facilitates its lysosomal degradation. J Am Soc Nephrol 20:990-1001.
Vitale, N., A. S. Caumont, S. Chasserot-Golaz, G. Du, S. Wu, V. A. Sciorra, A. J. Morris, M. A. Frohman, and M. F. Bader. 2001. Phospholipase D1: a key factor for the exocytotic machinery in neuroendocrine cells. EMBO J 20:2424-34.
Wang, X. 2000. Multiple forms of phospholipase D in plants: the gene family, catalytic and regulatory properties, and cellular functions. Prog Lipid Res 39:109-49.
Wang, X., J. H. Dyer, and L. Zheng. 1993. Purification and immunological analysis of phospholipase D from castor bean endosperm. Arch Biochem Biophys 306:486-94.
Wang, X., C. Wang, Y. Sang, C. Qin, and R. Welti. 2002. Networking of phospholipases in plant signal transduction. Physiol Plant 115:331-335.
Wang, X., C. Wang, Y. Sang, L. Zheng, and C. Qin. 2000. Determining functions of multiple phospholipase Ds in stress response of Arabidopsis. Biochem Soc Trans 28:813-6.
Wang, X., L. Xu, and L. Zheng. 1994. Cloning and expression of phosphatidylcholine-hydrolyzing phospholipase D from Ricinus communis L. J Biol Chem 269:20312-7.
Wangler, B., S. Schneider, O. Thews, E. Schirrmacher, S. Comagic, P. Feilen, C. Schwanstecher, M. Schwanstecher, C. Y. Shiue, A. Alavi, S. Hohnemann, M. Piel, F. Rosch, and R. Schirrmacher. 2004. Synthesis and evaluation of (S)-2-(2-[18F]fluoroethoxy)-4-([3-methyl-1-(2-piperidin-1-yl-phenyl)-butyl -carbamoyl]-

methyl)-benzoic acid ([18F]repaglinide): a promising radioligand for quantification of pancreatic beta-cell mass with positron emission tomography (PET). Nucl Med Biol 31:639-47.

Way, G., N. O'Luanaigh, and S. Cockcroft. 2000. Activation of exocytosis by cross-linking of the IgE receptor is dependent on ADP-ribosylation factor 1-regulated phospholipase D in RBL-2H3 mast cells: evidence that the mechanism of activation is via regulation of phosphatidylinositol 4,5-bisphosphate synthesis. Biochem J 346 Pt 1:63-70.

Wei, F. Y., K. Nagashima, T. Ohshima, Y. Saheki, Y. F. Lu, M. Matsushita, Y. Yamada, K. Mikoshiba, Y. Seino, H. Matsui, and K. Tomizawa. 2005. Cdk5-dependent regulation of glucose-stimulated insulin secretion. Nat Med 11:1104-8.

Whitaker, B. D., D. L. Smith, and K. C. Green. 2001. Cloning, characterization and functional expression of a phospholipase Dalpha cDNA from tomato fruit. Physiol Plant 112:87-94.

Worley, J. F., 3rd, M. S. McIntyre, B. Spencer, R. J. Mertz, M. W. Roe, and I. D. Dukes. 1994. Endoplasmic reticulum calcium store regulates membrane potential in mouse islet beta-cells. J Biol Chem 269:14359-62.

Xie, Z., W. T. Ho, and J. H. Exton. 1998. Association of N- and C-terminal domains of phospholipase D is required for catalytic activity. J Biol Chem 273:34679-82.

Xie, Z., W. T. Ho, and J. H. Exton. 2000. Association of the N- and C-terminal domains of phospholipase D. Contribution of the conserved HKD motifs to the interaction and the requirement of the association for Ser/Thr phosphorylation of the enzyme. J Biol Chem 275:24962-9.

Yang, J. S., H. Gad, S. Y. Lee, A. Mironov, L. Zhang, G. V. Beznoussenko, C. Valente, G. Turacchio, A. N. Bonsra, G. Du, G. Baldanzi, A. Graziani, S. Bourgoin, M. A. Frohman, A. Luini, and V. W. Hsu. 2008. A role for phosphatidic acid in COPI vesicle fission yields insights into Golgi maintenance. Nat Cell Biol 10:1146-53.

Yang, J. S., S. Y. Lee, S. Spano, H. Gad, L. Zhang, Z. Nie, M. Bonazzi, D. Corda, A. Luini, and V. W. Hsu. 2005. A role for BARS at the fission step of COPI vesicle formation from Golgi membrane. EMBO J 24:4133-43.

Yang, J. S., L. Zhang, S. Y. Lee, H. Gad, A. Luini, and V. W. Hsu. 2006. Key components of the fission machinery are interchangeable. Nat Cell Biol 8:1376-82.

Yang, S. F., S. Freer, and A. A. Benson. 1967. Transphosphatidylation by phospholipase D. J Biol Chem 242:477-84.

Yi, X., R. Bouley, H. Y. Lin, S. Bechoua, T. X. Sun, E. Del Re, T. Shioda, M. K. Raychowdhury, H. A. Lu, A. B. Abou-Samra, D. Brown, and D. A. Ausiello. 2007. Alix (AIP1) is a vasopressin receptor (V2R)-interacting protein that increases lysosomal degradation of the V2R. Am J Physiol Renal Physiol 292:F1303-13.